This project has received funding from the Shift2Rail Joint Undertaking under the European Union's Horizon 2020 research and innovation programme under grant agreement no. 881805 (LOCATE)

Deliverable D 4.3
Simulation and Post Processing Results Report

Project acronym:	LOCATE
Full title	Locomotive bOgie Condition mAinTEnance
Starting date:	07/01/2022
Duration (in months):	29
Call (part) identifier:	S2R-OC-IP5-01-2019
Grant agreement no:	881805
Due date of deliverable:	28/02/2022
Actual submission date:	
Responsible/Author:	IST
Dissemination level:	
Status:	

Reviewed: yes

Document history		
Revision	*Date*	*Description*
0.1		Draft version
0.2		Partners Contributions
1.0		First issue
1.1		Revised Issue

Report contributors		
Name	Beneficiary Short Name	Details of contribution
Jorge Ambrósio	IST	Structure of work and methods selection, contributions to the deliverable and document revision
João Pagaimo	IST	Development of tools, simulations and digital twins construction
Pedro Millan	IST	Modelling and analysis, digital twins development
João Costa	IST	Framework for the simulation work, design of experiments and surrogate models construction. Overview of digital twins development.
Adam Bevan	HUD	Contributions to the Deliverable and Review
Xiaoyuan Liu	HUD	Main contribution to Section 9

Contents

1. Executive summary

Project LOCATE aims at the development of tools and methodologies to implement a condition-based maintenance policy for railway locomotives. WP4 aims at the development of models and methods to monitor the condition of bogie components using computer simulations, focusing on bogie frame and wheelset damage, as well as degradation of elements of the suspension system.

The development of digital twins to support the maintenance decisions requires that appropriate models of the locomotive are available in realistic operation conditions. Due to the fact that freight locomotive have friction based damping suspension systems, a major effort in modelling the locomotive and developing realistic operation scenarios is done here. Besides the locomotive also typical wagons are modelled and linked to the locomotive in normal operation. The computational models are verified through the comparison of the vehicle response, recorded in a preliminary measurement campaign, with the response that results from computer simulations. This process of model verification or validation is still an open point in both the academic and industrial fields. The variability of the operating conditions and the parameter uncertainty are considered in the definition of the simulations using experimental design techniques. These strategies also contribute to solve the problem of the high computational cost associated with simulations of highly non-linear railway dynamics using detailed vehicle models. The simulated vehicle response is measured using a series of virtual accelerometers distributed on the bogie components and the results are post-processed to obtain features that have different levels of sensitivity to the degradation of the bogie components. The post-processing involves a variety of methods including the analysis of signals in the frequency domain using the concept of transmissibility, in addition to the use of regression and statistical tools to model the vehicle response in the time domain. Condition classification methodologies are proposed to detect and locate damage on the bogie frame and the failure of suspension elements.

The final results is the construction of digital twins for the cases and scenarios in which they are feasible, the identification of their range of application and the limitations observed. In particular digital twins for the condition monitoring of the locomotive bogie structural heath and for the suspensions are successfully developed and presented. Although attempted, the digital twin for the structural health of the wheelsets presents limitations in its use due to its lack of sensitivity to intermediate health conditions of the wheelsets. In the process a methodological framework is presented to allow the use of the developments obtained in this task to be used in other applications in which the identification of physically based digital twins, for maintenance or safety applications, are of importance.

2. Abbreviations and acronyms

Acronym	Description
FGC	Ferrocarrils de la Generalitat de Catalunya
RLS	Recursive Least-square
TD	Technology Demonstrator
WA	Work Action
WP	Work Package

3. Background

The present document constitutes the Deliverable D4.3 “Simulation and Post Processing Results Report” in the framework of Tasks 4.3 and 4.4 of WP4 – Reference Behaviour.

4. Objective/Aim

This deliverable reports the development of models and methods to monitor the condition of bogie components using computer simulations. These simulations describe the nominal and abnormal behaviour of the locomotive, defining a data library for the reference behaviour of the vehicle. These methods can be further tested in real operation scenarios to assess their applicability in supporting the monitoring of the vehicle condition.

The final results are the construction of digital twins for the cases and scenarios in which they are feasible, the identification of their range of application and the limitations observed. In particular digital twins for the condition monitoring of the locomotive bogie structural heath and for the suspensions are successfully developed and presented. Although attempted, the digital twin for the structural health of the wheelsets presents limitations in its use due to its lack of sensitivity to intermediate health conditions of the wheelsets. In the process a methodological framework is presented to allow the use of the developments obtained in this task to be used in other applications in which the identification of physically based digital twins, for maintenance or safety applications, are of importance.

5. Vehicle and Track Models

The vehicle and track models representing the vehicle-track interaction are required to study their dynamic behaviours. Therefore, the multibody models of the locomotive and freight wagons are developed in the simulation code MUBODyn. These are described in the following sections together with the track models. To ensure that the models developed are representative of the locomotive under investigation in LOCATE, a verification strategy for comparison between simulations and measurements is proposed and applied to verify the locomotive model.

5.1. Vehicle Models

The dynamic simulations require the definition of models that incorporate the geometrical and mechanical properties of the locomotive and wagons. Such models must accurately capture the phenomena associated with the vehicle dynamics in order to represent the real operation. Focus is on the modelling of the locomotive components, which requires a detailed representation of the suspension mechanisms. To allow a study of the dynamics of the locomotive in the defective condition, these models must be able to represent the different behaviours of the components. A detailed description of the multibody model of the locomotive is given below. The models of the wagons and knuckle couplers are considered in preliminary simulations, to assess the effect of the presence of the wagons in the quantities measured in the bogies of the locomotive.

5.1.1. FGC 254 Series Locomotive

The FGC 254 freight locomotive, illustrated in Figure 1, is a diesel-electric locomotive composed of a vehicle body two bogie frames and 6 wheelsets. The vehicle body carries a 10 tonnes 8V diesel engine, traction related equipment and has two driver cabs, one on each end of the vehicle. It is supported by the two bogies through a set of mechanical elements that link it to the bolster, constituting the bogie-body connection. The bogie has two tiers of suspension, the first linking the axle boxes to the bogie frame, and the second connecting the bogie frame to the bolster. The axle boxes are linked to the bogie frame through horn guides and helical springs, while the bogie is connected to the bolster using rubber springs and guide limits. Each bogie has three powered axles individually driven by electric traction motors. Each electric motor is partially supported by both the bogie frame and the wheelset it drives. The general technical characteristics of the locomotive are presented in Table 1.

In the multibody model developed in MUBODyn, the vehicle body, bogie frames, bolsters, wheelsets and electric motors account for most of the inertia of the vehicle. Compared to the springs of the suspensions, these bodies are of a very high stiffness and are assumed as rigid bodies in the model. Springs, horn guides, friction surfaces, centreplates and guide limits constrain the relative movement of the bodies and are modelled as kinematic joints and force elements. The bogie structure is illustrated in Figure 1, and highlights the primary suspension, the bogie-bolster connection and the bogie-body connection. The connection between the electric motor and the bogie frame/wheelset is simplified. The electric motors are rigidly connected to the bogie frame. The inertia properties, as well as the initial positions and velocities of the centre of mass of the bodies are given in Annex A together with a detailed description of the modelled elements.

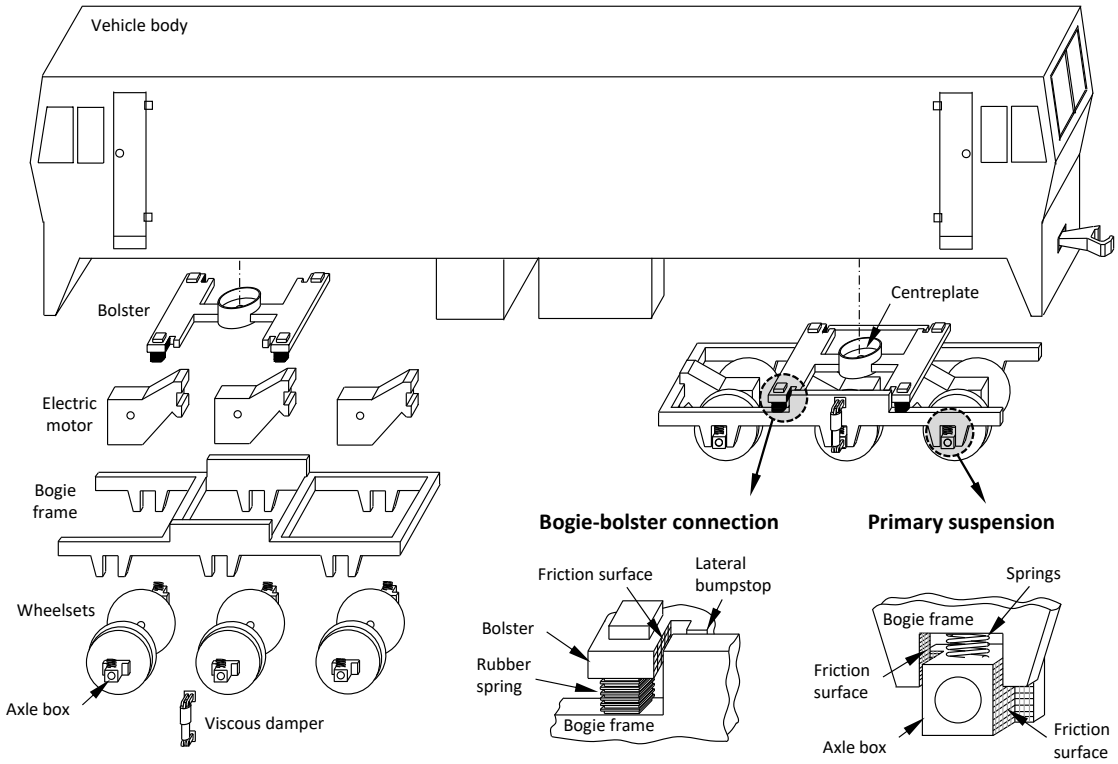

Figure 1 – Schematic representation of the locomotive and bogies with suspension mechanisms highlighted.

Table 1 – Technical characteristics of the locomotive FGC 254.

Track gauge	1.000 m (Metric gauge)
Wheel diameter (new condition)	0.914 m
Wheelset rolling line distance (new condition)	1.066 m
Wheelset weight (including axle gear)	1.243 t (approx.)
Bogie weight (w/ wheelsets, motors, braking gear, etc)	14.0 t (approx.)
Vehicle body weight (half consumables)	50.860 t (approx.)
Consumables weight (fuel, water and sand)	4.79 t (approx.)
Electric motor weight	2.002 t
Bogie centre pivot distance	9.5 m
Vehicle height (max.)	3.8 m
Vehicle width	2.67 m
Vehicle length (including couplers)	16.346 m
Maximum service speed	90 km/h
Power output	1214 kW
Braking	Dynamic/Pneumatic
UIC locomotive axle arrangement	Co'Co'

5.1.1.1. Primary Suspension

The primary suspension transmits the loads between the bogie frame and the axle boxes. It filters the vibrations from the wheelset to the bogie frame and dissipates energy through friction damping on the surfaces of the horn guides and viscous dampers, as illustrated in Figure 1. It also ensures the guidance of the vehicle. The axle boxes are connected to the bogie frame through two vertical concentric helical springs, and horn guides aligned with friction surfaces that allow longitudinal and lateral displacements within defined clearances, as shown in Figure 2. The axle boxes and wheelsets connect through bearings, which are modelled with revolute joints, only allowing the relative pitch rotation between the two bodies. The concentric helical springs are modelled using three orthogonal linear force elements that represent their axial and shear stiffness, as illustrated in Figure 2. The viscous damper is modelled using one axial linear force element.

The horn guides are modelled by three cylindrical joints with clearance, as in Figure 2. The cylindrical joints with clearance penalise the radial displacements and axial misalignment between the two bodies. Physically, a cylindrical joint with clearance represents a cylinder inside a tube with radial clearance. Normal forces develop when contact occurs in the radial direction and friction forces arise when there is a relative tangential displacement at the contact point. Although cylindrical joints with clearances have a circular cross-section, the adopted radii used here are large enough to approximate flat surfaces. The longitudinal guides are modelled using two intersecting cylindrical joints with clearance, as depicted in Figure 2, defining the real longitudinal clearance. In the lateral direction the reduced longitudinal clearance does not allow significant yaw rotations due to the two flaps that limit the lateral displacement. This enables a simplified modelling in which the lateral clearance is represented by one cylindrical joint with clearance aligned with the wheelset axle. This simplification reduces the model complexity and the computational effort while guarantees that the suspension geometry is accurately represented.

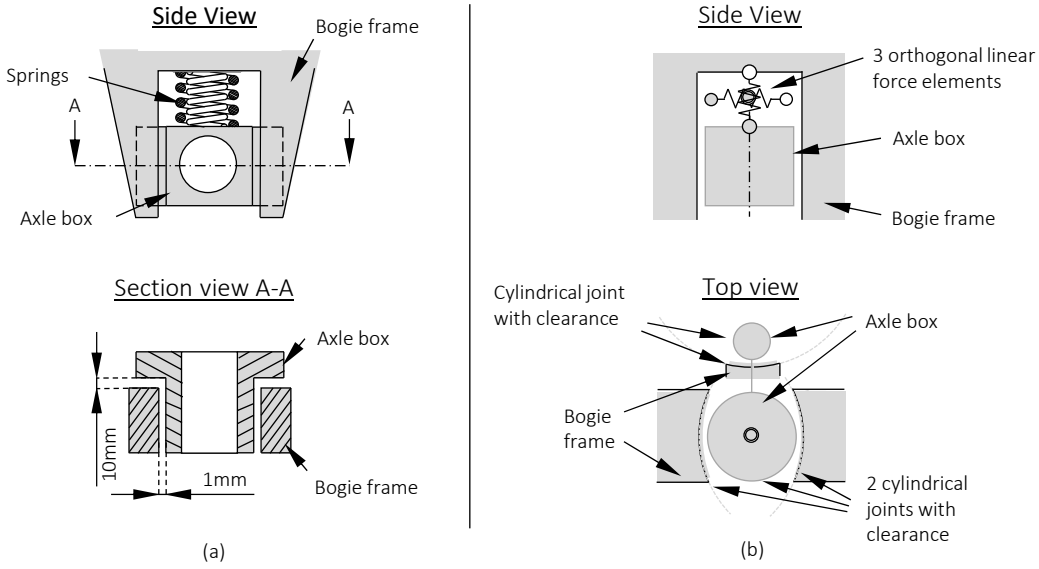

Figure 2 – Schematic representation of primary suspension: (a) actual mechanism and (b) multibody model.

5.1.1.2. Bogie-Bolster Connection

Rubber springs and limit guides form the bogie-bolster connection at four different points, as depicted in Figure 1. The rubber springs in the bogie-bolster connection transmit vertical, lateral and longitudinal loads and dampen the vibrations. Rubber springs have non-linear elastic and damping behaviour with hysteresis, where part of the energy is dissipated due to internal friction. Generally, accurate modelling of rubber elements is challenging, as observed in [1,2]. In this work, the rubber elements models are simplified. To define the behaviour of the rubber spring in the three directions, three linear force elements, each consisting of a spring and damper in parallel, are defined, orthogonal to each other, as illustrated in Figure 3.

The guides limit the relative displacements between the bogie frame and bolster in the lateral and longitudinal directions, being modelled as revolute joints with clearance, as depicted in Figure 3. The revolute joint with clearance penalizes the radial displacement and axial misalignment between the two bodies, as well as the axial displacement but not the axial rotation. From the physical point of view, the revolute joints with clearance represent a cylinder inside a hollow cylinder, where the inner body movement is limited in the radial and axial directions by inner surfaces of the outer body. The lateral guide is modelled with the contact between the bases of the cylinders while the longitudinal guide is represented with the contact between the cylinder walls.

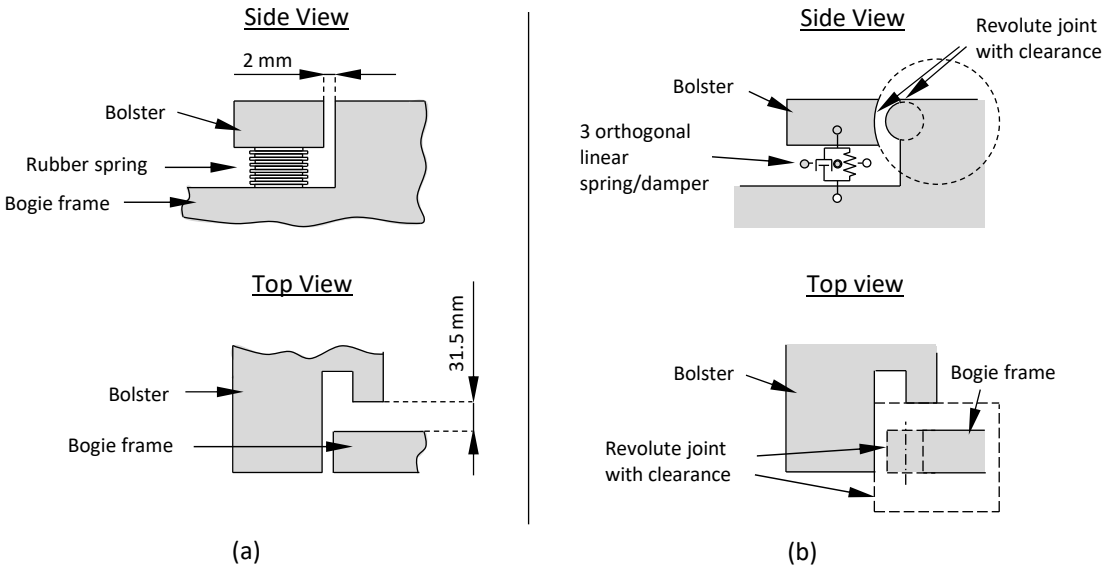

Figure 3 – Schematic representation of bogie-bolster connection (a) real sub-systems; (b) multibody model of the sub-system.

5.1.1.3. Bogie-Vehicle Body Connection

The vehicle body connects to the bogie through the centreplate, as depicted in Figure 4. The centreplate connection allows the steering of the bogies and transmits the vertical, lateral and longitudinal forces, as well as the roll and pitch rotation moments. The contacting surfaces between the pivot and centreplate are lined with friction pads that provide yaw damping. The connection at the centreplate-pivot is defined within a radial clearance, depicted in Figure 4.

The centreplate-pivot connection is modelled by 4 revolute joints, as depicted in Figure 4. The formulation of the revolute joint with clearance in MUBODyn does not allow to capture the yaw friction moments developed at the centreplate-pivot bases. This happens because the contact between the bases of the cylinders is detected at its centre points. Even though the use of one revolute joint could be sufficient to capture the radial clearance and the contact forces in the radial directions, when there is a rotation around the axis of the cylinders, the moment arm is zero, hence leading to a null friction moment. The use of the four revolute bushings overcomes this limitation as the four inner cylinders rotate around the vertical axis of the centreplate and allow a friction moment to develop. When the pivot is displaced sideways, and contact occurs at the centreplate walls, the normal and tangential forces are captured. It must be noted that the clearance on the radial direction is a better modelling method as the number of revolute joints increases. However, the use of four revolute joints offers a reasonable trade-off between model complexity and physical accuracy.

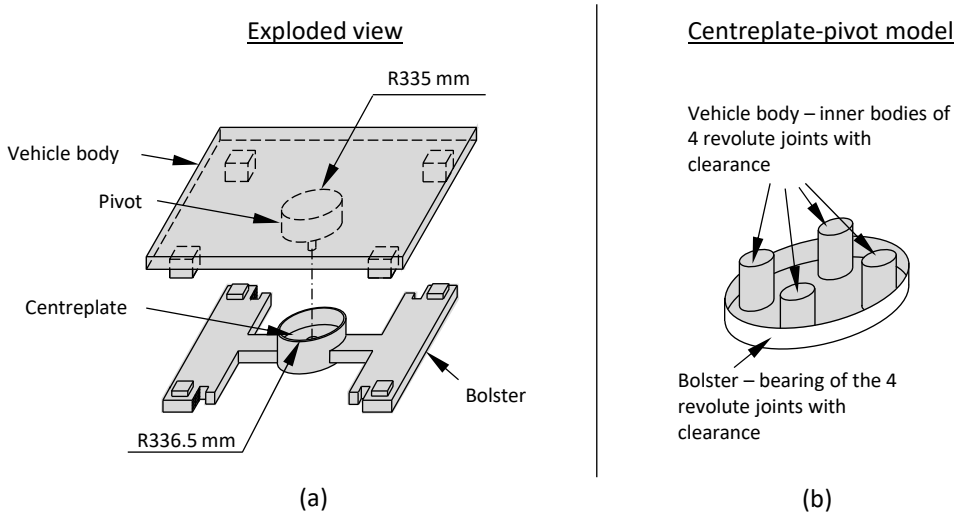

Figure 4 – Schematic representation of (a) vehicle body-bogie connection and (b) multibody model of centreplate-pivot.

5.1.2. FGC 62.000 Series Wagons

The modelling of the freight wagon was not envisaged in the technical annex of the LOCATE project. However, in order to perform the dynamics analysis of the locomotive in realistic operation conditions, for the development of the digital twins, the dynamic effects due to the wagon pull is very important. Therefore, freight wagons of the type used in the daily activities of FGC are modelled here also.

The FGC 62.000, depicted in Figure 5, is a freight wagon composed of the vehicle body and two three-piece-bogies with constant damping [3–5]. The vehicle body is supported by the two three-piece bogies through a set of mechanical elements, which link to the bolster. The bogie consists of three main pieces, i.e., the two side frames and the bolster, plus two wheelsets. The bolster rests on vertical helical springs that connect it to the side frames while the side frames rest on the axle boxes on top of rubber elements that isolate the high-frequency vibrations from the

wheel-rail contact. The technical characteristics of the FGC 62.000 are presented in Table 2. A simplified multibody model of the freight wagon was developed in MUBODyn, using linear force elements to represent the suspension systems. The model is described in Annex B.

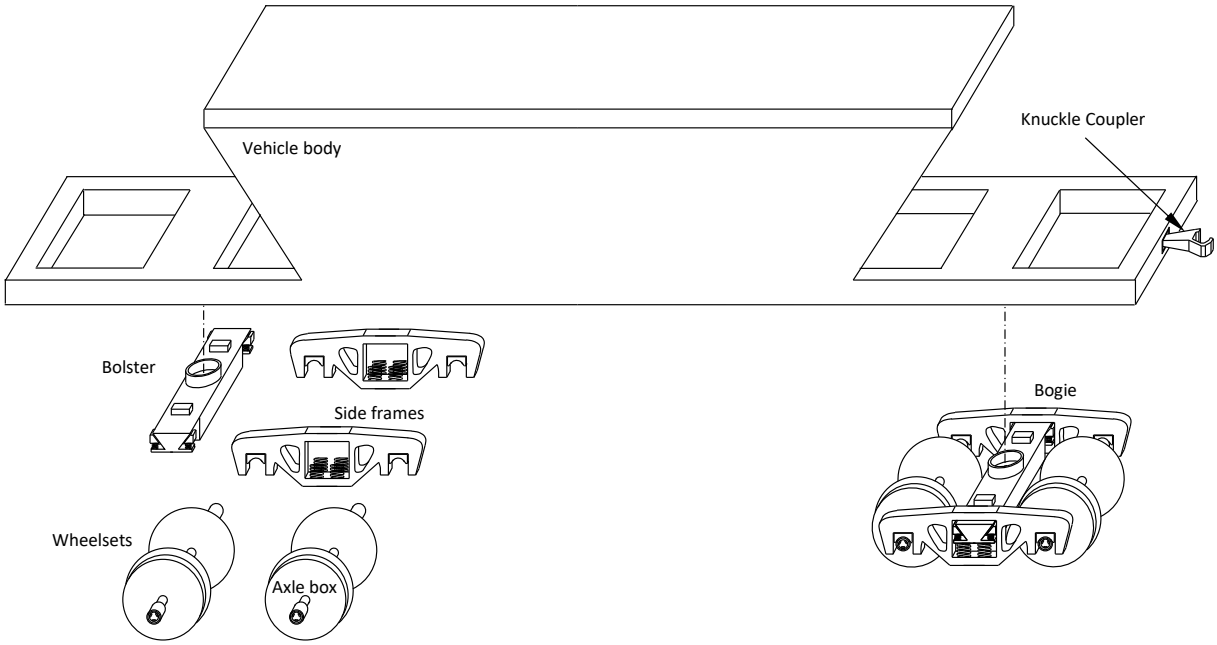

Figure 5 – Schematic representation of the freight wagon FGC 62.000

Table 2 – Technical characteristics of the freight wagon FGC 62.000.

Track gauge	1.000 m (Metric gauge)
Wheel diameter (new condition)	0.762 m
Wheelset rolling line distance (new condition)	1.066 m
Wheelset weight (including axle box)	0.990 t (approx.)
Bogie weight (w/ wheelsets, axle boxes, etc)	3.238 t (approx.)
Vehicle body weight (tare)	13.970 t (approx.)
Vehicle body weight (laden)	59.572 t (approx.)
Bogie centre pivot distance	9.6 m
Vehicle height (max.)	3.74 m
Vehicle width	2.75 m
Vehicle length (including couplers)	13.633 m

5.1.3. Knuckle coupler

Both the locomotive FGC 254 and freight wagons FGC 62.000 are equipped with knuckle couplers to connect adjacent vehicles. The knuckle coupler mechanism, shown in Figure 6, consists of two stiff bodies and one suspension element. The stiff bodies are the knuckle, used to connect the adjacent vehicles. The follower is connected to the knuckle at one end allowing limited relative pitch and yaw, and connected to the vehicle body at the other end through a translation joint and a draft gear. The draft gear transmits the longitudinal forces between the follower and the vehicle body by friction elements and steel helical springs or rubber components. The draft gear presents a highly non-linear

behaviour which depends on whether the system is loading or unloading, and on the difference of relative velocities between adjacent vehicles. Due to the limited information on the coupler characteristics, a simplified multibody model of the coupler is developed. The values presented in [6] are used as reference for the coupler geometry, while the stiffness of the draft gear is considered linear based on [7]. The description of the coupler model can be found in the Annex C.

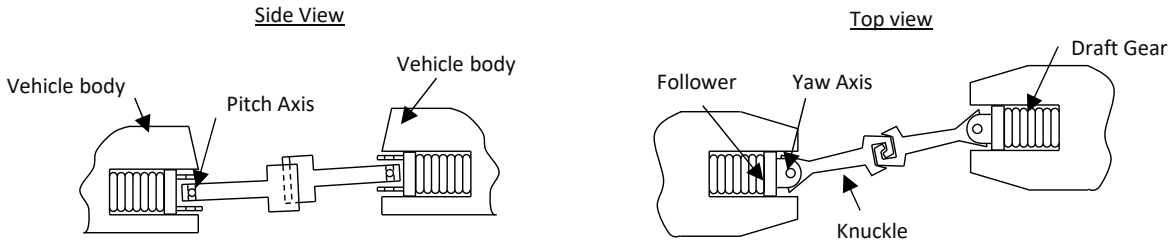

Figure 6 – Schematic representation of knuckle couplers.

5.2. Track Geometry

The nominal geometry of a track is usually described by five parameters: curvature κ, cross-level *cl*, elevation *h*, gauge *G*, and rail inclination β. The first three are functions of track coordinate, while gauge and rail inclination are usually constant throughout the track. Figure 7 depicts the curvature, cross-level, and elevation of two track sections used in this work. One track section belongs to the Quatre Camins – Santa Coloma de Cervelló line, on the outskirts of Barcelona, in general characterized by longer straight track sections. The second track section belongs to the Manresa – Súria line, located in a mountainous area, and characterized by a large number of medium and small radius curves. Figure 8 illustrates the gauge, rail inclination, and cross-level for cross-section. Track irregularities are deviations from the track nominal geometry described as function of track coordinate. The longitudinal level and alignment are respectively the vertical and lateral misalignment of the track, and the cross-level variation and gauge variation are the difference between measured and ideal values of both rails. Figure 9 depicts the track irregularities of the track section in Figure 7. For rail vehicle simulations, the nominal geometry and track irregularities were pre-processed and superimposed to obtain the position and direction of the rails [8,9].

5.3. Verification process in the context of LOCATE

This section aims at a comparison of the measured and simulated quantities to verify the computational model of the locomotive. The measured quantities are firstly described and followed by a preliminary assessment of the impact of coupled wagons in the simulations results of the locomotive. Then, a verification process is proposed and applied to evaluate the computational model of the locomotive.

5.3.1. Measured Quantities

To verify and compare the computational model with the real locomotive it requires a comparison between the measured and simulated quantities. The measured quantities for comparison are described in Figure 10, whose selection is explained in LOCATE Deliverable D3.2. The setup includes one inertial measurement unit (IMU), one unidirectional accelerometer and one displacement sensor. In total, the quantities consist of two angular velocities, three accelerations and one displacement. Other quantities were obtained in the preliminary campaign, however the selected quantities are the most suitable for the verification of the computational multibody model.

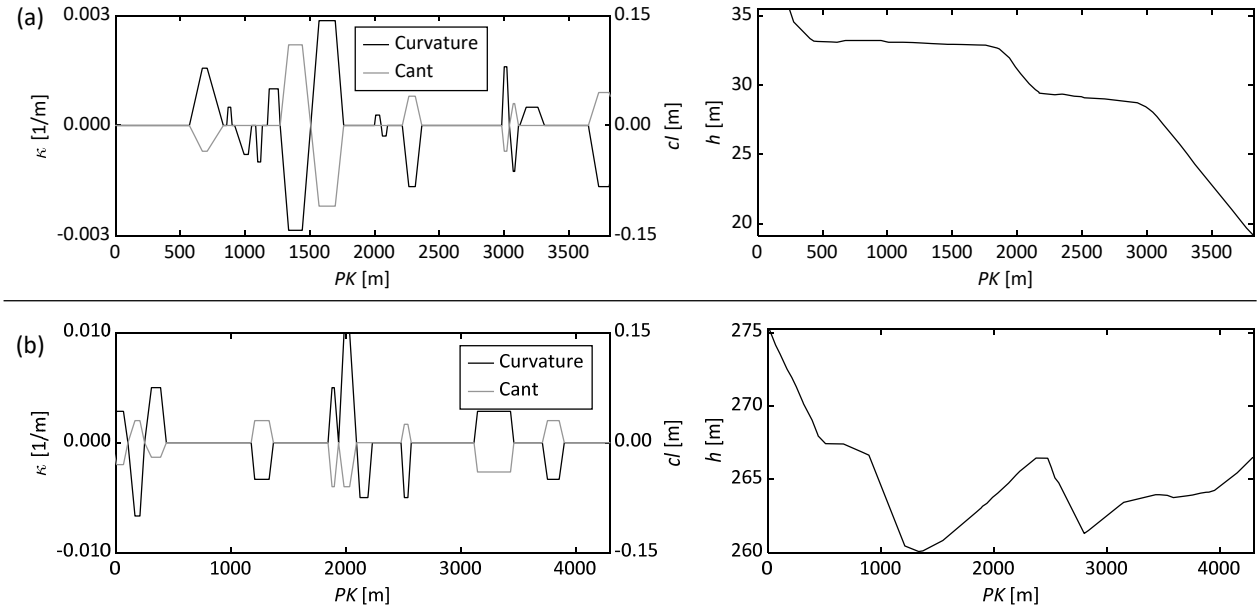

Figure 7 – Curvature, cross-level, and elevation of the (a) QC-CL and (b) MA-SU sections.

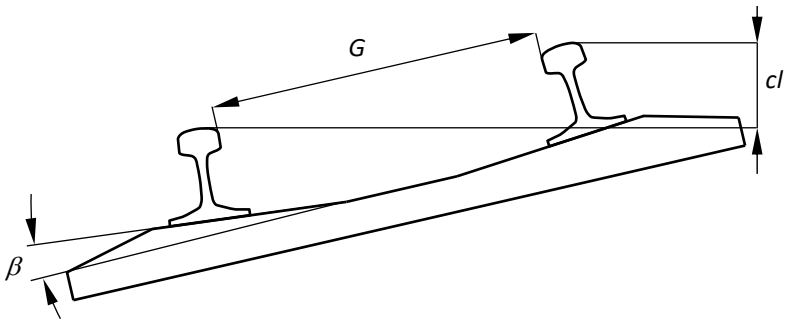

Figure 8 – Gauge, rail inclination, and cross-level.

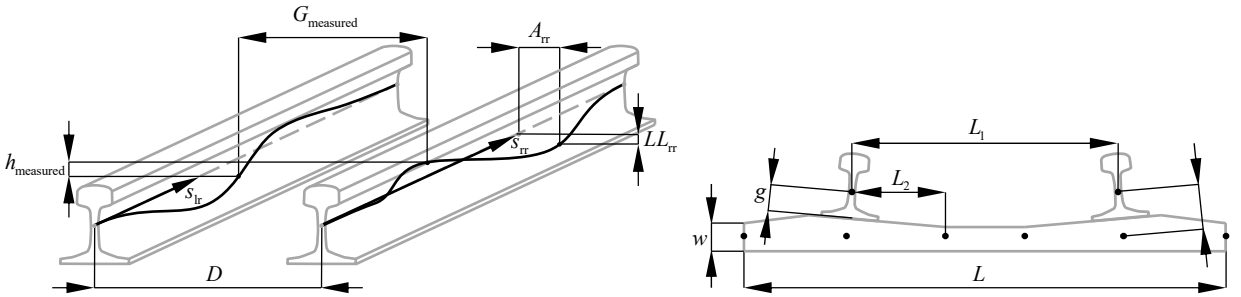

Figure 9 – Longitudinal level, alignment, cross-level variation, and gauge variation of the QC-CL section.

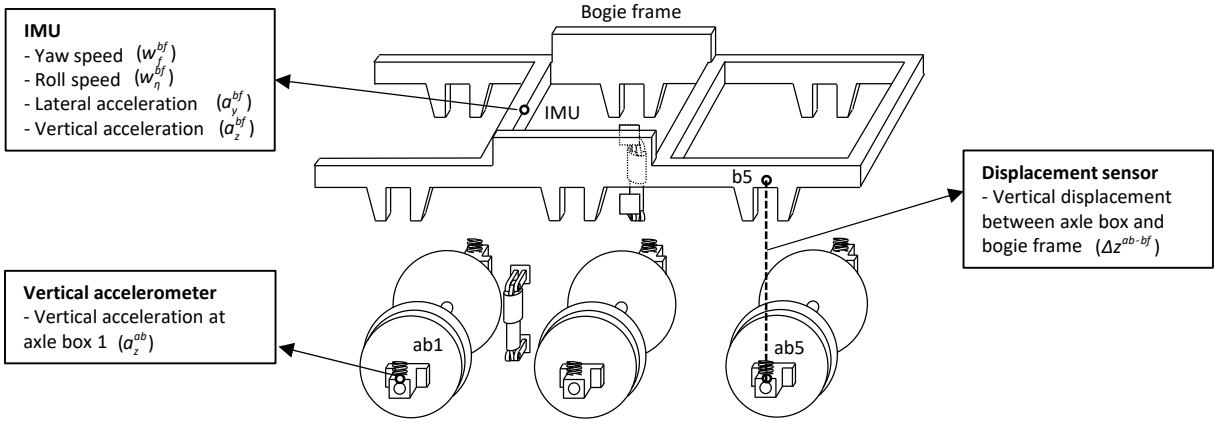

Figure 10 – Quantities for comparison between on-track measurements and simulation results.

5.3.2. Wagons Impact on Locomotive Dynamics

This section evaluates the impact of coupled wagons on the dynamics of the locomotive bogie to understand the necessity for considering them in the simulations. Two simulations of the locomotive running alone and coupled to two trailing wagons are developed. The simulation conditions represent those obtained in the preliminary measurement campaign, where the vehicle runs at a variable speed in the track segment Manresa-Suria. The lateral and vertical accelerations measured at the bogie frame, depicted in Figure 11, indicate a smaller impact of the coupled wagons in the curves, in contrast to a more significant impact in the straight sections. In addition, the lateral accelerations are more affected by the coupled wagons than the vertical accelerations. Nevertheless, the impact of the coupled wagons in the locomotive bogie dynamics is considered small and the inclusion of the wagons increases the amount of uncertainty. Therefore, the simulations used for the locomotive verification and further analysis of the locomotive in abnormal conditions only consider the locomotive running alone. This allows a reduction of the computational effort and avoids considering the complex effects of the longitudinal train dynamics [10].

5.3.3. Verification Strategy

The current standards include strategies for the validation of computational models of railway vehicles for vehicle acceptance [11], however, the framework of these strategies differ from the aim of the LOCATE project. Therefore, the measurement system and operation conditions are not the same. The requirement of measurements at specific points in the vehicle at specific track sections and at approximately constant speeds is not met in LOCATE. Hence, an adapted method for the verification of the computational model is defined to meet the project aims. The proposed methodology is based on the strategy presented in the standard, consisting in the comparison between statistical quantities of the measured and simulated signals in track sections with constant curvature and cant. The proposed method is described in Table 3. The quantities are selected according to those available data from the measurement campaign. The filtering of the signals is based on the standard [11]. No limits values are defined since these are not regarded in the standard. Therefore, the proposed strategy allows a verification by evaluation of the quantities rather than a validation by comparison to limit values.

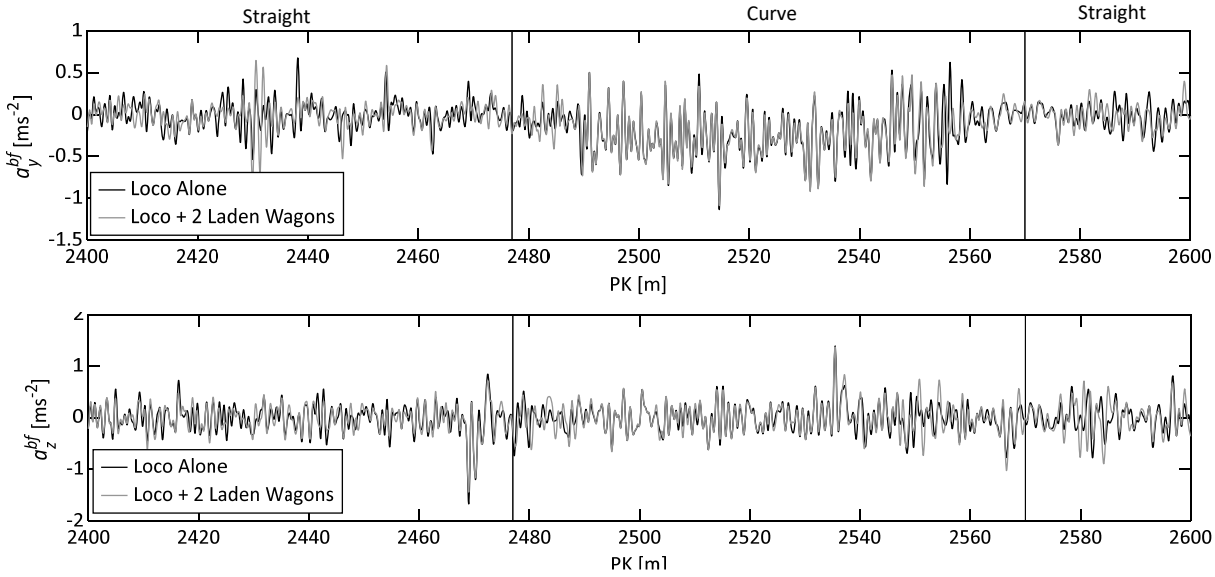

Figure 11 – Simulation results for lateral and vertical accelerations measured at the bogie frame for the locomotive running alone and with two coupled wagons.

5.3.4. Verification Results of Locomotive Model

The verification of the locomotive model consists in the comparison of the measured and simulated quantities when the locomotive is running at variable speeds in two specific track segments: Manresa – Suria and Quatre Camins – Santa Coloma Cervello. The track segments are approximately 2 km long, with curves and straight sections with variable radius and lengths. The signals are evaluated in different sections with constant radius, as suggested in the standard [11]. At each section the signals are filtered and processed according to Table 3 to obtain the maximum and average values. Table 4 describes the characteristics from the sections selected from each track segment. In total, 10 straight sections and 10 curves are considered.

Table 3 – Quantities for model verification with respect to on-track test in the context of LOCATE.

Quantity	Notation	Unit	Filtering	Processing	Definition of Sv, Mv	Differences
Bogie frame lateral acc. maximum	$a^{bf}_{y,\max}$	m/s^2	Low pass filter 10 Hz	0.15/99.85 % - value	Sv, Mv = $\lvert a^{bf}_{y,\max} \rvert$	Dv = (Sv-Mv) *Mv/|Mv|
Bogie frame vertical acc maximum	$a^{bf}_{z,\max}$	m/s^2	Low pass filter 10 Hz	0.15/99.85 % - value	Sv, Mv = $\lvert a^{bf}_{z,\max} \rvert$	
Axlebox vertical acc maximum	$a^{ab}_{z,\max}$	m/s^2	Low pass filter 20 Hz	0.15/99.85 % - value	Sv, Mv = $\lvert a^{ab}_{z,\max} \rvert$	
Displ axle-box to bogie frame, avg	$\Delta z^{ab-bf}_{\max}$	m	Low pass filter 0.1Hz to 4Hz	50% value	Sv, Mv = $\lvert \Delta z^{ab-bf}_{\max} \rvert$	
Roll angle of bogie frame, average	$w^{bf}_{\eta,avg}$	º/s	Low pass filter 0.1Hz to 4Hz	50% value	Sv, Mv = $\lvert w^{bf}_{\eta,avg} \rvert$	
Yaw angle of bogie frame, average	$w^{bf}_{\phi,avg}$	º/s	Low pass filter 0.1Hz to 4Hz	50% value	Sv, Mv = $\lvert w^{bf}_{\phi,avg} \rvert$	

Table 4 – Description of track sections used for the model verification.

Segment: Manresa - Súria				
Section	Type	Radius [m]	Cant [m]	Length [m]
1	Curve	350	0.03	40
2	Curve	150	0.03	25
3	Curve	200	0.02	60
4	Straight	-	-	100
5	Straight	-	-	100
6	Straight	-	-	100
7	Curve	300	0.03	100
8	Straight	-	-	100
9	Straight	-	-	100
10	Curve	100	0.06	30

Segment: Quatre Camins - Santa Coloma Cerveló				
Section	Type	Radius [m]	Cant [m]	Length [m]
1	Straight	-	-	100
2	Straight	-	-	100
3	Curve	640	0.035	20
4	Curve	1267	0.0	20
5	Curve	1002	0.0	50
6	Curve	350	0.110	85
7	Curve	350	0.110	85
8	Straight	-	-	100
9	Straight	-	-	80
10	Straight	-	-	50

The verification results are shown in Figure 12 to Figure 17 and include the time-domain signals for each quantity, with the track section highlighted in grey, filtered according to Table 3. The average and maximum values for both measurements and simulations at each section are also shown. In addition, the differences (D_v) between measurements and simulations are represented by bar plots together with the mean and standard deviation. The comparison of the measured and simulated time signals shows a good match for most of the quantities. Similarly, the mean and the standard deviation of the quantities at the specific track sections indicates that the measurements and simulations are often similar. The uncertainties regarding the exact wheel profile, the track irregularities, and the clearances at the suspension elements during the measurement campaign are unknown. Additionally, the evaluation of a friction damped vehicle for the purpose of a computational validation is considerably difficult as described in [12,13]. Finally, the coupling of the locomotive to trailing wagons and the measurement of operation at variable speed are other sources of uncertainties causing modelling difficulties. With the available data and consideration of

the realistic and detailed modelling of the vehicle and track, the results suggest a reasonable proximity between the simulations and the measured data.

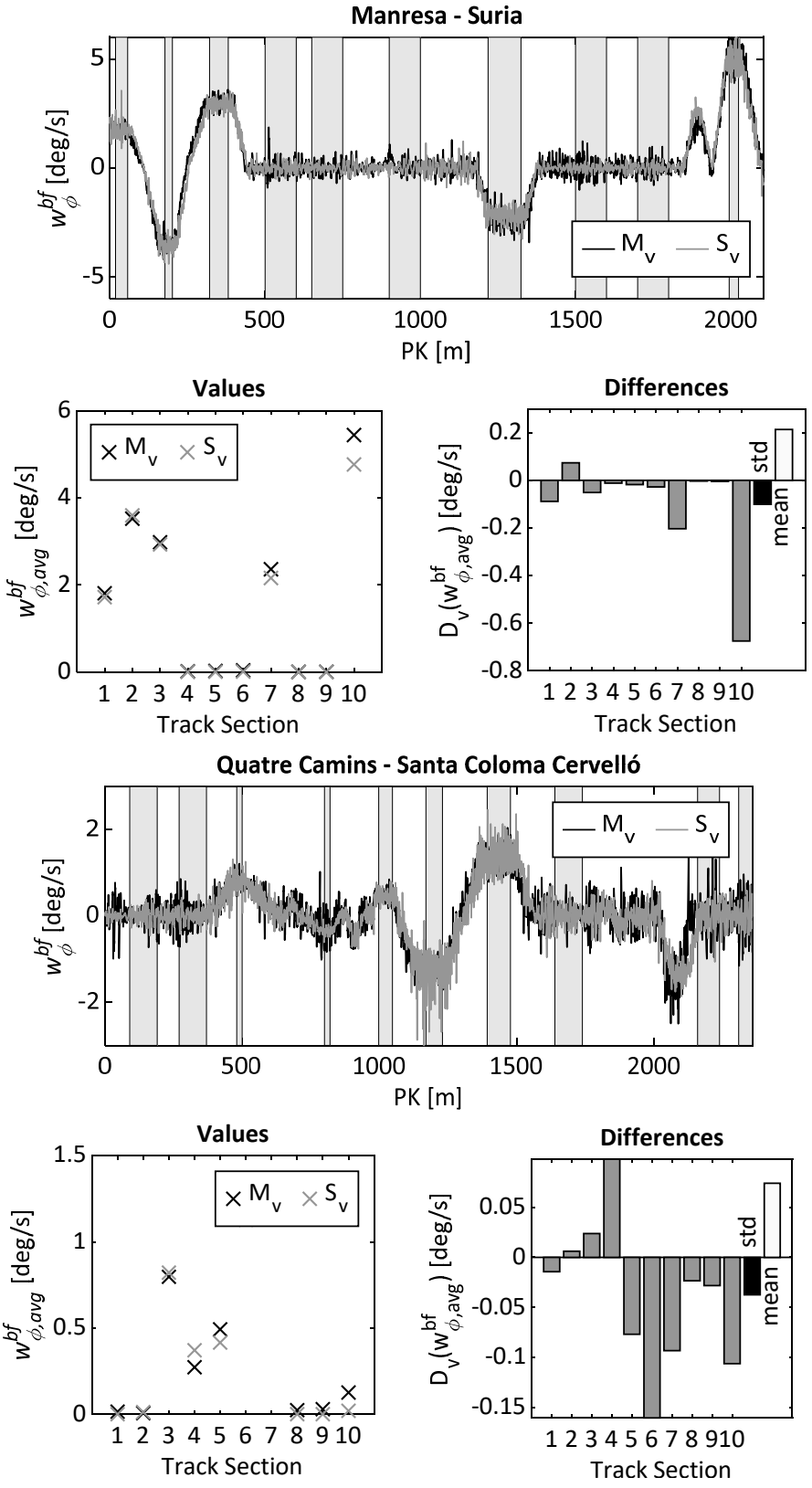

Figure 12 – Verification results: yaw speed of the bogie frame.

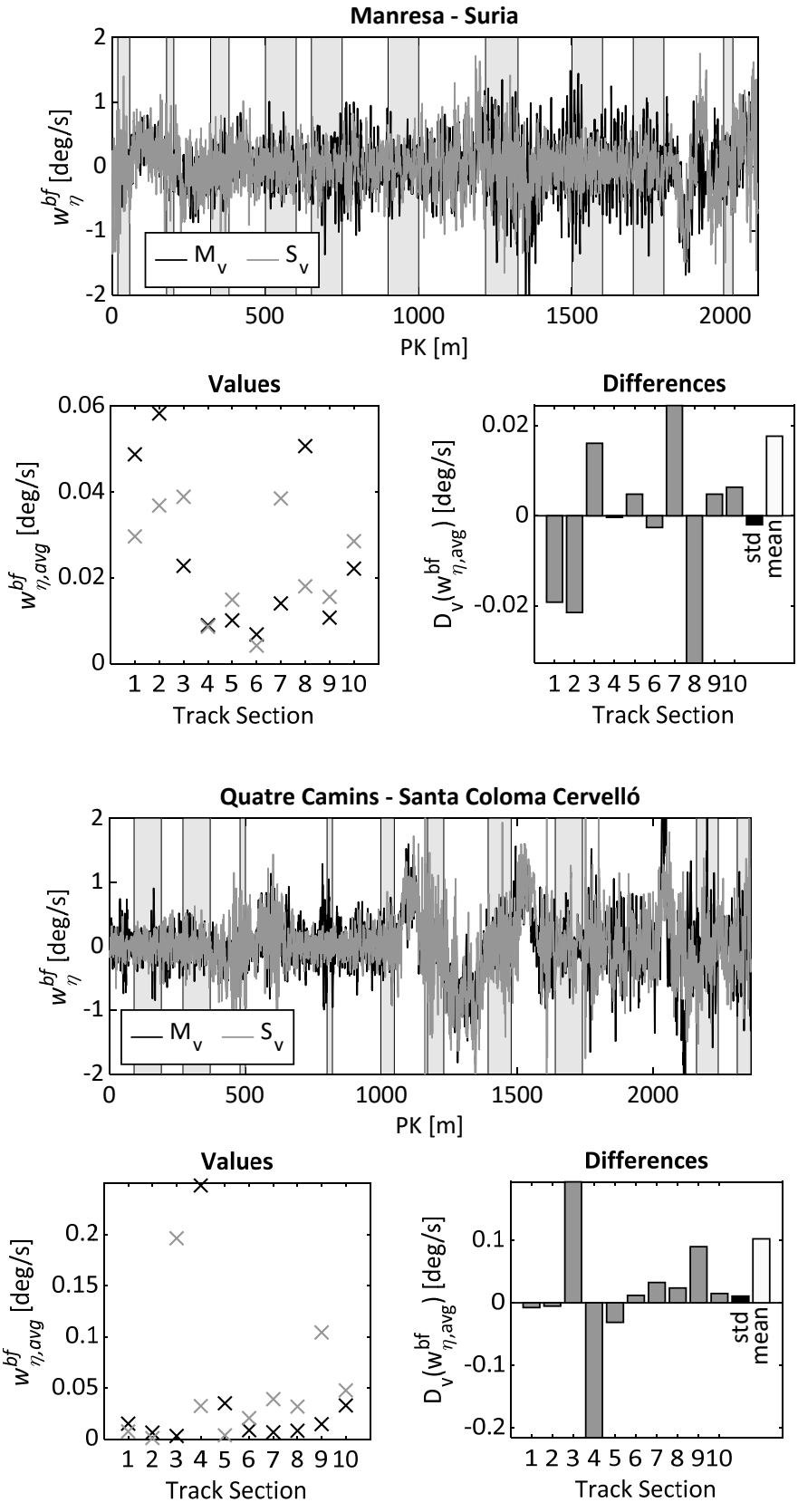

Figure 13 – Verification results: roll speed of the bogie frame.

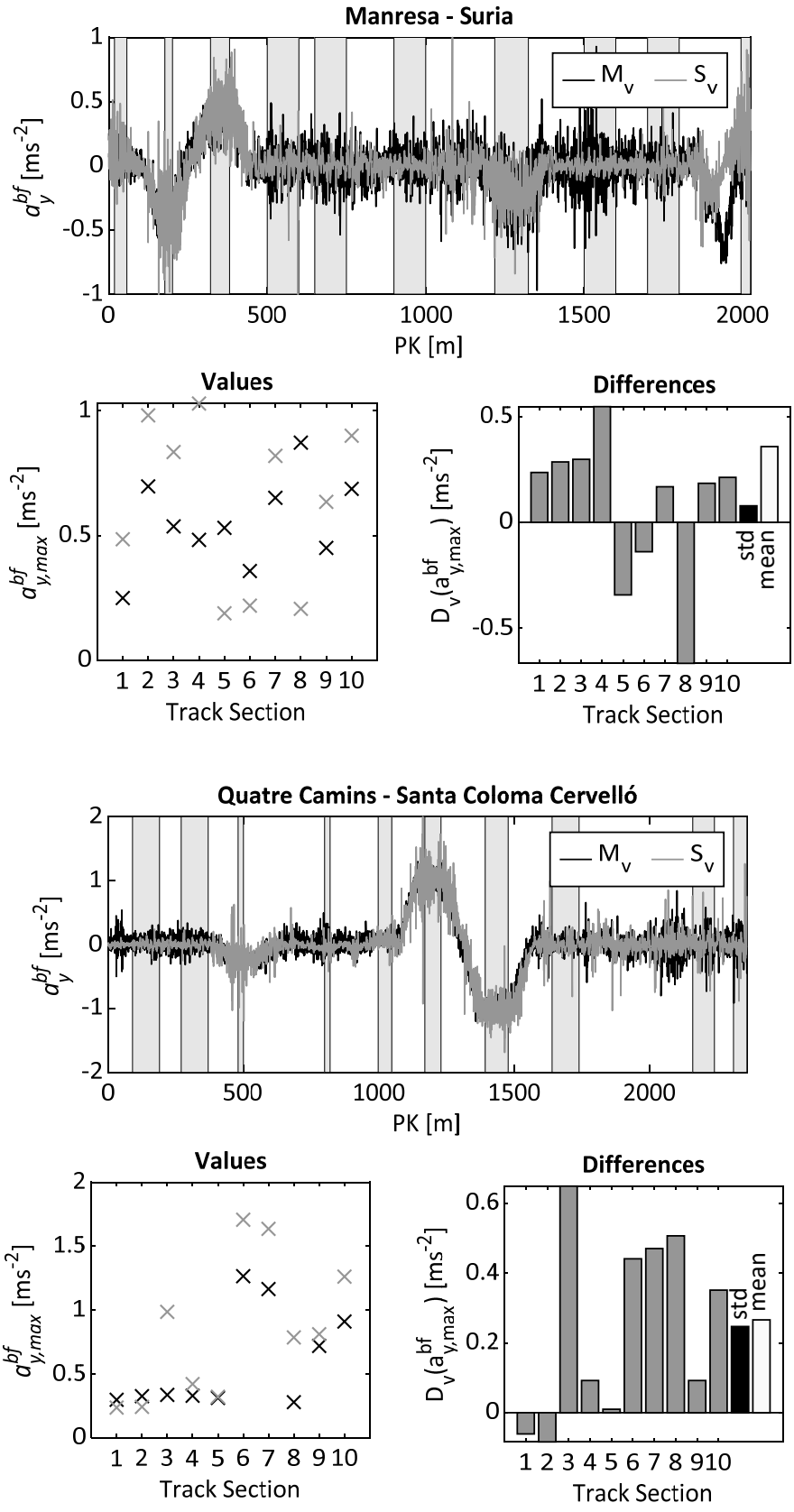

Figure 14 – Verification results: lateral acceleration of the bogie frame.

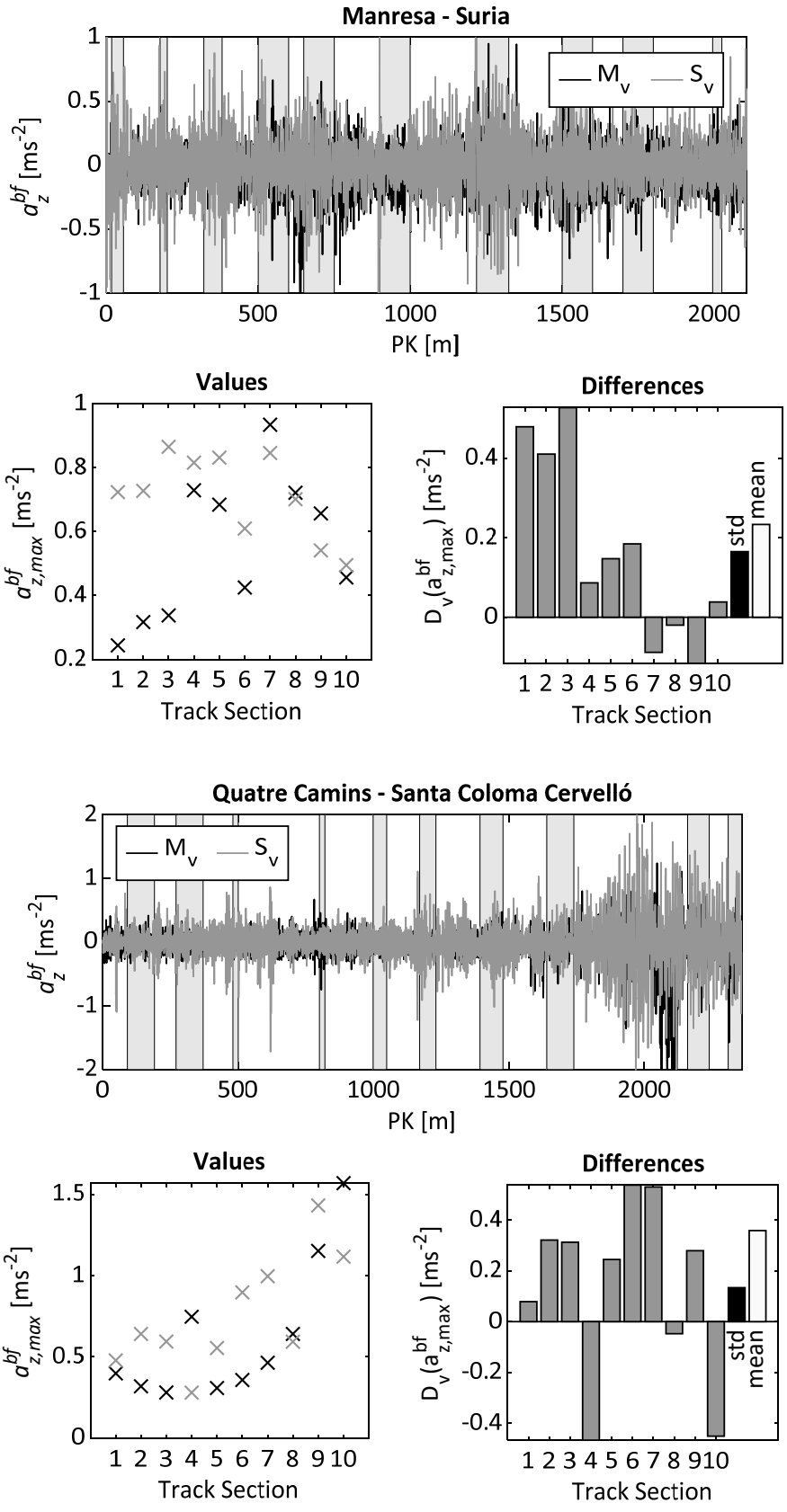

Figure 15 – Verification results: vertical acceleration of the bogie frame.

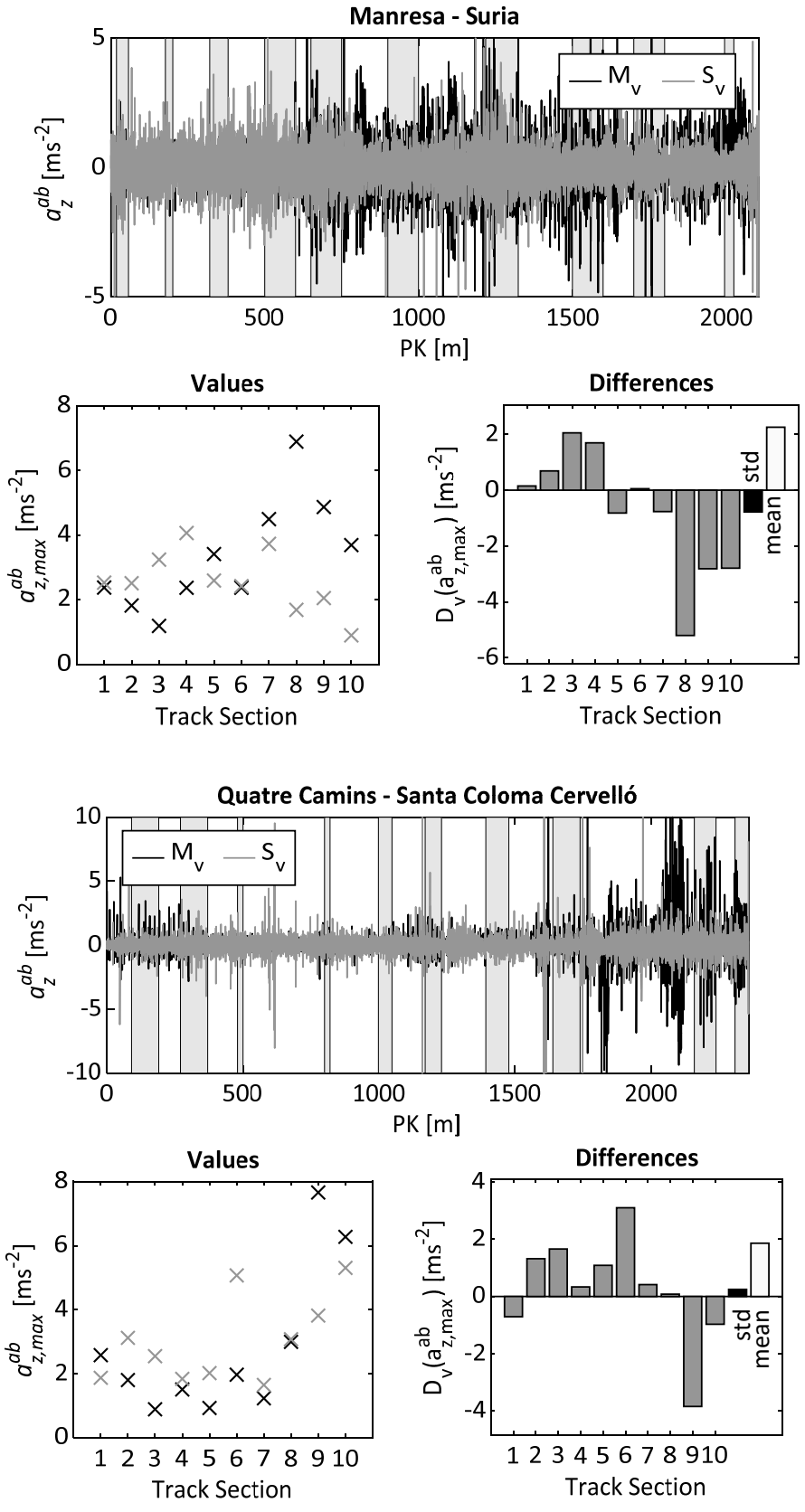

Figure 16 – Verification results: vertical acceleration of the axle box.

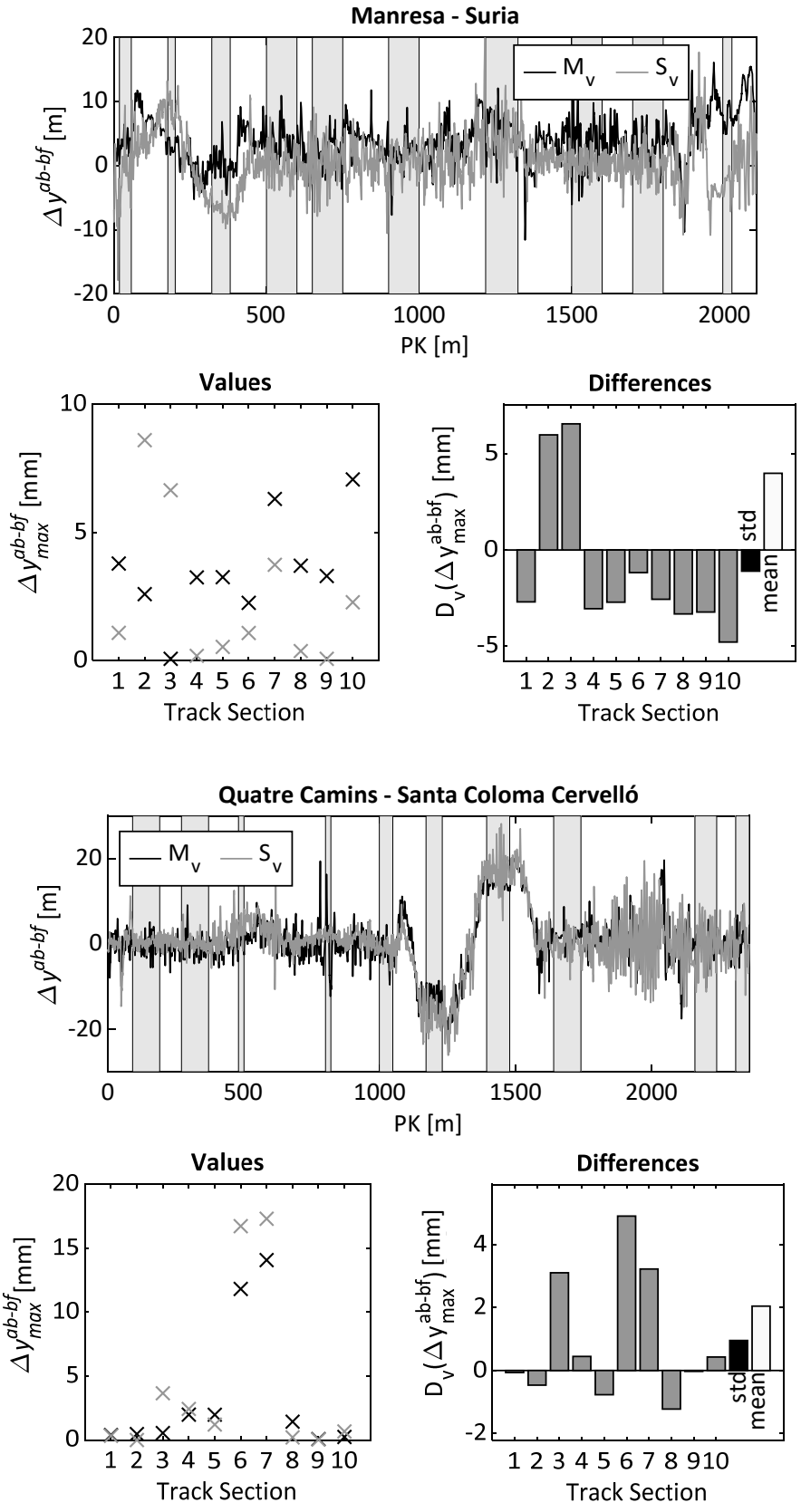

Figure 17 – Verification results: vertical displacement between the axle box and bogie frame.

6. Methods

6.1. Multibody Formulation

The dynamic analysis of a multibody system involves the study of its motion and the internal and external forces developed during a certain time period. A general multibody model is defined as a collection of rigid bodies interconnected by kinematic joints and force elements. The kinematic joints constrain the relative motion between the bodies, while the force elements represent the internal forces that develop between the bodies due to their relative motion. External forces may also be applied to the system components, as a consequence of their interaction with the surrounding environment, such as those developed in imperfect kinematic joints or due to the wheel-rail contact. Both internal and external forces are described by using suitable constitutive relations between kinematic quantities. The multibody simulation algorithm is represented in Figure 18, and follows the sequence: (*i*) set the initial time $\mathbf{t}_0$, positions of bodies $\mathbf{q}_0^{\#}$, and velocities $\dot{\mathbf{q}}$ of the multibody model; (*ii*) assemble the mass matrix $\mathbf{M}$, the Jacobian matrix associated with the constraint equations $\mathbf{\Phi}_q$, the force vector $\mathbf{g}$, and the vector of the right-hand side of the acceleration constraint equations $\mathbf{Y}$; (*iii*) solve the equations of motion to determine the vectors of the accelerations $\ddot{\mathbf{q}}$ and Lagrange multipliers $\boldsymbol{\lambda}$; (*iv*) determine the auxiliary vector $\dot{\mathbf{h}}_t = \begin{bmatrix}\dot{\mathbf{q}} & \ddot{\mathbf{q}}\end{bmatrix}_t^T$; (*v*) integrate vector $\dot{\mathbf{h}}_t$ to obtain $\mathbf{h}_{t+\Delta t} = \begin{bmatrix}\mathbf{q} & \dot{\mathbf{q}}\end{bmatrix}_{t+\Delta t}^T$; (*vi*) update time step $t = t + \Delta t$; (*vii*) stop simulation if $t > t_{end}$, otherwise go to step (*ii*).

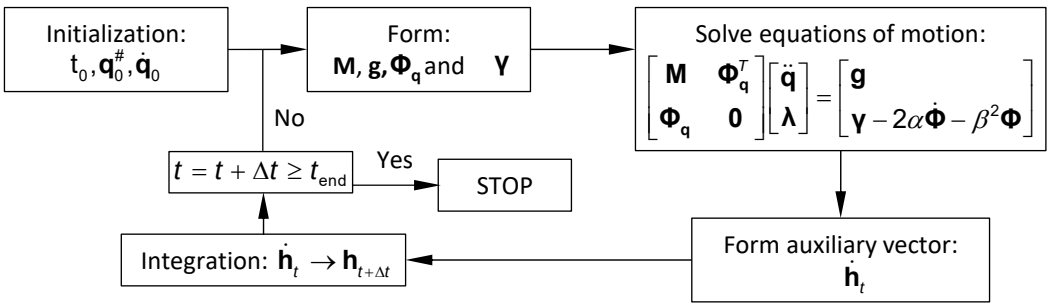

Figure 18 – Direct integration algorithm to develop the multibody simulation.

In the equations of motion, shown in Figure 18, $\mathbf{\Phi}$ is the vector of the kinematic constraint equations, $\dot{\mathbf{\Phi}}$ is the first time derivative of the constraint equations and α and β are the parameters of the Baumgarte stabilization method [14]. The time integration of the vector $\dot{\mathbf{h}}_t$ is performed using the Gear algorithm [15], which is a time integration method with variable time step and variable order. In this work Cartesian coordinates and Euler parameters describe the position and orientation of the bodies.

The bodies of the locomotive model considered in this work are interconnected by force elements, perfect kinematic joints, and imperfect kinematic joints. The force elements contribute to the force vector $\mathbf{g}$ by developing forces due to the relative motion between the bodies. Perfect kinematic joints [16], on the other hand, are defined by algebraic equations, expressed in terms of the coordinates of the connected bodies, that contribute to the Jacobian matrix $\mathbf{\Phi}_q$ and to the acceleration equation right-hand-side vectors $\mathbf{Y}$. Imperfect kinematic joints impose the kinematic

constraints through sets of contact forces due to the contact between the bodies on selected surfaces, contributing to force vector $\mathbf{g}$.

The multibody formulation can be extended to include the structural flexibility of the bodies, which is described using nodal deformations **u**' [17]. The full system of equations of motion is expressed by:

$$\begin{bmatrix} \mathbf{M}_r & \mathbf{M}_{rf} & \mathbf{\Phi}_{\mathbf{q}r}^T \\ \mathbf{M}_{fr} & \mathbf{M}_{ff} & \mathbf{\Phi}_{\mathbf{q}f}^T \\ \mathbf{\Phi}_{\mathbf{q}r} & \mathbf{\Phi}_{\mathbf{q}f} & \mathbf{0} \end{bmatrix} \begin{Bmatrix} \ddot{\mathbf{q}}_r \\ \ddot{\mathbf{u}}' \\ \boldsymbol{\lambda} \end{Bmatrix} = \begin{Bmatrix} \mathbf{g}_r \\ \mathbf{g}_f \\ \boldsymbol{\gamma} \end{Bmatrix} - \begin{Bmatrix} \mathbf{s}_r \\ \mathbf{s}_f \\ \mathbf{0} \end{Bmatrix} - \begin{bmatrix} \mathbf{0} & \mathbf{0} & \mathbf{0} \\ \mathbf{0} & \mathbf{K}_{ff} & \mathbf{0} \\ \mathbf{0} & \mathbf{0} & \mathbf{0} \end{bmatrix} \begin{Bmatrix} \mathbf{0} \\ \mathbf{u}' \\ \mathbf{0} \end{Bmatrix} \tag{1}$$

where $\mathbf{M}_{ff}$ is the lumped mass matrix of the flexible body and $\mathbf{M}_{rf}$ is the matrix of the coupling terms between the rigid and flexible motions. $\mathbf{s}_r$ and $\mathbf{s}_f$ constitute the rigid and flexible components of the vector of quadratic velocity terms. $\mathbf{K}_{ff}$ is the standard stiffness matrix, which can be obtained from any available finite element software. The reference conditions that ensure the uniqueness of the flexible displacement field are the mean axis conditions [18]. If the number of nodal coordinates is too large, the mode component synthesis can be used to reduce the problem dimension, under the assumption of small and linear elastic deformations. In these conditions, the nodal displacements, velocities, and accelerations can be expressed using the matrix of modes of vibration **X**, according to:

$$\begin{aligned} \mathbf{u}' &= \mathbf{X}\mathbf{w} \\ \dot{\mathbf{u}}' &= \mathbf{X}\dot{\mathbf{w}} \\ \ddot{\mathbf{u}}' &= \mathbf{X}\ddot{\mathbf{w}} \end{aligned} \tag{2}$$

where **w** is the vector of modal coordinates, that replace the nodal coordinates **u**'. The dimensions of vector **w** are equal to the number of modes of vibration considered in the modal matrix **X**. The orthonormality conditions of the mass and stiffness matrix are:

$$\begin{aligned} \mathbf{X}^T\mathbf{M}_{ff}\mathbf{X} &= \mathbf{I} \\ \mathbf{X}^T\mathbf{K}_{ff}\mathbf{X} &= \mathbf{\Lambda} \end{aligned} \tag{3}$$

where $\mathbf{\Lambda}$ is a vector of the squares of the natural frequencies associated with the modal matrix **X**. Consequently, the equations of motion undergo a transformation from Cartesian to modal coordinates:

$$\begin{bmatrix} \mathbf{M}_r & \mathbf{M}_{rf}\mathbf{X} & \mathbf{\Phi}_{\mathbf{q}_r}^T \\ \mathbf{X}^T\mathbf{M}_{fr} & \mathbf{I} & \mathbf{X}^T\mathbf{\Phi}_{\mathbf{q}_f}^T \\ \mathbf{\Phi}_{\mathbf{q}_r} & \mathbf{\Phi}_{\mathbf{q}_f}\mathbf{X} & \mathbf{0} \end{bmatrix} \begin{Bmatrix} \mathbf{q}_r \\ \mathbf{X}^T\ddot{\mathbf{u}}' \\ \boldsymbol{\lambda} \end{Bmatrix} = \begin{Bmatrix} \mathbf{g}_r \\ \mathbf{X}^T\mathbf{g}_f \\ \boldsymbol{\gamma} \end{Bmatrix} - \begin{Bmatrix} \mathbf{s}_r \\ \mathbf{X}^T\mathbf{s}_f \\ \boldsymbol{\gamma} \end{Bmatrix} - \begin{Bmatrix} \mathbf{0} \\ \mathbf{\Lambda}\mathbf{w} \\ \mathbf{0} \end{Bmatrix} \tag{4}$$

The flexible formulation is complemented by the use of the virtual bodies methodology, that allows the functional connection between the rigid and flexible bodies using kinematic joints and force elements [19,20].

In this work, the general purpose multibody software MUBODyn [21] is used, which includes modelling features such as wheel-rail contact [22], allowing the study of railway dynamics. It also includes a large collection of kinematic joints, force elements, imperfect kinematic joints, and a library of normal and friction contact force models. MUBODyn also comprises a flexible multibody dynamics package.

6.2. Transmissibility

The concept of transmissibility is commonly defined, for single degree-of-freedom systems and assuming harmonic motion, as the ratio between the amplitude of the response and the amplitude of the imposed motion. This concept can also be extended to systems with multiple degrees of freedom, including those that are used to represent continuum structures using a process of discretisation. Figure 19 illustrates a system with multiple degrees of freedom characterised by a vector of amplitudes of harmonic forces $\mathbf{F}_A$ applied on a subset of points A, the vector of amplitudes of the responses $\mathbf{X}_U$ on a subset of points U, and a vector of amplitudes of the responses $\mathbf{X}_K$ on a subset of points K.

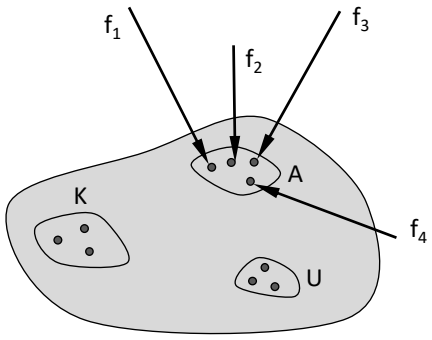

Figure 19 – System with subsets A, K and U.

The responses $\mathbf{X}_U$ and $\mathbf{X}_K$ are related with the forces through the receptance matrices $\mathbf{H}_{UA}$ and $\mathbf{H}_{KA}$ according to the expressions:

$$\begin{aligned} \mathbf{X}_U &= \mathbf{H}_{UA}\mathbf{F}_A \\ \mathbf{X}_K &= \mathbf{H}_{KA}\mathbf{F}_A \end{aligned} \tag{5}$$

The two equations can be related by eliminating $\mathbf{F}_A$, as in:

$$\mathbf{X}_U = \mathbf{H}_{UA}\mathbf{H}_{KA}^{-1}\mathbf{X}_K = \mathbf{T}_{UK}\mathbf{X}_K \tag{6}$$

where $\mathbf{T}_{UK}$ is the transmissibility matrix, which establishes the relationship between the response vectors $\mathbf{X}_U$ and $\mathbf{X}_K$. The invertibility of $\mathbf{H}_{KA}$ in Eq. (6) requires that the number of points in subset A equals the number of points in subset K. If the number of points in subset K exceeds the number of points in subset A, the pseudo-inverse matrix $\mathbf{H}_{KA}^{+}$ must be used. Eq. (6) shows that the transmissibility matrix $\mathbf{T}_{UK}$ does not depend on the amplitudes of the forces, and for this reason the entries of the matrix are called global transmissibilities. However, it is also possible to directly divide the magnitudes of the responses on any two points to define local transmissibilities, which are scalar entities. For example, dividing two known scalar amplitudes X_r and X_s, renders:

$$\tau_{rs} = T_{rs} = \frac{X_r}{X_s} \tag{7}$$

where τ_{rs}, or T_{rs}, is a scalar quantity, and r and s are indices that identify the measured points of the structure. Even though the above expressions concerning the transmissibilities are deduced assuming harmonic loading and motion, it can be shown that they are also valid for other types of loading, such as random excitation [23].

6.2.1. Transmissibility Damage Indicator

The concept of transmissibility raises an opportunity for condition monitoring through the assessment of changes in the response of the structure. The Transmissibility Damage Indicator (TDI) is an approach developed to detect and quantify structural damage, proposed by Maia et al. [24]. The development of TDI is inspired by the Response Vector Assurance Criterion (RVAC), defined by Heylen et al. [25] as the correlation between the frequency response functions of the undamaged and damaged structures for a given frequency. One relevant feature of TDI is that is does not require a previous modal identification of the structures, nor the knowledge of the forces involved, depending only on the measured response of the structure. The transmissibility can be evaluated in the frequency domain using the power spectral density (PSD) of the response. Also, the transmissibility curves do not reflect the maxima and minima of the FRFs, hinting they have a local nature that suggests their significance to detect damage.

The rationale of the TDI is that when a structure is damaged, there are changes in the transmissibilities of the system. Matrix $\mathbf{T}^n(\omega)$ is defined by the local transmissibilities between all the N measured points of the structure in nominal condition, as a function of the frequency ω, according to:

$$\mathbf{T}^n(\omega)=\begin{bmatrix} \tau_{11}^n(\omega) & \tau_{12}^n(\omega) & \cdots & \tau_{1N}^n(\omega) \\ \tau_{21}^n(\omega) & \tau_{22}^n(\omega) & \cdots & \tau_{2N}^n(\omega) \\ \vdots & \vdots & \ddots & \vdots \\ \tau_{N1}^n(\omega) & \tau_{N2}^n(\omega) & \cdots & \tau_{NN}^n(\omega) \end{bmatrix} \tag{8}$$

Likewise, matrix $\mathbf{T}^d(\omega)$ expresses the local transmissibilities of the structure in the unknown condition. For the sake of simplicity, hereafter $\mathbf{T}^d(\omega)$ is called the transmissibility matrix of the structure in the damaged condition. The Response Vector Assurance Criterion (RVAC) [24] defines, for each frequency, the correlation between the values of the local transmissibilities of the undamaged and damaged structures. The RVAC is originally defined considering a sequential progression over the points of the structure and is expressed by:

$$RVAC(\omega)=\frac{\left|\sum_{r=1}^{N-1}\tau_{rs}^n(\omega)\tau_{rs}^d(\omega)\right|^2}{\sum_{r=1}^{N-1}\left(\tau_{rs}^n(\omega)\tau_{rs}^n(\omega)\right)\sum_{r=1}^{N-1}\left(\tau_{rs}^d(\omega)\tau_{rs}^d(\omega)\right)} \quad , \quad s=r+1 \tag{9}$$

Assuming the forces are always applied in the same locations, the TDI is a normalisation of the contributions of RVAC over N_ω frequencies of interest, as in:

$$TDI=\frac{1}{N_\omega}\sum_{\omega}\frac{\left|\sum_{r=1}^{N-1}\tau_{rs}^n(\omega)\tau_{rs}^d(\omega)\right|^2}{\sum_{r=1}^{N-1}\left(\tau_{rs}^n(\omega)\tau_{rs}^n(\omega)\right)\sum_{r=1}^{N-1}\left(\tau_{rs}^d(\omega)\tau_{rs}^d(\omega)\right)} \quad , \quad s=r+1 \tag{10}$$

TDI is valued between 0 and 1, and values close to unit indicate there is a strong correlation between the nominal condition and the measured response, suggesting the structure is healthy. Lower values of TDI suggest the structure is damaged.

The geometry of the structures analysed in the framework of LOCATE is intricate, and this motivated the development of alternative expressions for TDI, based on the original formulation of TDI. These expressions concern with how the transmissibilities of the different measured points of the structure are correlated. The sequential scheme presented in the original formulation is:

$$s=r+1 \tag{11}$$

meaning the transmissibilities are evaluated in successive pairs of points in terms of the indices

that identify them. In terms of the transmissibility matrices, this means relating all the entries of the upper diagonal. One first alternative, named symmetric scheme, is defined considering the transmissibilities of all the measured points in the structure are involved in the calculation of TDI for each frequency, defined by the expression:

$$r = 1,...,N \quad , \quad s = 1,...,N \quad , \quad r \neq s \tag{12}$$

In terms of the transmissibility matrices, this means relating all the entries of the matrices, except the entries in the main diagonal. A second alternative, named non-symmetric scheme, involves considering only the entries of the upper triangles of the transmissibility matrices, excluding the entries in the main diagonal, according to:

$$r = 1,...,(N-1) \quad , \quad s = (r+1),...,N \tag{13}$$

These three approaches provide different results in terms of the values of TDI.

The use of the TDI method to assess the condition of structures relies on the processing of the response according to the methodology depicted in Figure 20. The signals in the time domain, in general accelerations, velocities, or displacements, obtained either through dynamic simulations or experimental testing, are transformed to the frequency domain through the computation of the PSDs of those signals. The PSDs of the structure in nominal condition, that represent the nominal response, are combined to define the nominal transmissibility matrix $\mathbf{T}^n(\omega)$, which is a three-dimensional matrix that is a function of the frequency and the indices r and s of the measured points. Conversely, the PSDs of the structure in the unknown condition to be assessed are used to define the transmissibility matrix of damaged structure $\mathbf{T}^d(\omega)$. The value of TDI is then computed by combining the entries of matrices $\mathbf{T}^n(\omega)$ and $\mathbf{T}^d(\omega)$ are combined to compute the value of TDI.

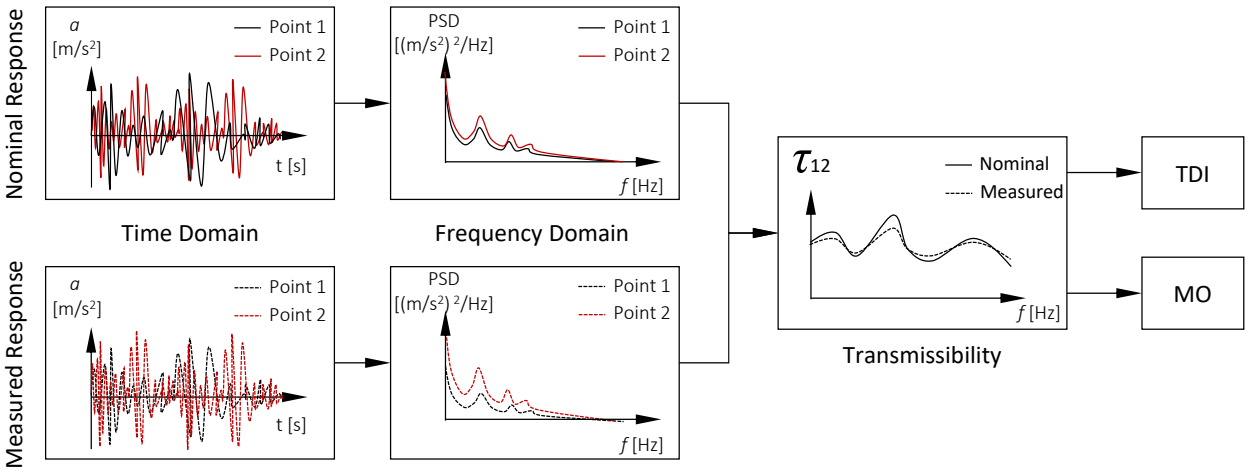

Figure 20 – Methodology for condition monitoring using the Transmissibility Damage Indicator (TDI) and Maximum Occurrences (MO) methods.

6.2.2. Maximum Occurrences

The Maximum Occurrences method, also called Frequency of Maximum Differences algorithm, is proposed by Sampaio et al. [26,27] for the localisation of damage, after proper damage detection is achieved. For each frequency, the transmissibility matrices $\mathbf{T}^n(\omega)$ and $\mathbf{T}^d(\omega)$ are used to compute the subtraction:

$$\Delta\mathbf{T} = \mathbf{T}^n(\omega) + \mathbf{T}^d(\omega) \tag{14}$$

and the coordinate pair (r,s) of the entry of $\Delta\mathbf{T}$ with the highest value is recorded as the maximum occurrence for that frequency. All the occurrences of maxima at each coordinate pair are summed according to the expression:

$$\Delta\mathbf{T}^* = \Delta\mathbf{T} + \Delta\mathbf{T}^T \tag{15}$$

and the indices of the entry of $\Delta\mathbf{T}^*$ with the highest value suggest the most probable location for damage is between the points of the pair. It is worth highlighting that the sum of the occurrences associated with each pair of points (r,s) is the sum of the contribution from both the upper and lower triangles of $\Delta\mathbf{T}$, as per Eq. (15).

6.3. Design and Analysis of Computer Experiments

The degradation of the suspension elements is studied using Design and Analysis of Computer Experiments (DACE). The vehicle dynamics are analysed using computer codes and comprehensively testing the degradation of the suspension elements becomes time-consuming due to the expensiveness of the code, the high number of simulations, or both. A DACE approach allows finding surrogate models, cheaper models that can replace the computer code. The process entails: (a) defining an input space, usually a hyperrectangle; (b) filling the input space with points, where each point is a set of inputs of the computer code; (c) evaluating the code at these points; (d) estimating a surrogate model; and (e) assessing the surrogate.

In this section, x_j represent the j^{th} input of a computer code, $\mathbf{x}_i = [x_1, x_2, \ldots, x_k]$ a k-dimensional vector comprising the inputs, and $\mathbf{X}$ an $n \times k$ design matrix organized as

$$\mathbf{X} = \begin{bmatrix} \mathbf{x}_1 \\ \vdots \\ \mathbf{x}_n \end{bmatrix}. \tag{16}$$

Moreover, $y(\mathbf{x})$ represents the output of the computer code, and $\mathbf{y}_\mathbf{x} = \left[y(\mathbf{x}_1), \ldots, y(\mathbf{x}_n)\right]^T$ is $n \times 1$ vector comprising the evaluations of the code at $\mathbf{X}$.

6.3.1. Designs

This work considers a custom design and Latin Hypercubes Designs (LHDs). An LHD is obtained by dividing the domain of each input into n cells and randomly permutating these cells. The result are n random points in the input space that, projected on a specific input, guarantee one sample per cell, i.e., the marginals of the inputs are uniform. Figure 21 (a) depicts an example of an LHD. In short, LHDs assume inputs are equally important and try to fill the input space as best as possible without repeating observations.

The custom design takes two inputs, $\mathbf{x} = \left[x_1, x_2\right]^T$, and assumes a reference value for x_2, x_{2r}.

Let x_1 be divided into n_1 cells, and n_2 be the number of x_2 points inside each cell. The custom design ensures that x_2 is sampled n_2 times in each cell, and that the sample includes x_{2r}. Figure 21(b) illustrates an example of a custom design. An intermediate step divides the input space into smaller cells to ensure a single sample per cell along x_1 (uniform marginal), and a single sample per cell along x_2, except for the reference value, which is sampled n_1 times (non-uniform marginal). The design produces $n=n_1 \times n_2$ points. The rationale behind this non-uniform sampling is that it is essential to predict x_{2r} accurately over the whole input space.

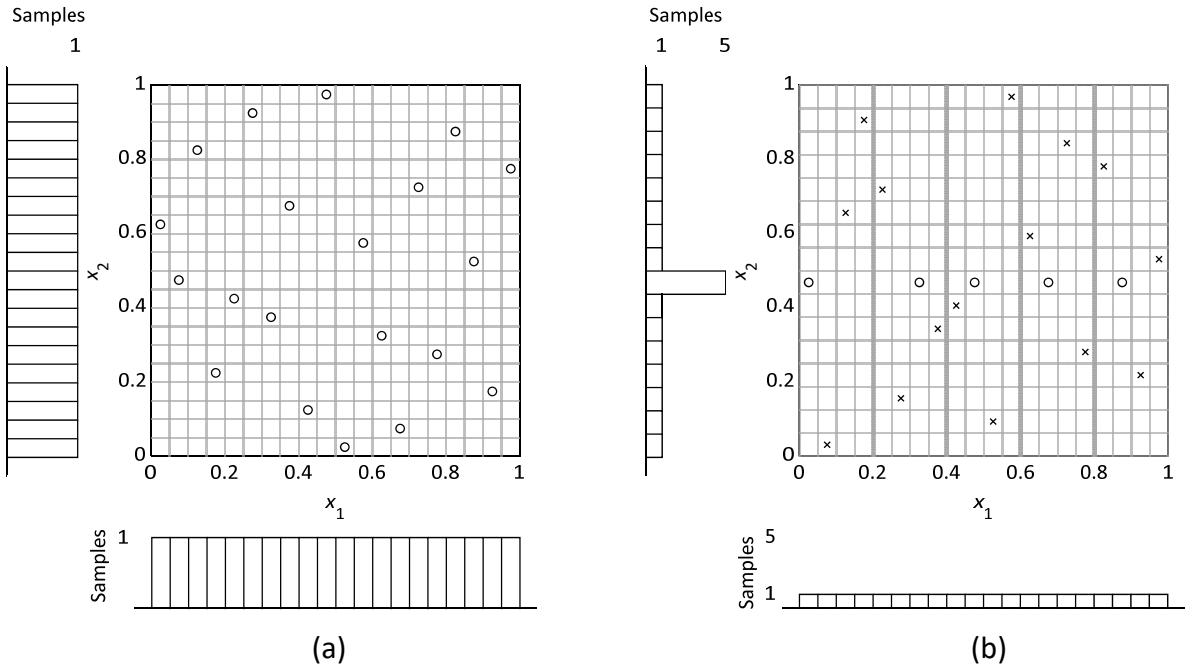

Figure 21 – (a) LHD with n=20 and (b) custom design with n_1=5, n_2=4, and x_{2r}=0.5.

6.3.2. Gaussian Process Surrogates

This work uses Gaussian Process (GP) surrogate modelling due to its flexibility to fit a broad class of response functions and capture non-linearities. If a stochastic process represents the output of the computer code as [28]

$$y(\mathbf{x}) = \mu + z(\mathbf{x}), \tag{17}$$

where μ is the overall mean and $z(\mathbf{x})$ is a zero-mean stationary Gaussian Process (GP), the best linear unbiased predictor of Eq. (17) is [28,29]:

$$\hat{y}(\mathbf{x}) = \hat{\mu} + \mathbf{r}(\mathbf{x})^T (\mathbf{R}_\mathbf{x} + g\mathbf{I})^{-1} (\mathbf{y}_\mathbf{x} - \mathbf{1}_n \hat{\mu}), \tag{18}$$

with mean squared error [28]

$$s^2(\mathbf{x}) = \hat{\sigma}^2 \left(1 + g - \mathbf{r}(\mathbf{x})^T (\mathbf{R}_\mathbf{x} + g\mathbf{I})^{-1} \mathbf{r}(\mathbf{x}) + \frac{(1 - \mathbf{1}_n^T (\mathbf{R}_\mathbf{x} + g\mathbf{I})^{-1} \mathbf{1}_n)^2}{\mathbf{1}_n^T (\mathbf{R}_\mathbf{x} + g\mathbf{I})^{-1} \mathbf{1}_n} \right). \tag{19}$$

In Eqs. (18) and (19), $\mathbf{r}(\mathbf{x}) = \left[r(\mathbf{x}, \mathbf{x}_1), \ldots, r(\mathbf{x}, \mathbf{x}_n) \right]^T$ is a n×1 vector comprising the correlations

between **x** and the design points, $\mathbf{R}_{\mathbf{x}}$ is an $n \times n$ matrix comprising the correlations between the design points as $R_{ij} = r(\mathbf{x}_i, \mathbf{x}_j)$, **I** is the $n \times n$ identity matrix, $\mathbf{1}_n$ is an $n \times 1$ vector of 1s, g is the nugget parameter, and σ^2 is the variance. The correlation function used is the separable Gaussian correlation function, which is given by [30]:

$$r(\boldsymbol{\theta}, \mathbf{x}, \mathbf{x}') = \exp\left(-\sum_{j=1}^{k} \vartheta_j \left| x_j - x_j' \right|^2 \right), \tag{20}$$

where $\vartheta_j > 0$ is the rate parameter of the j^{th} input. This correlation function is suitable to model continuous and smooth surfaces. The estimates of μ, σ^2, $\boldsymbol{\theta}$, and g are obtained using maximum likelihood estimation. μ and σ^2 have closed-form expressions given by [31]:

$$\begin{aligned} \hat{\mu} &= (\mathbf{1}_n^T (\mathbf{R}_{\mathbf{x}} + g\mathbf{I})^{-1} \mathbf{1}_n)^{-1} (\mathbf{1}_n^T (\mathbf{R}_{\mathbf{x}} + g\mathbf{I})^{-1} \mathbf{y}_{\mathbf{x}}) \\ \hat{\sigma}^2 &= \frac{(\mathbf{y} - \mathbf{1}_n \hat{\mu})^T (R_{\mathbf{x}} + g\mathbf{I})^{-1} (\mathbf{y} - \mathbf{1}_n \hat{\mu})}{n} \end{aligned}, \tag{21}$$

while $\boldsymbol{\theta}$ and g are estimated using numerical optimization because there is no analytical solution.

6.3.3. *k*-fold cross-validation

The performance of the surrogates is assessed using *k*-fold cross-validated metrics. *k*-fold cross-validation is a technique that partitions the data into *k* folds (subsets) of approximately equal size. It uses (k – 1) folds to estimate the surrogate and the remaining one for validation. The process is repeated *k* times, and each fold is used exactly once for validation. For clarity, the points in the (k – 1) folds are referred to hereafter as training set and the points in the left-out subset as the test set. The metric is calculated *k* times, one for each fold, using the true values of the test set and the predictions given by the estimated surrogates on the test set. The average of the *k* metrics provides an estimate of the metric. This work considers two metrics: the coefficient of determination, R^2, to assess fit and the Mean Absolute Percentage Error, *MAPE*, to assess error. Cross-validated metrics are evaluated using $k = 5$, a typical number of folds [32].

6.3.4. Sensitivity analysis

The sensitivity analysis used here is based on the following variance decomposition of $y(\mathbf{x})$ [31]:

$$\mathbb{V} = \sum_{j=1}^{k} \mathbb{V}_j + \sum_{i=1}^{k} \sum_{j>1}^{k} \mathbb{V}_{ij} + \ldots + \mathbb{V}_{1\ldots k}, \tag{22}$$

where

$$\begin{aligned} \mathbb{V} &= \mathbb{V}\left[y(\mathbf{x}) \right] \\ \mathbb{V}_j &= \mathbb{V}\left[\mathbb{E}\left[y \middle| x_j \right] \right] \\ \mathbb{V}_{ij} &= \mathbb{V}\left[\mathbb{E}\left[y \middle| x_i, x_j \right] \right] - \mathbb{V}_i - \mathbb{V}_j \end{aligned}, \tag{23}$$

and higher-order variances are derived recursively in a similar fashion. In Eq. (23), operators $\mathbb{V}[\,]$ and $\mathbb{E}[\,]$ denote variance and expectation. In summary, Eq. (22) decomposes the variance of $y(\mathbf{x})$ in terms attributable to the inputs and their interactions, which in turn allows defining sensitivities indices as [33]

$$S_Q = \frac{\mathbb{V}_Q}{\mathbb{V}}, \tag{24}$$

where $Q \subseteq \{1,\ldots,k\}$. Particularly interesting here are the first-order sensitivity indices, S_j, corresponding to the proportion of variance due to input x_j, and the second-order sensitivity indices, S_{ij}, corresponding to the proportion of variance due to the combined effect of inputs x_i and x_j. The sensitivity indices are evaluated using the surrogate model, $\hat{y}(\mathbf{x})$, a quasi-Monte Carlo integration [31,33,34], and Latin hypercube sampling.

6.3.5. Variance-based limits

Limits are found by exploring the response and its conditional variance in discrete subregions of the input space. Input x_1 is divided into n cells, and x_2 is divided into two cells by a reference value, x_{2r}, resulting in $2n$ cells in total. This discretization assumes variable x_2 has two different regimes, above and below x_{2r}. Assume that $x_{2low} < x_{2r}$ is a lower limit for x_2, and let $\mathbb{V}_{sub}$ denote the variance of the response in subdomain $\mathcal{X}_{low} = [x_{1lb}, x_{1ub}]\times[x_{2lb}, x_{2r}]$, where x_{ilb} and x_{iub} are the lower and upper bound of the i^{th} input in the subdomain. Additionally, let $\mathbb{V}_{2sum} = \mathbb{V}[y(\mathbf{x}|x_2)] + \mathbb{V}[y(\mathbf{x}|x_1, x_2)]$ denote the sum of the conditional variances involving x_2 in subdomain $\mathcal{X}'_{low} = [x_{1lb}, x_{1ub}]\times[x_{2low}, x_{2r}]$. A limit for x_{2low} can be found by imposing the condition $\mathbb{V}_{2sum} = \alpha\mathbb{V}_{sub}$, where $\alpha \in [0, 1]$. In other words, x_{2low} defines the point at which the variances associated with x_2 in $\mathcal{X}'_{low}$ match α% of the variance in $\mathcal{X}_{low}$. The process is similar for the upper limit. Assume that $x_{2up} > x_{2r}$, where x_{2up} is the upper limit for x_2, and let $\mathbb{V}_{sub}$ denote the variance in $\mathcal{X}_{up} = [x_{1lb}, x_{1ub}]\times[x_{2r}, x_{2ub}]$ and $\mathbb{V}_{2sum}$ the sum of conditional variances involving x_2 in $\mathcal{X}'_{up} = [x_{1lb}, x_{1ub}]\times[x_{2r}, x_{2up}]$. A Limit for x_{2up} can be found using the same expression. Finally, the response limits are the maximum and minimum of $y(\mathbf{x})$ in $\mathcal{X}'_{low} \cup \mathcal{X}'_{up}$. Figure 22 illustrates the process for $n = 5$.

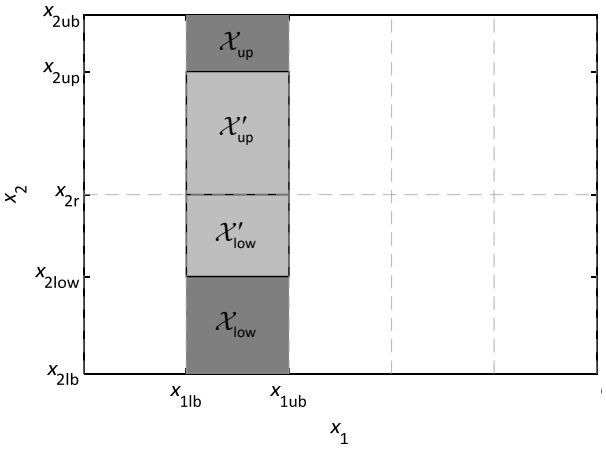

Figure 22 – Subdomains $\mathcal{X}_{low}$ and $\mathcal{X}_{up}$ in dark grey, and $\mathcal{X}'_{low}$ and $\mathcal{X}'_{up}$ in light grey. Note that $\mathcal{X}'$ overlaps $\mathcal{X}$.

7. Studies for Condition Monitoring Using Transmissibilities and Surrogate Models

The work developed in WP4 focuses on bogie frame damage, wheelset fatigue cracking, and degradation of the primary suspension elements. Structural damage and component degradation change the modal properties of the locomotive (natural frequencies, vibrations modes, and deflections shapes), which are related to the mechanical properties of the locomotive components (stiffness, mass, and damping). Therefore, the vibrational characteristics of the locomotive might be useful for condition monitoring, and computer simulations allow safely assessing the degradation of components. Particularly, a multibody formulation with an appropriate vehicle-track interaction model ensures the vehicle is excited by realistic loads.

7.1. Structural Damage of Bogie Frame

Although, the FGC 254 series of locomotives does not have a history of developing bogie cracks, the study of this failure mode is relevant for the railway industry, including vehicle manufacturers, railway operators, and technical regulators. The causes of the development of bogie cracks range from fatigue due to loads during the operation to collisions with objects during the operation. This subsection provides an analysis on the detection of bogie cracks using computational tools, which supports the development of a methodology to monitor the bogie condition using the selected sensor data.

7.1.1. Identification of Critical Locations

The absence of a history of crack initiation and propagation in the bogies of the FGC 254 locomotives implies that the analysis requires the definition of critical locations in the bogie. These physical points in the structure are determined using standard EN 13749, which regulates the methods required to assess the design of bogie frames [35]. This standard defines the considerations and provides examples of static and dynamic tests to evaluate the suitability of bogie designs. The critical locations are also established by prioritising the welded connections of the bogie frame, which are especially prone to crack propagation [36–38].

Annex F of EN 13749 details the static test programmes that can be used to verify the static strength requirements, to verify a FEM model, and to support the design life estimation. The static test programme for bogies of locomotives under normal service loads resulting from operation running is stated in point F.2.2.2 Loads resulting from bogie running. A 3D model of the bogie frame is developed in a 3D CAD software and the static analysis is performed using a finite element software, following the considerations of the standard. The finite element model comprises approximately forty five thousand structural 3D 10-node tetrahedral solid elements, with three nodal displacement degrees of freedom. The static load arrangement and the boundary conditions are an adaptation of the examples provided in the standard to the configuration of the bogie, considering three axles, and four connection points between the frame and the bolster. The magnitudes of the normal service loads are specified in section C.4.2. Normal service loads. The total vertical force applied on each bogie frame is:

$$F_z = \frac{\left(M_v - 2m^+\right)g}{2} \tag{25}$$

where M_v is the total vehicle mass, m^+ is the bogie mass, and g is the gravity acceleration. The transverse force applied to each bogie frame is:

$$F_y = \frac{F_z + m^+ g}{4} \tag{26}$$

The longitudinal force applied to each wheel due to the tractive effort is:

$$F_x = 0.1\frac{M_v g}{n_a} \tag{27}$$

where n_a is the total number of axles. Figure 23 depicts a simplified diagram of the loads distribution and the boundary conditions. Concerning the boundary conditions, the bogie frame is clamped on the top surface of the middle right horn guide, preventing all the displacements of the nodes of this surface. The bogie frame is simply supported on the top surface of the remaining horn guides, preventing only the vertical displacements of the nodes. Three different load scenarios are considered, and the set of forces associated with the first scenario is:

$$\begin{cases} F_{z1} = F_{z2} = F_{z3} = F_{z4} = F_z/4 \\ F_{m1} = F_{m2} = F_{m3} = F_m \end{cases} \tag{28}$$

where F_{zi} is the vertical force acting on each of the four rubber springs. F_{mj} is the weight of a traction motor. The loads associated with the second scenario are:

$$\begin{cases} F_{z1} = F_{z2} = F_{z3} = F_{z4} = F_z/4 \\ F_{m1} = F_{m2} = F_{m3} = F_m \\ F_{y1} = F_{y2} = F_{y3} = F_{y4} = F_{y5} = F_{y6} = F_y/6 \end{cases} \tag{29}$$

where F_{yj} is the transverse force applied on each pair of horn guides. The loads associated with the third scenario are:

$$\begin{cases} F_{z1} = F_{z2} = F_{z3} = F_{z4} = F_z/4 \\ F_{m1} = F_{m2} = F_{m3} = F_m \\ F_{x1} = F_{x2} = F_{x3} = F_{x4} = F_{x5} = F_{x6} = F_x \end{cases} \tag{30}$$

where F_{xk} is the longitudinal force applied on each of the six horn guides.

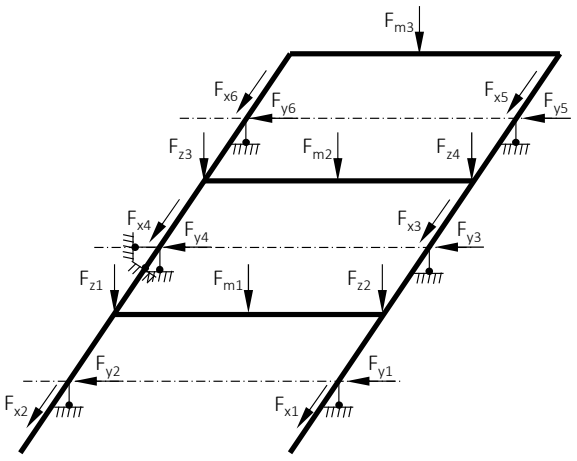

Figure 23 – Schematic representation of the static test programme.

The output quantities of the static analysis are the distribution of the von-Mises stress along the structure, depicted in Figure 24. The candidates to critical locations are the areas of higher stress concentration, subjected to tension or shear forces, which contribute to the propagation of cracks. Additionally, the effect of the mesh discretisation on the magnitude of stress must be recognised - the formulation of the finite elements presents a singularity, such that the smaller the discretisation in sharp corners, the higher the stress concentration values.

Figure 24 depicts three positions that are candidates for critical locations. Location 1 is a sharp transition between a bore and a stiffener on the right side frame, when the bogie is subjected to load scenario 1. This location is discarded as a critical location because the magnitude of stress is magnified by the proximity to the clamped connection on the middle right set of horn guides. Location 2 is defined by two edges of the welded connection between the front transversal beam and the right side frame, when the bogie is subjected to load scenario 2. This is a relevant location because the lateral forces due to the action of the front wheelset result in the development of traction forces in the welded connection, that may contribute to the propagation of cracks in this area. However, and as expected, the maximum stress is well under the limits of steel, for the load case considered. Location 3 is a bore in the left side frame. This area is disregarded as a relevant candidate for critical location because it does not involve welded joints or sharp corners where crack initiation and propagation are expected. The further analysis of location 2 is favoured due to the presence of the welded connection. Additionally, it is expected that damage in location 2 results in a larger change of the modes of vibration of the bogie frame, in particular the lateral movement of the sections of the side frames that protrude in the longitudinal direction.

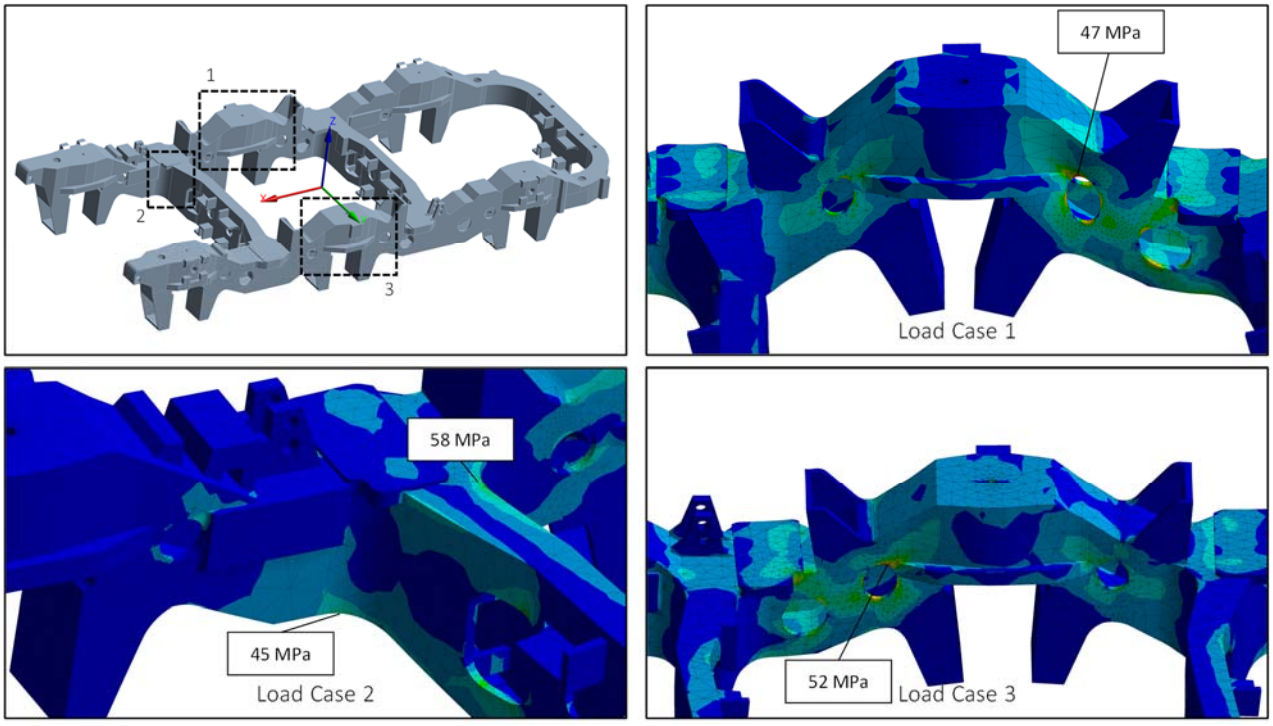

Figure 24 – Candidates of critical locations in the bogie frame.

7.1.2. Modal Analysis

The modal analysis aims at the study of the vibrational characteristics of structures. This type of analysis supports the development of models that can accurately describe the dynamics of structures, allowing their further analysis, optimisation, and the definition of limits in the operating conditions. Most finite element software provide tools to perform the modal analysis, requiring the definition of a FEM model similar to that of a standard linear static analysis. The modal analysis is a linear analysis, requiring a linearised model of the bogie frame and ignoring physical non-linearities such as the absence of normal and tangential forces between the surfaces of the crack, that are involved in the crack breathing mechanism [39]. The output of the modal analysis is a vector of natural frequencies and the associated matrix of modes of vibration.

The baseline FEM model developed is the same previously used in the static analysis, but in free-free conditions. The analysis of the influence of structural damage of the bogie frame on its vibration characteristics is supported by a set of scenarios characterised by different magnitudes of the crack area: 0%, 20%, 63%, and 100% of the area of the cross-section of the connection between the transversal beam and the side frame.

Table 5 shows the natural frequencies of the four different models, ordered in ascending order. The first six natural frequencies are associated with the six rigid-body modes of vibration and this is the reason why they are not shown. The results show that a crack with 20% of the area of the cross-section causes a negligible impact on the natural frequencies of the bogie frame. The increase in the crack area results in moderate changes of the vectors of natural frequencies: only the scenarios of 100% crack area presents noticeable changes in the natural frequencies, and the different frequencies are impacted in distinct magnitudes. These results suggest that the natural frequencies alone are not a sensitive damage indicator. Additionally, from a practical point of view, obtaining the natural frequencies of the real structure is a complex task that would require a large number of sensors.

Table 5 – Natural frequencies associated with the 4 scenarios for the bogie frame condition.

Mode		7	8	9	10	11	12	13	14	…	30	…	50
Natural frequency [Hz]	Nominal	30.57	46.56	51.95	52.33	60.79	73.40	112.09	113.06	…	309.85	…	561.51
	Damaged (20%)	30.56	46.56	51.91	52.46	60.80	73.39	112.24	112.93	…	309.73	…	561.56
	Damaged (63%)	29.30	38.63	46.53	51.96	59.58	71.51	110.54	112.58	…	306.98	…	558.68
	Damaged (100%)	13.19	14.98	26.94	37.82	46.88	54.30	61.63	70.12	…	271.54	…	541.20

The matrix of modes of vibration presents information which is complementary to the natural frequencies. The values of the modal matrix that are associated with the three translational degrees of freedom of one node *n* of the bogie frame are given by:

$$\mathbf{X}_{n,\xi/\eta/\zeta} = \begin{Bmatrix} x_{n,1,\xi} & \cdots & x_{n,M,\xi} \\ x_{n,1,\eta} & \cdots & x_{n,M,\eta} \\ x_{n,1,\zeta} & \cdots & x_{n,M,\zeta} \end{Bmatrix} \tag{31}$$

where *M* is the total number of modes of vibration considered. Figure 25 depicts the values of a node located on the top surface of the front right horn guide of the bogie frame, identified with number 2 on Figure 27. The results reveal that the modes of vibration are influenced by damage

and that the magnitude of damage results in different changes in the magnitude of the amplitudes. For example, the 10th mode of vibration, which is depicted in Figure 26, is associated with the lateral movement of the front ends of the side frames, and is disturbed by the existence of the crack in position 2, as shown in Figure 25.

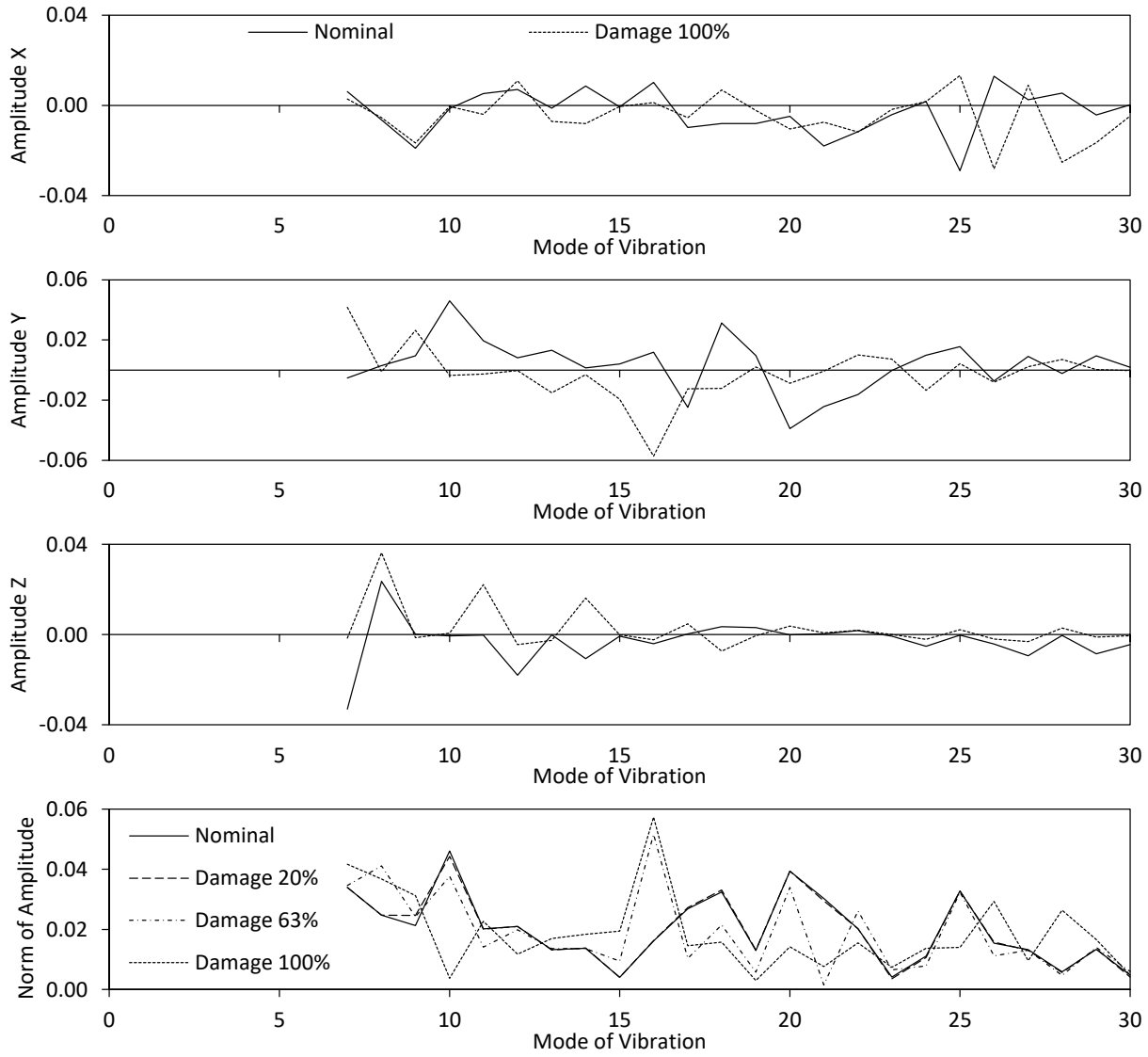

Figure 25 – Amplitudes of the entries of the matrix of modes of vibration associated with a node on the top surface of the front right horn guide.

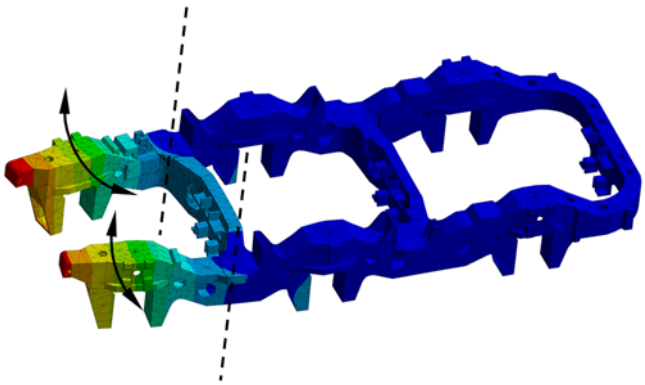

Figure 26 – Bogie frame deformation associated with the 10th mode of vibration – lateral movement of the front ends of the side frames, in phase opposition.

7.1.3. Flexible Multibody Simulations

The assessment of the condition of the bogie frame using computational tools is supported by multibody simulations to simulate the vehicle-track interaction, including the dynamics of the bogie frame. The vehicle model follows the description of Section 5.1.1., with some adaptations. The rigid body of the bogie frame is replaced by a flexible model. Also, the imperfect kinematic joints, that represent the clearances and friction damping in the primary suspension, are replaced by linear elements such as springs and dampers, to improve the numerical efficiency of the simulations. The flexible multibody simulations are performed using a straight track section, with synthetic track irregularities that follow the statistical properties of a real track section from FGC. The locomotive moves at a constant speed of 60 km/h.

As explained in Section 6.1., the flexible multibody formulation used employs the mode component synthesis, which defines that the structural deformations are described using a set of modes of vibration of the structure. Therefore, the structural flexibility of the bogie frame is defined in the vehicle model using the vector of natural frequencies **f** and the associated matrix of modes of vibration **X**. Each crack size scenario is associated with a pair of natural frequencies vector and matrix of modes of vibration, presented in subsection 7.1.2. The choice of the mode shapes considered is relevant. There is the need to reduce the number of flexible degrees of freedom to minimise the number of equations of motion that must be solved, and the number of modal coordinates that must be integrated to obtain the positions and velocities. There is also the priority of minimising the highest natural frequency considered, allowing the maximisation of the time step used in the integration scheme. However, the increase of the number of modes of vibration improves the accuracy of the description of the deformations of the bogie frame. The choice for the 30 lowest flexible modes of vibration, associated with a frequency range of approximately 15-375Hz, provides a reasonable compromise between all these factors, and includes several modes of vibration that involve the lateral movement of the side frame in the vicinity of the crack.

The flexible model of the bogie frame also includes 18 nodes that are distributed in the bogie frame, as shown in Figure 27. These nodes represent a baseline system of sensors, which is reduced after the results of the simulations are post-processed and interpreted. Nodes 12 to 18 are distributed in the vicinity of the crack, with the purpose of recording local changes in the

accelerations. Nodes 5 to 11 are positioned symmetrically with respect to the plane of symmetry of the bogie frame oriented in the longitudinal direction, and define a reference that can be used to evaluate asymmetries in the dynamics of the structure. Nodes 1 to 4 are distributed in outer points of the bogie frame with the intention of determining changes of the vibrations of the bogie frame, in a more global scale.

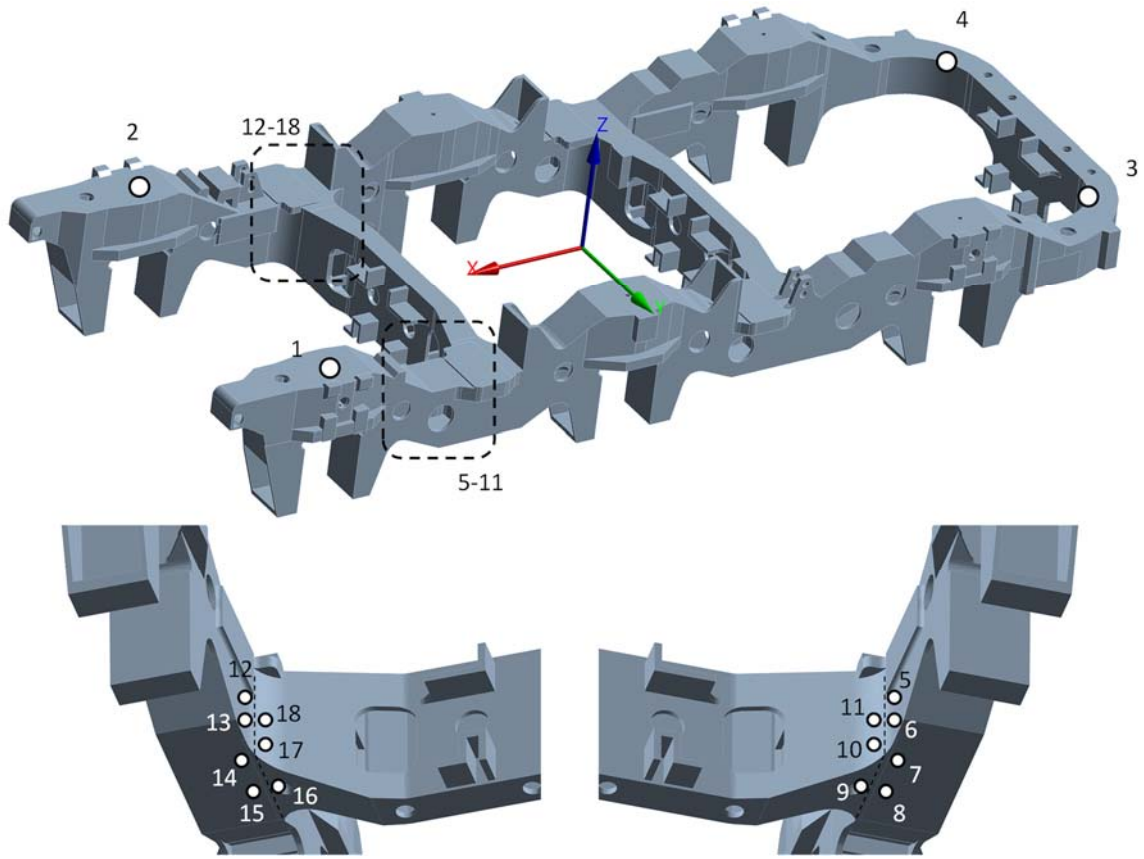

Figure 27 – Baseline set of virtual accelerometers.

The outputs of the simulations that are relevant for monitoring the condition of the bogie frame are the lateral accelerations of the 18 sensors depicted in Figure 27. In theory, both the longitudinal and vertical accelerations could also be used to define the transmissibilities between the points, but the results show the lateral accelerations are the most sensitive to presence of the crack defined for the study. The accelerations are post-processed according to Figure 20 on section 6.2.1 to obtain the transmissibilities. Figure 28 illustrates the types of results obtained in different scenarios. Figure 28 (a) shows the two transmissibility curves $\tau_{13}(\omega)$ between sensors 1 and 3, for the locomotive running in two subsequent track sections, each with a duration of 20 seconds. The condition of the bogie frame is nominal in both sections, therefore the differences in the curves are explained by the effect of the different track irregularities found in the two track sections. Figure 28 (b) depicts the two transmissibility curves $\tau_{13}(\omega)$, for the locomotive running in the same track section during 40 seconds and using the nominal bogie frame model and the model associated with 100% crack area. These preliminary results show that the transmissibilities are affected by the existence of damage with moderate dimension.

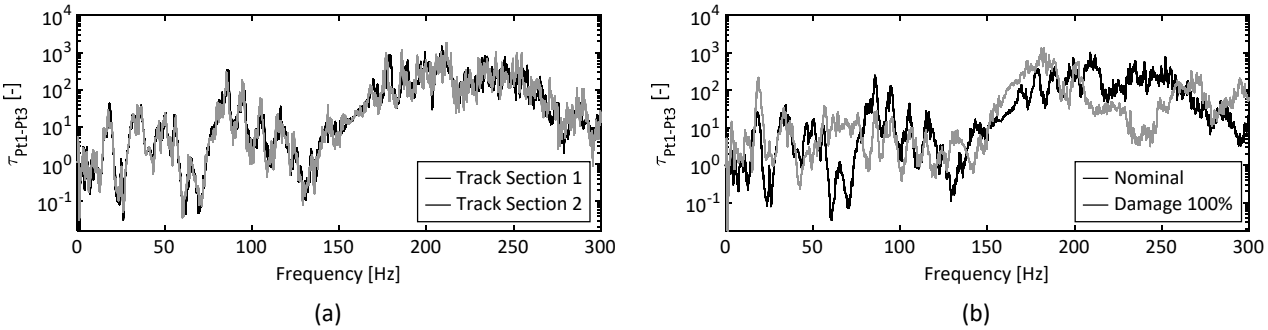

Figure 28 – Transmissibility curves relative to the lateral accelerations on sensors 1 and 3: (a) comparison of two different short track sections with bogie in nominal state, and (b) comparison in a long track section with bogie in nominal and fully damaged state.

7.1.4. Transmissibility-based Damage Indicators

This section focuses on the use of the method of the Transmissibility Damage Indicator (TDI) and the method of Maximum Occurrences (MO), presented in Section 6.2., with the goal of monitoring the condition of the bogie frame. These methods explore the changes in the transmissibilities, that are computed using the Power Spectral Densities of the lateral accelerations measured in the virtual sensors depicted in Figure 27. Table 6 reports the values of TDI that are the result of post-processing the outputs of the set of dynamic simulations in the frequency range of 10-150 Hz. This frequency range focuses on the lower frequencies of the response of the bogie frame, which is most accurately simulated by the flexible model. Additionally, this is the frequency range where the values of TDI are most consistent with the magnitude of damage for the simulations performed.

Table 6 presents 5 different scenarios, from the top to the bottom of the table. “Nominal Two Track Sections 20s” refers to a single simulation of the locomotive running in perfect conditions, and the values of TDI result from the comparison of the response in two subsequent track sections, each one amounting to 20 seconds of running. The aim of this comparison is the assessment of the impact of the length of the time signals on TDI, considering that the track irregularities that excite the locomotive are not perfectly ergodic relative to the track distance. “Nominal Two Track Sections 40s” is associated with a similar simulation, this time considering two subsequent track sections, each one amounting to 40 seconds of running. The results of the two simulations are close to unity, confirming the bogie frame is not damaged, and the values of scenario “Nominal Two Track Sections 40s” are consistently higher than the values of scenario “Nominal Two Track Sections 20s”. This result shows that the increase in the length of the time signals used to compute the PSDs is positive, because it contributes to reduce the effect of the differences in the track irregularities on the values of TDI.

The values of TDI associated with the 3 damage scenarios are the result of the comparison, in the same track section, of the simulated response of the vehicle in nominal condition with the simulated responses of the vehicle using 3 different bogie frame models that comprise a crack. The results show that the values of TDI decrease with the increase in the crack area. However, the values of TDI for the scenario of 20% crack area are virtually unitary and even higher than the values of scenario “Nominal Two Track Sections 40s”. This result shows that the impact of the differences in the track irregularities exceeds the effect of the existence of the bogie crack with

20% crack size. In the other scenarios, the values of TDI present noticeable reductions, and are consistently lower with the increase in damage size, as expected. These results suggest that the method of TDI is adequate to detect moderate to large, local bogie frame damage, while the sensitivity of the method is low for small magnitudes of damage. A TDI value of 0.7 is a reference threshold that can be used to identify the existence of damage in the structure, in circumstances similar to those of the simulations.

The method for the calculation of TDI is also a relevant factor that has an influence on the results. The sequential scheme consistently provides the higher values of TDI but requires the definition of the sequence used to relate the responses between the different sensors. This may not be a trivial task depending on the geometry of the structure, and the sensor data available, but has the potential to contribute to the process of damage localisation. The non-symmetric and symmetric schemes do not require such a sequence, instead relating all the transmissibilities between the sensors. The non-symmetric scheme provides values of TDI higher than those using the symmetric scheme. The symmetric scheme is moderately more sensitive to the existence of damage, but also more sensitive to external perturbations unrelated with the vehicle condition, such as the differences in the track irregularities.

The five rightmost columns of Table 6 are associated with 5 different sensor sets considered in the analysis, from a larger sample not presented for the sake of brevity. The results show there is a trade-off between the quantity of sensors and the sensitivity to damage. The increase in the number of sensors is followed by an increase of the sensitivity of TDI to damage, but also to the external perturbations.

Table 6 – Results of TDI considering different scenarios, methods of calculation, and sensors sets.

		Sensors				
		1,3,4,2	1,11,18,2	1,11,3,4,18,2	1,5,11,3,4,18,12,2	1,5,11,8,3,4,15,18,12,2
Nominal Two Track Sections 20s	Sequential scheme	0.9625	0.9796	0.9391	0.9359	0.9297
	Non-symmetric scheme	0.9611	0.9764	0.9267	0.9202	0.9158
	Symmetric scheme	0.9301	0.9432	0.9096	0.9046	0.9044
Nominal Two Track Sections 40s	Sequential scheme	0.9830	0.9874	0.9781	0.9756	0.9701
	Non-symmetric scheme	0.9803	0.9795	0.9678	0.9600	0.9562
	Symmetric scheme	0.9680	0.9674	0.9565	0.9494	0.9469
Damage 20% 40s	Sequential scheme	0.9993	0.9999	0.9991	0.9982	0.9972
	Non-symmetric scheme	0.9993	0.9995	0.9980	0.9923	0.9923
	Symmetric scheme	0.9989	0.9991	0.9977	0.9919	0.9920
Damage 63% 40s	Sequential scheme	0.9222	0.9184	0.8054	0.7019	0.6884
	Non-symmetric scheme	0.9099	0.8236	0.7551	0.6856	0.6647
	Symmetric scheme	0.7490	0.6788	0.6404	0.6068	0.5961
Damage 100% 40s	Sequential scheme	0.6791	0.8777	0.6227	0.5579	0.3104
	Non-symmetric scheme	0.6548	0.7491	0.4814	0.4174	0.2679
	Symmetric scheme	0.4833	0.5295	0.3715	0.2883	0.2636

The method of the Transmissibility Damage Indicator for damage detection can be complemented by the method of Maximum Occurrences to locate the structural damage. Figure 29 depicts three matrices of Maximum Occurrences for the sensor system involving sensors 1, 2, 11 and 18. Each matrix is associated with a different magnitude of crack area and the results are obtained considering the frequency range of 10-150 Hz. The colours of the squares are a measure of the number of occurrences. The matrix on the left shows the sensor pair with the maximum number of occurrences for 20% crack area is (2-11), which, according to an inspection of Figure 29, cannot be associated with any particular location of the bogie frame. The matrix in the middle, associated with the scenario of 63% crack area, shows the sensor pair with the highest number of occurrences is (2-18), which in fact corresponds to the area where the crack is located, in the connection between the right side of the front truss and the right side frame. The matrix in the right, associated with the scenario of 100% crack area, also successfully indicates the sensor pair (2-18). Figure 30 shows similar results for the sensor system involving sensors 1, 2, 3, 4, 11 and 18. The sensor pair with the maximum number of occurrences is consistently (2,18). The combined inspection of the results in Figure 29 and Figure 30 suggests that the increase in the number of sensors may improve the sensitivity of the method of Maximum Occurrences and enhance the capacity to locate the damage.

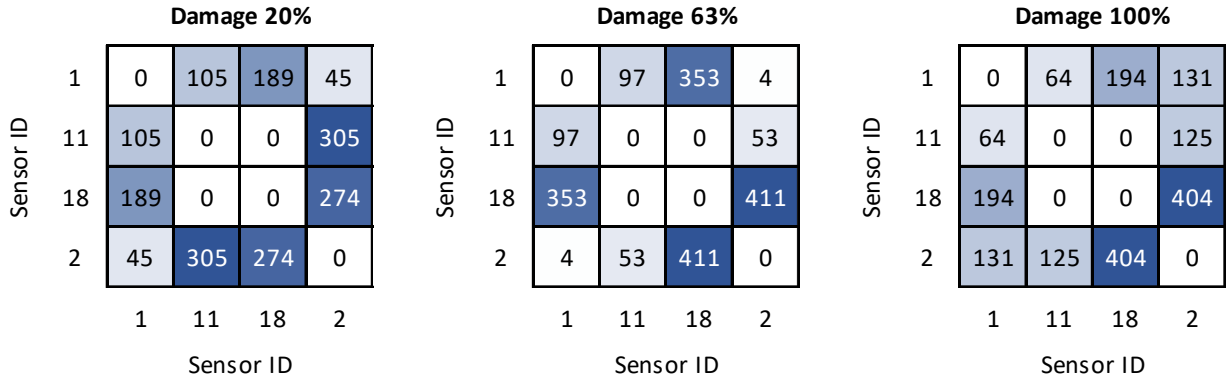

Figure 29 – Matrices of Maximum Occurrences for sensor system (1,11,18,2).

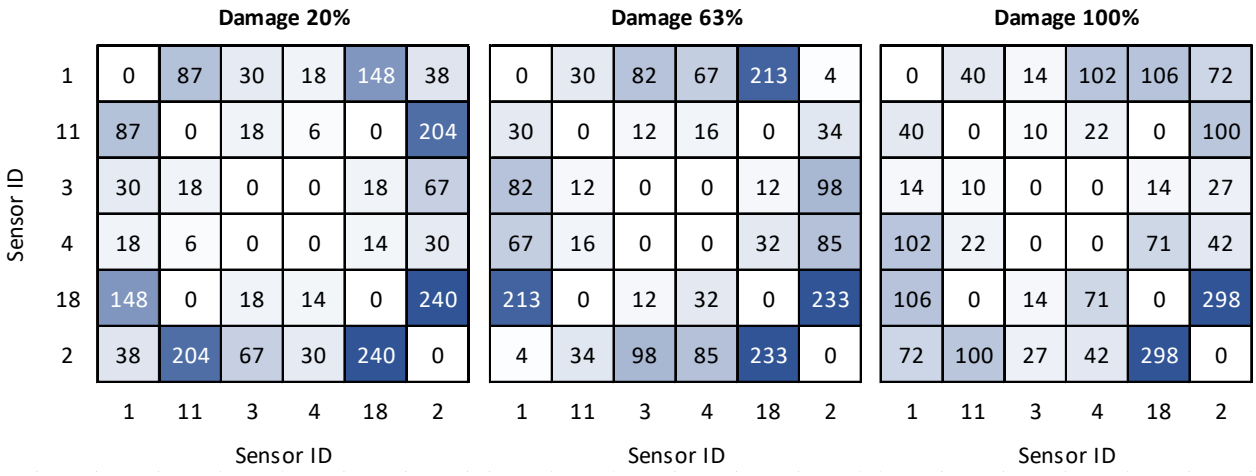

Figure 30 – Matrices of Maximum Occurrences for sensor system (1,11,3,4,18,2).

7.2. Structural Damage of Wheelsets

The wheelsets are one of the most safety-critical components of any railway vehicle and one of their most relevant failure modes is the propagation of axle cracks. The cause for the propagation of cracks in the axle of the wheelset is fatigue due to the cyclic axial traction and compression loading that the axles endure during the regular operation. This subsection aims at assessing the viability of the detection of wheelset cracks using computational tools.

The wheelset is a challenging component to monitor, due to the adverse conditions of operation and the axial rotation motion, despite its importance from the safety point of view. Access to the axle during the operation is impractical without wireless technology and the protection of the measuring equipment is precarious. One alternative, discussed in complementary projects such as INNOWAG, is the measurement of the longitudinal accelerations of the axle boxes to search for harmonics that can be associated with the speed of revolution of the axle. Project LOCATE employs the use of flexible multibody simulations to study the possibility of detecting changes in the response of the structural components. These simulations require a prior modal analysis to extract the natural frequencies and modes of vibration.

7.2.1. Impact of cracks on the modal properties of the wheelset

The modal analysis of the wheelset requires the geometrical modelling of the component using a 3D CAD software and technical drawings. To assess the effect of damage on the modal properties, four different models are developed: one model without damage; a second model with a crack with a depth of 10% of the axle diameter; a third model with a crack with a depth of 25% of the axle diameter; a fourth model with a crack with a depth of 50% of the axle diameter. The crack is shaped as a minor segment of a circle, perpendicular to the axis of the wheelset, and is located at mid-distance between the wheels. The model is discretised using solid finite elements, as show in Figure 31.

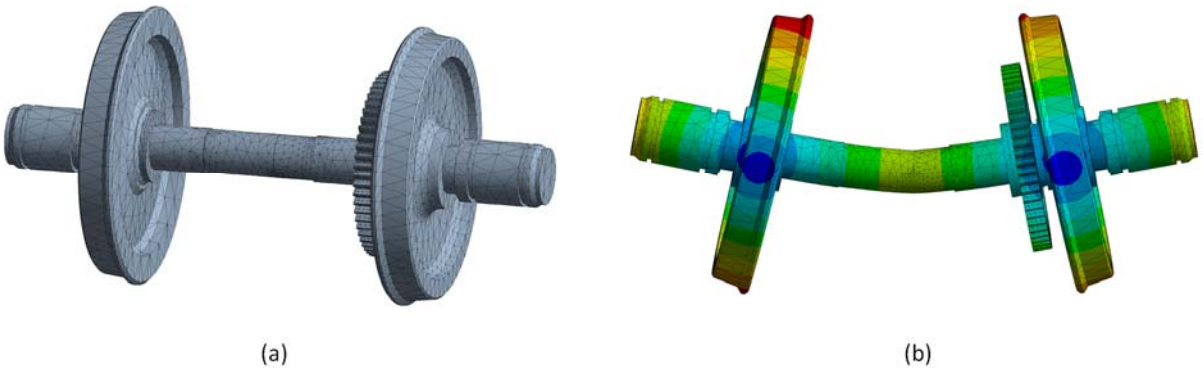

Figure 31 – Graphical representation of the wheelset: (a) model discretised by solid finite elements, and (b) first bending moment of the wheelset.

Table 7 presents the values of the natural frequencies as a function of the axle condition. The 8th and 9th mode shapes are the first and second bending modes, which are the ones relevant for the measurement of the radial vibrations of the wheelset. The first bending mode is depicted in Figure 31 (b). The results show that the for the damage cases of 10% and 25% crack depth the natural are frequencies are marginally affected by the damage. In the most adverse case, of 50% crack depth the natural frequencies are more sensitive to the crack, but this scenario most probably exceeds the limit after which it is not possible to correct the damage and the crack propagates at an exponential rate, until catastrophic damage occurs.

The assessment of the condition of wheelsets using computational tools requires alternative methods to those used in the previous section for the analysis of cracks in the bogie frame. Additionally, the difficulty of developing methods to monitor the structural condition of wheelsets is aggravated by other problems. It is impractical to measure the vibrations of the wheelset directly, and the feasibility of the indirect measurement of the vibrations on the axle box is yet to be confirmed. Also, the timely detection of changes in the response of the wheelset in an environment polluted by the vibrations that result from the wheel-rail contact is not trivial.

Table 7 – Natural frequencies associated with the four levels of wheelset condition.

Mode		7	8	9	10	11	12	13	14	15	16	17	18
Natural frequency [Hz]	Nominal	75.22	88.92	89.00	160.47	160.79	242.70	286.24	287.07	333.61	395.56	395.77	395.79
	Damaged (10%)	75.14	88.68	88.91	160.56	160.93	242.89	286.34	287.08	333.92	395.84	395.87	395.95
	Damaged (25%)	74.52	86.23	88.60	160.56	160.77	242.53	284.43	286.02	333.75	395.68	395.79	395.85
	Damaged (50%)	71.22	74.41	85.75	161.12	161.41	241.35	277.11	285.43	336.28	396.45	396.75	396.81

7.3. Degradation of suspension elements

The failure modes or degraded elements in this section concern the helicoidal springs and viscous dampers of the primary suspension, illustrated in Figure 32. These elements connect the axle boxes to the bogie frame and were identified as critical components defined in LOCATE Deliverable 4.1.

The failure modes are modelled by changing the mechanical properties of the multibody models described in Section 5.1.1. Specifically, the axial and shear stiffness of the springs and the damping coefficient of the dampers. An increase in stiffness represents a jammed spring, while a decrease in stiffness represents a buckled or broken spring. A reduction of the damping coefficient represents a leaking damper, while an increase of the damping coefficient represents a blocked damper.

The condition of the springs and dampers is monitored by the sensors depicted in Figure 32. The sensors are one biaxial accelerometer in each axle box, six biaxial accelerometers in the bogie frame, one at the end of each spring, and one IMU in the centre of the bogie frame. The sensor layout is based on the preliminary measurement campaign described in Deliverable 3.2, but includes more sensors. One benefit of the computational model is that the number of sensors is unlimited. Moreover, the simulation results might provide insight on sensor placement for future measurement campaigns.

Hereafter, the simulation results presented concern the rigid multibody simulations of the model described in Section 5.1.1. The signals from the multibody simulations are reported at 1000Hz and filtered with a 20Hz low-pass filter.

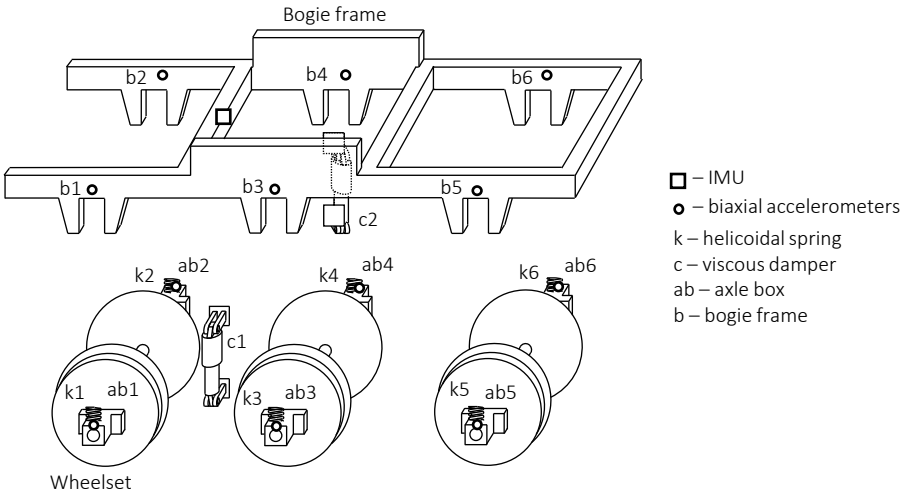

Figure 32 – Suspension elements and sensors used for condition monitoring of the primary suspension.

7.3.1. Design Variables and Experimental Setup

The design variables are the vehicle speed, v, spring stiffness, k_i, and damping coefficient, c_i. The subscript i refers to the numbering in Figure 32. Curvature is not used as a design variable. Curvature implies other considerations concerning cross-level and vehicle speed, and building an input space that respects the relationships between these variables is challenging. Moreover, available track data consists mainly of straight segments and does not provide enough information to define the boundaries of such input space reliably. For these reasons, the same track is used in every simulation, and it comprises a single straight section. The simulation time is 200 s to ensure measured signals have the same length across simulations. Considering a straight track allows exploring the symmetry of the suspension. The designs consider only failures on the left side of the bogie, namely in elements k_1, k_3, k_5, and c_1. The track irregularities should be different for each run so that the surrogate generalizes well to other irregularities. Since the available irregularity data covers about 5 km, the existing irregularities are used to estimate a vector autoregressive model. The vector autoregressive model allows generating irregularities with the same spatial correlations as the measured irregularities and thus, eliminates the problem of data availability.

7.3.2. Designs

The custom designs are used to study isolated failures, i.e., one faulty component while the others are healthy. The custom design approach is used to ensure the nominal value of the component is correctly represented in the surrogate. Inputs x_1 and x_2 are the speed, v, and the faulty component property, q_i, i.e., k_i for the spring and c_i for the damper. The lower and upper bounds of v and q_i are respectively [25, 70] km/h and $[0.1q_n, 1.9q_n]$, where q_n is the nominal value of the faulty component ($k_n = 0.680\times10^6$ and $c_n = 0.020\times10^6$ Ns/m). The healthy components (remaining inputs) are normally distributed in the interval $[0.9q_n, 1.1q_n]$ to consider some variability about their true value. The total number of points in each design is 25 ($n_1 = 5$ and $n_2 = 5$).

7.3.3. Threshold Definition Using Surrogate Models

The goal is to find surrogates for the statistical quantities of measured signals, namely, mean and standard deviation. Two types of GP models were explored: interpolation and regression. The observations of the GP interpolation model are the statistical quantities of the whole signal (200 s). For the GP regression, the observations are the statistical quantities of five signals obtained by partitioning the measured signal into five (5×40 s). In other words, the GP regression considers five observations per set of inputs.

It is necessary to cover several combinations of statistical quantity, measure, position, body, and faulty component. For example, one might be interested in the mean of the lateral acceleration at position 2 of the bogie frame when k_1 is faulty or the standard deviation of the vertical acceleration at position 4 of the axle box when c_2 is faulty. Additionally, there are two types of of models (interpolation and regression) for every combination. In total, 416 models were estimated to cover every combination of isolated failures on the left side of the bogie. A three-stage screening process was applied to find reliable models. The metrics hereafter are cross-validated metrics. The first stage compared the R^2 between the interpolation and regression models and dropped the one with the lowest score. The second stage dropped models with an $R^2 \leq 0.8$ and $MAPE \geq 0.1$. The second stage ensured that the remaining 104 models had a good fit and low prediction error. However, these metrics only ensure the surrogates provide good predictions and not that the faulty components influence the predictions. Therefore, the third stage is a sensitivity analysis using LHDs with 2×10^5 points. Models with $S_{\text{fault}} \leq 0.2$ were dropped, where S_{fault} is the sensitivity index associated with the faulty component. Table 8 lists the remaining models at the end of the screening process and their sensitivity indices. These surrogates have few elements in common. They are GP regressions and represent the standard deviation of the lateral accelerations of the bogie. Depending on the model, the faults explain between 24 to 48% of the variance, and second-order sensitivities are negligible. Finally, there are two symmetries. First, sensitivities of surrogates modelling positions above the same wheelset (positions 1&2, 3&4, and 5&6) are equal. Additionally, Table 9, which lists the parameters of the models, shows that these coefficients are virtually the same. In other words, despite the failure being on the left side of the bogie, the sensors on the left and right sides are measuring the same. Second, the surrogates of positions above the first and second wheelset (positions 1, 2, 3, and 4) are sensitive to failures in k_1, and surrogates of positions above the second and third wheelset (positions 3, 4, 5, and 6) are sensitive to failures in k_5.

Limits for the response were found for the standard deviation of the lateral acceleration of the bogie frame at position $i = 1, 3, 5$ when k_i is faulty, i.e., for surrogates modeling sensors directly connected to faulty springs. Limits values were found using the variance-based approach described in 6.3.5 and considering $x_1 = v$ and $x_2 = k$, and $x_{2r} = k_n$. v was discretized into five intervals, the same number used to generate the designs, and limit stiffness value for each interval were found for $\alpha = 0.05, 0.10, 0.15$. In Figure 33, the dashed grey lines show the input space discretized into cells. The greyed-out areas correspond to the region between the k_{low} and k_{up} for $\alpha = 0.05$ in each speed interval. The regions obtained for $\alpha = 0.10, 0.15\%$ are omitted to avoid cluttering the figure. For each speed interval and $\alpha = 0.05, 0.10, 0.15$, the figure depicts points corresponding to maxima of the response as “o” and points corresponding minima as “×”. Finally, these points are connected by lines to show how the response limits change with v. The upper stiffness limits for k_1 and k_3 decrease as speed increases. The algorithm could not find upper limits for k_3, which means the variances due to k_3 never reach $\alpha\%$ of the variance in the cell (the variance is mostly

due to v). This behaviour difference relative to k_1 and k_2 is likely due to the damper installed next to k_3. The lower stiffness limits are less sensitive to v and show similar behaviour for the three springs. Table 10 lists the values of the surrogate at these points, i.e., maxima and minima according to α for each speed interval.

Table 8: Sensitivity indices of the isolated failure models

GP type	Statistical quantity	Measure	Body	Faulty component	Sensor position	Sensitivity indices S_v	S_{fault}	$S_{v,fault}$
Regression	Standard deviation	Lateral acceleration	Bogie frame	k_1	1	0.52	0.48	0.00
					2	0.52	0.47	0.01
					3	0.68	0.32	0.01
					4	0.68	0.32	0.01
				k_3	1	0.72	0.27	0.01
					2	0.72	0.28	0.00
					3	0.77	0.23	0.00
					4	0.77	0.23	0.00
					5	0.77	0.23	0.00
					6	0.77	0.23	0.00
				k_5	3	0.72	0.28	0.00
					4	0.72	0.27	0.00
					5	0.60	0.40	0.00
					6	0.60	0.40	0.00

Table 9: Parameters of the GP models.

Model					Parameters					Metrics	
Statistical quantity	Measure	Body	Component	Sensor	β	σ^2	ϑ_v	ϑ_{fault}	g	R_2	$MAPE$
Standard deviation	Lateral acceleration	Bogie frame	k_1	1	-0.7020	0.5044	0.0179	0.0272	0.0014	0.9986	0.0091
				2	-0.7018	0.5045	0.0179	0.0272	0.0014	0.9932	0.0175
				3	-0.2707	0.1492	0.0156	0.0359	0.0030	0.9915	0.0196
				4	-0.2706	0.1493	0.0156	0.0359	0.0030	0.9919	0.0197
			k_3	1	-1.2089	0.2026	0.0156	0.0359	0.0040	0.9964	0.0106
				2	-1.2086	0.2026	0.0156	0.0359	0.0040	0.9906	0.0213
				3	-0.3555	0.0842	0.0118	0.0625	0.0063	0.9956	0.0114
				4	-0.3547	0.0843	0.0118	0.0625	0.0063	0.9993	0.0080
				5	-0.1494	0.0948	0.0118	0.0625	0.0089	0.9983	0.0082
				6	-0.1491	0.0948	0.0118	0.0625	0.0089	0.9993	0.0084
			k_5	3	0.2101	0.0607	0.0118	0.0625	0.0076	0.9983	0.0085
				4	0.2106	0.0607	0.0118	0.0625	0.0076	0.9979	0.0120
				5	1.1978	0.1186	0.0156	0.0359	0.0050	0.9889	0.0213
				6	1.1979	0.1186	0.0156	0.0359	0.0050	0.9892	0.0225

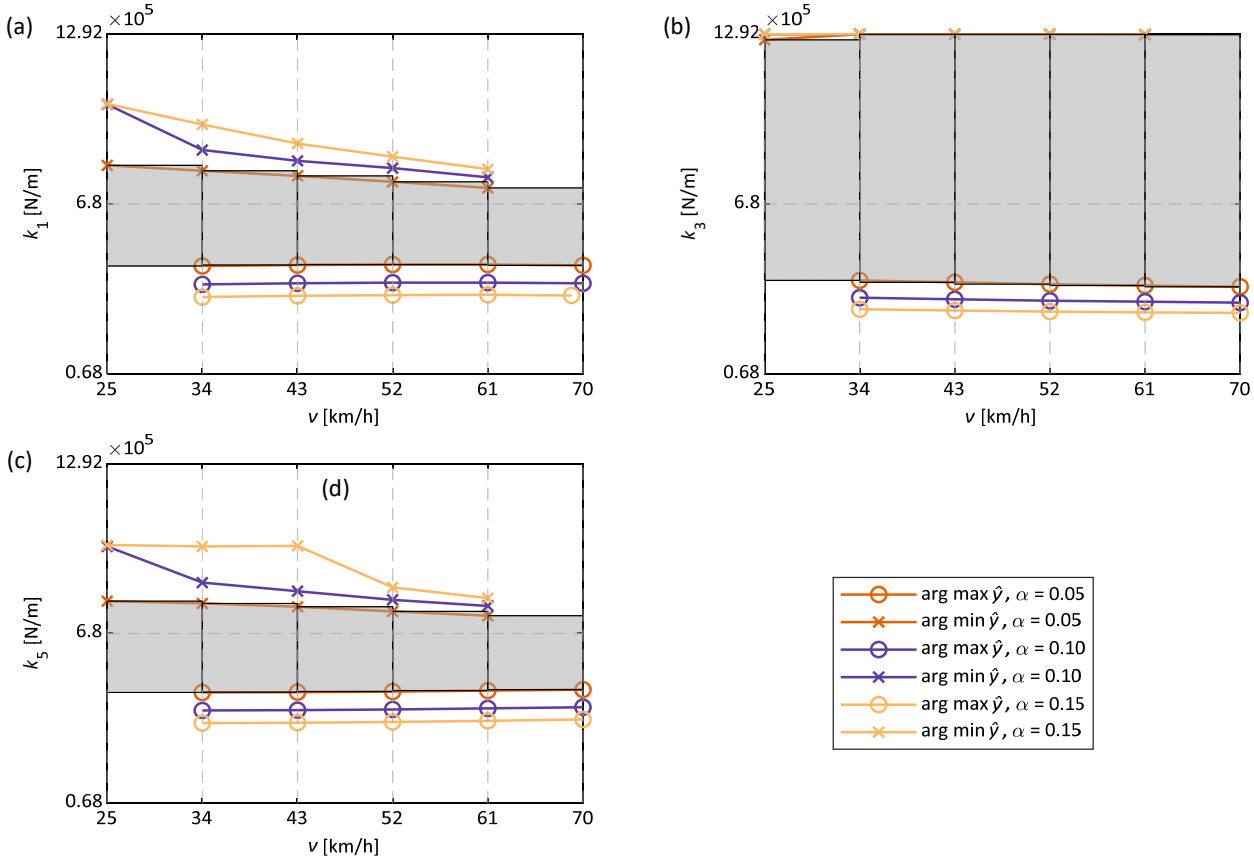

Figure 33: Upper and lower stiffness limits in the design space for α = 0.05 and arguments of the maxima and minima of the response for α = 0.05, 0.10, and 0.15: (a) k_1 and sensor 1, (b) k_3 and sensor3, and (c) k_5 and sensor 5.

Table 10 – Maxima and minima of the response in the input space.

Component, sensor position	α		v [km/h] [25, 34]	[34, 43]	[43, 52]	[52, 61]	[61, 70]
k_1,1	0.05	y_{min}	0.1492	0.2451	0.3251	0.3868	0.4288
		y_{max}	0.3261	0.3982	0.4499	0.4813	0.4938
	0.10	y_{min}	0.1379	0.2374	0.3189	0.3811	0.4246
		y_{max}	0.3517	0.4218	0.4714	0.5002	0.5099
	0.15	y_{min}	0.1379	0.2317	0.3134	0.3771	0.4217
		y_{max}	0.3713	0.4399	0.4877	0.5145	0.5223
k_3,3	0.05	y_{min}	0.1105	0.1692	0.2266	0.2796	0.3265
		y_{max}	0.2207	0.2745	0.3231	0.3645	0.3979
	0.10	y_{min}	0.1093	0.1692	0.2266	0.2796	0.3264
		y_{max}	0.235	0.2882	0.3363	0.3772	0.41
	0.15	y_{min}	0.1093	0.1692	0.2266	0.2796	0.3264
		y_{max}	0.2459	0.2988	0.3463	0.3869	0.4191
k_5,5	0.05	y_{min}	0.1404	0.2031	0.2656	0.3253	0.3791
		y_{max}	0.2634	0.3264	0.386	0.4395	0.485
	0.10	y_{min}	0.1312	0.197	0.2603	0.3205	0.3743
		y_{max}	0.2825	0.346	0.4062	0.4602	0.5059
	0.15	y_{min}	0.1312	0.1932	0.2539	0.3165	0.3711
		y_{max}	0.2971	0.361	0.4216	0.4759	0.5219

7.3.4. Condition Monitoring Using Transmissibilities

This section focuses on the use of the Transmissibility Damage Indicator method (TDI) and the Maximum Occurrences method (MO), described in Section 6.2., with the aim of detecting damage in the springs and dampers of the primary suspension. The transmissibilities between the Power Spectral Densities (PSD) of the accelerations measured at the virtual sensors in the axle boxes and bogie frame, depicted in Figure 32, are employed in the analysis.

Figure 34 shows the transmissibilities between the PSD of the lateral and vertical accelerations measured at the axle box and bogie frame in position 1. Three cases are shown that correspond to: the vehicle in nominal condition; stiffness of spring k1 is 200% of the nominal value; and stiffness of spring k1 is 10% of the nominal value. The simulations correspond to the locomotive running at 60 km/h for 200s in a straight track with real irregularities. The results show a significant difference between the nominal case and that corresponding to the stiffness decrease. In contrast, the results between the nominal case and the stiffness increase are similar. Additionally, the transmissibilities using the lateral accelerations, in Figure 34 (a), shows a stronger sensitivity to the spring stiffness decrease than those using the vertical accelerations, in Figure 34 (b). The TDI is appropriate to detect and quantify such differences in transmissibilities.

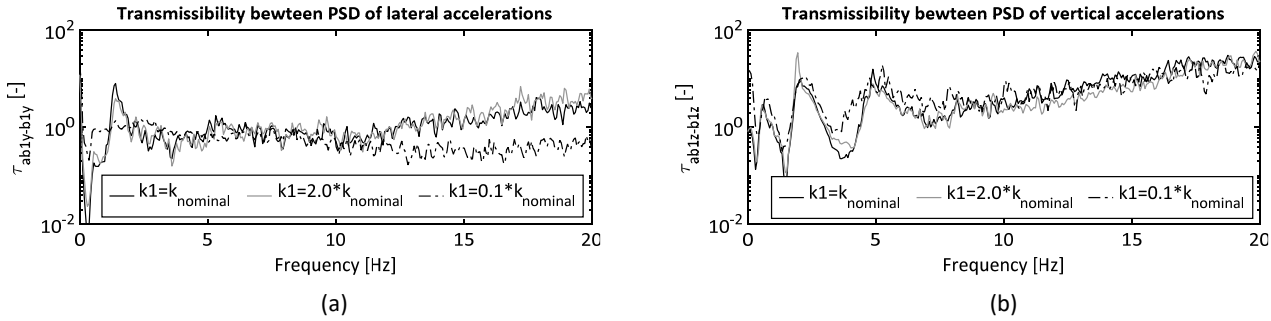

Figure 34 – Transmissibility between the PSD of the (a) lateral and (b) vertical accelerations measured at axle box 1 and bogie 1 for changes in the stiffness of spring k1.

The simulations of the design of experiments for single failures, described in Section 7.3.2., is used hereafter to study the TDI and MO methods. The TDI method requires a reference, corresponding to the vehicle in nominal conditions. Since the simulations are performed at different constant speeds, it requires a database of the nominal responses of the locomotive that covers the range of velocities used in the design. Hence, 18 simulations that correspond to the locomotive in nominal conditions running at speeds between 25 km/h and 70 km/h, with a step of 2.5 km/h, are performed. Thus, the maximum speed difference that can occur between a simulation from the design and the corresponding reference is of 1.25 km/h. This is considered acceptable and realistic, since during real operation the exact repeatability of velocities is unlikely. The reference and design simulations consist on the vehicle running for 200s in the same straight track with real irregularities.

The TDI value is calculated using pairs or groups of four sensors. In the first case, it considers the transmissibility between the signals at the axle box and the closest sensor in the bogie frame. In the second case, it considers the transmissibilities between the four sensors associated to one wheelset. This is done to associate each TDI value to a spring, damper or wheelset. The transmissibilities can be obtained for the PSDs of the vertical or lateral accelerations measured at the axle boxes and bogie frame. The following four cases were considered: 1) only vertical accelerations; 2) only lateral accelerations; 3) combining the lateral accelerations at the axle boxes and vertical accelerations at the bogie frame; 4) combining the vertical accelerations at the axle boxes and lateral accelerations at the bogie frame. In what follows, the results for cases 2) and 4) are shown, as these show the most significant sensitivity to damage. Nevertheless, cases 1) and 3) also show a reasonable sensitivity.

Figure 35 shows the TDI values (in the horizontal axis) as a function of the variation of the spring stiffness (in the vertical axis), corresponding to case 2) – transmissibilities between the lateral accelerations at the axle boxes and bogie frame. In the present case and in all that follows, the TDI values are calculated using the symmetric scheme, described in Section 6.2.1., since it shown consistently the best results. The bold darks circles in Figure 35 represent the TDI values for the combinations of signals in the vicinity of the damage. In contrast, the coloured lighter circles correspond to groups of sensors that are not directly associated to the damaged element.

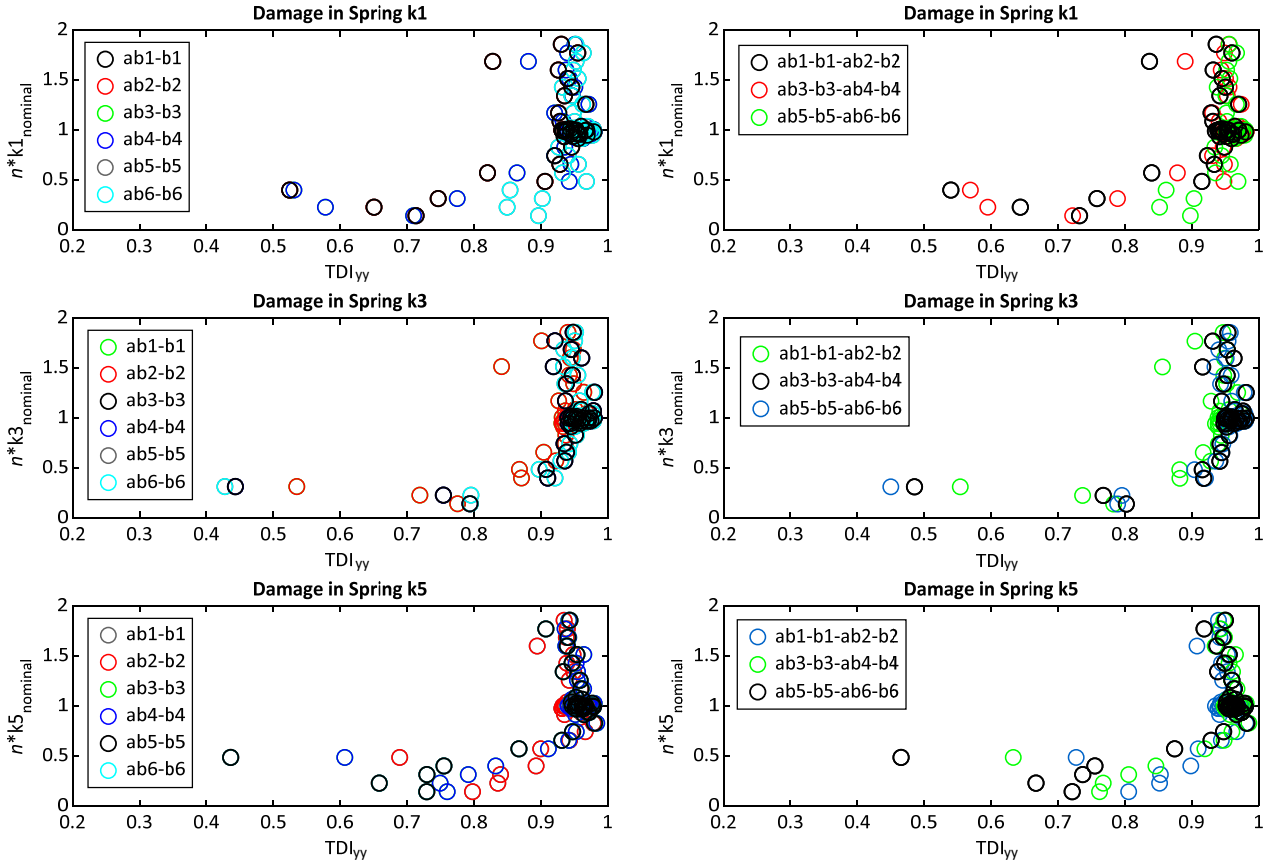

Figure 35 – TDI results using lateral accelerations measured at the axle boxes and bogie frame for simulations considering single failures of springs.

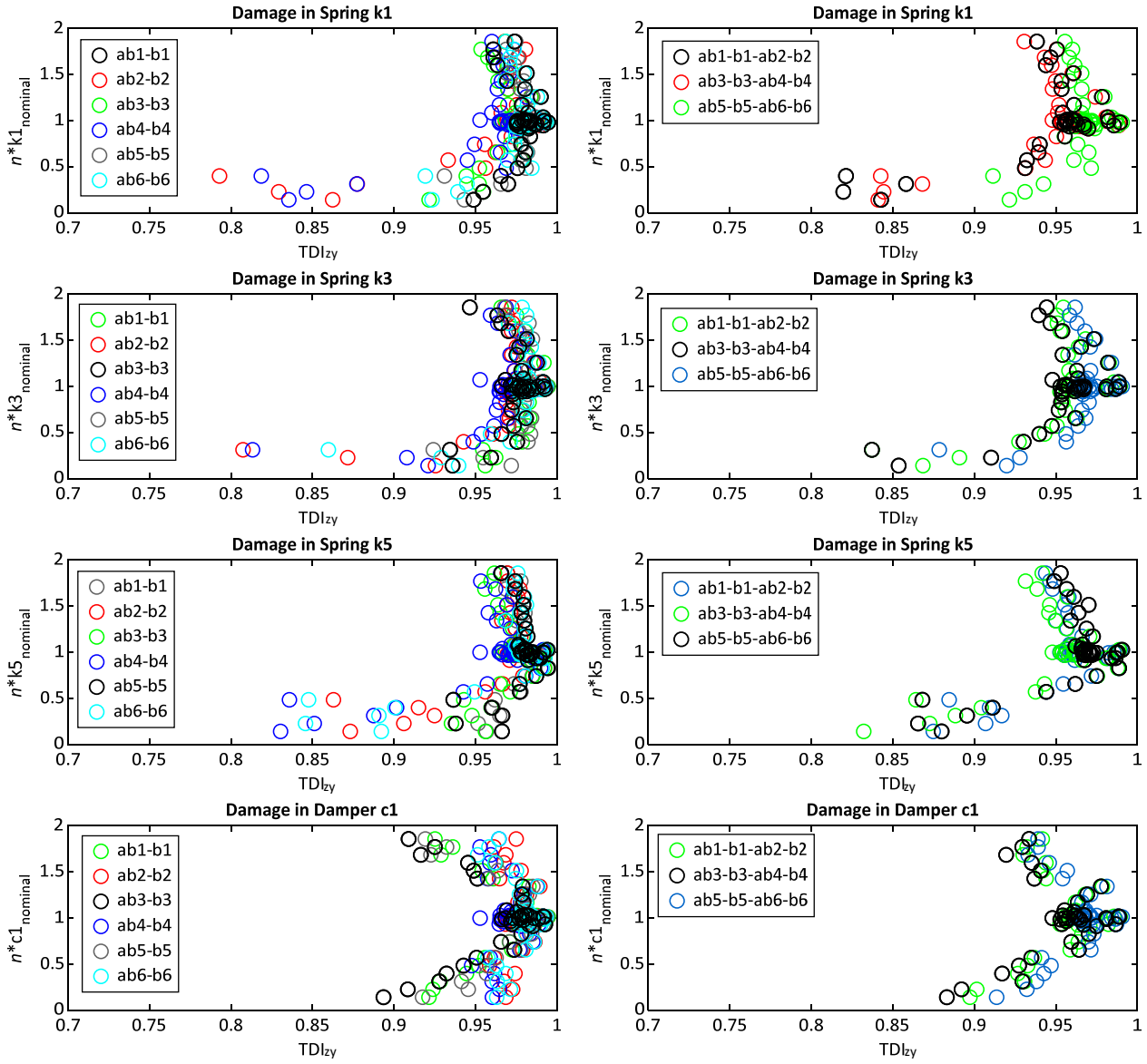

Figure 36 – TDI results combining the vertical accelerations measured at the axle boxes and lateral accelerations at the bogie frame for simulations considering single failures of springs and the viscous damper.

The results show a significant sensitivity to the decrease in the spring stiffness in opposition to a low sensitivity in the case of stiffness increase. The results also show a significant impact of the stiffness reduction in all combinations of sensors, making it difficult to locate the damage through the lowest value between the different pairs/groups of sensors. The simulations of damage in the viscous damper and corresponding TDI values are omitted as these do not show any sensitivity to the variation in the damping coefficient.

Figure 36 shows the TDI values corresponding to case 4) – transmissibilities between the vertical accelerations at the axle boxes and the lateral accelerations at the bogie frame. The results show a good sensitivity to the spring stiffness decrease when using groups of four points. In addition, when varying the damper properties, the TDI shows a significant sensitivity to both the

increase and decrease of the damping coefficient, either using pairs or groups of 4 points.

Figure 37 shows how the definition of thresholds for the TDI can be used for the detection of damage on both springs and dampers. Figure 37 (a) suggests that a reduction of 50% in the stiffness of spring k1 is associated to TDI values below 0.8. Similarly, Figure 37 (b) suggests that a reduction or increase in 40% of the damping coefficient implies TDI values below 0.95. However, it is difficult to determine whether the damage in the damper corresponds to an increase or decrease in the damping coefficient. In all cases, the TDI method does not allow to locate the damaged element. The damage of one component implies significant changes in all groups of sensors and often the lowest TDI value does not correspond to the location of the damaged component.

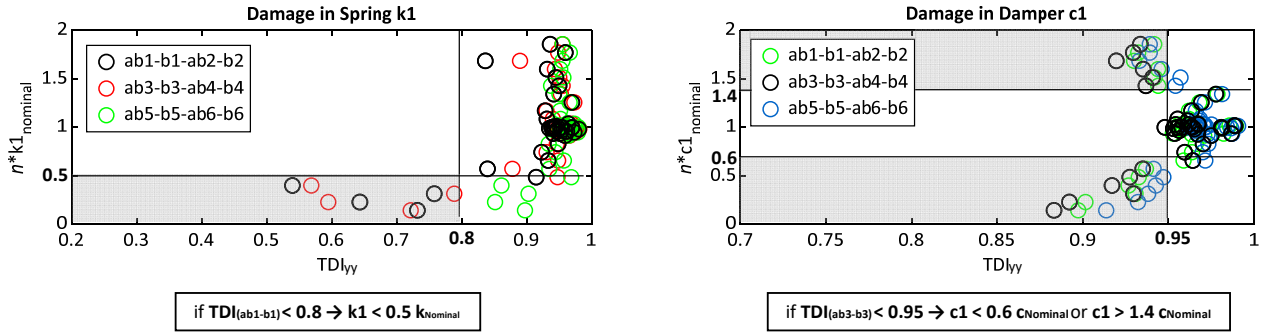

Figure 37 – Threshold for damage detection using the TDI_{yy} for the failure of (a) spring 1 (b) damper 1.

The MO method, described in Section 6.2.2., can be used to complement the TDI method in the localisation of the damage. Table 11 shows the results of the MO method using the trasmissibilities between the lateral accelerations at the axle boxes and bogie frame. The results focus on the reductions of the springs stiffnesses, since these are effectively detected using the TDI. The method evaluates, at each frequency, the pair of sensors where the difference between the nominal and measured transmissibilities is the largest, adding one to the wheelset, ws, associated to that pair. The method shows a good accuracy in identifying the wheelset associated to the damaged element when this occurs in the springs of the leading and trailing wheelsets. However, when the damage is in the middle wheelset, k3, the maximum occurrences are constantly in the trailing wheelset, ws 3. According to the results, when there is a stiffness reduction in one of the springs, the use of the maximum occurrences can identify whether the damage is in a spring in the leading wheelset, or in opposition, in the middle or trailing wheelsets. In the case of damage in the viscous damper, the maximum occurrences proved ineffective on locating it. Other possibilities using the MO method were explored, including the use of vertical and lateral accelerations at axle boxes and bogie frame, as well as the study of pairs of sensors in each wheel. However, none of the possibilities provided any valuable information.

Table 11 – Results of maximum occurrences method, between 1-20 Hz, for locating the wheelset connected to a buckled/broken spring.

Damage in spring 1 (wheelset 1)				Damage in spring 3 (wheelset 2)				Damage in spring 5 (wheelset 3)			
n*k1$_{nom}$	ws 1	ws 2	ws 3	n*k3$_{nom}$	ws 1	ws 2	ws 3	n*k5$_{nom}$	ws 1	ws 2	ws 3
0.40	**189**	70	54	0.31	91	59	**163**	0.49	36	68	**209**
0.57	**144**	75	94	0.66	89	80	**144**	0.66	84	76	**153**
0.23	**165**	72	76	0.23	101	84	**128**	0.40	49	63	**201**
0.74	**125**	84	104	0.74	101	89	**123**	0.74	81	84	**148**
0.31	**144**	91	78	0.14	109	49	**155**	0.31	63	72	**178**
0.83	99	73	**141**	0.91	**116**	87	110	0.83	**116**	101	96
0.14	109	**133**	71	0.49	107	85	**121**	0.23	49	62	**202**
0.91	**108**	104	101	0.57	84	**120**	109	0.57	83	84	**146**
0.49	**119**	93	101	0.40	88	100	**125**	0.14	69	84	**160**
0.66	**110**	101	102	0.83	94	104	**115**	0.91	100	**115**	98

So far, the TDI values were calculated using a nominal reference of the vehicle running in the exact same track as the measured scenario. To evaluate the impact of using different track sections between the nominal and measured cases, the TDI values were obtained by comparison of the vehicle running in two different straight sections with statistically similar irregularities. In addition, the signals are also shortened, corresponding to the locomotive travelling for 100s in the straight track. Figure 38 shows the results obtained when using the same track sections and signals of 200s length, in the left, and the results for 100s length signals where the nominal and measured simulations were obtained on different straight tracks. The results show a general decrease of the TDI values corresponding to the nominal situation, as highlighted, but the sensitivity to the stiffness decrease remains. Therefore, the TDI method does not require that the nominal and damaged cases are compared in the exact same track sections. If two straight track sections have similar irregularities, the transmissibilities can be compared to obtain the TDI and assess the suspension condition.

The TDI method can be implemented for testing in real operation. In this work, some of the sources of variability in real operation were considered, including the variation of all suspension properties around +/- 10% of its nominal value and the use of different track sections and velocities between nominal and measured cases. In all cases, the method shows promising results. If the time signals of the accelerations are long enough and consider the locomotive running at approximately constant speed in a straight track, the PSDs can be used to compute the TDI values. The method requires the nominal response that could be obtained by the sensoring system after a maintenance action to verify the integrity of all components. The condition can be continuously monitored by calculation of the PSD of the signals and respective TDI values.

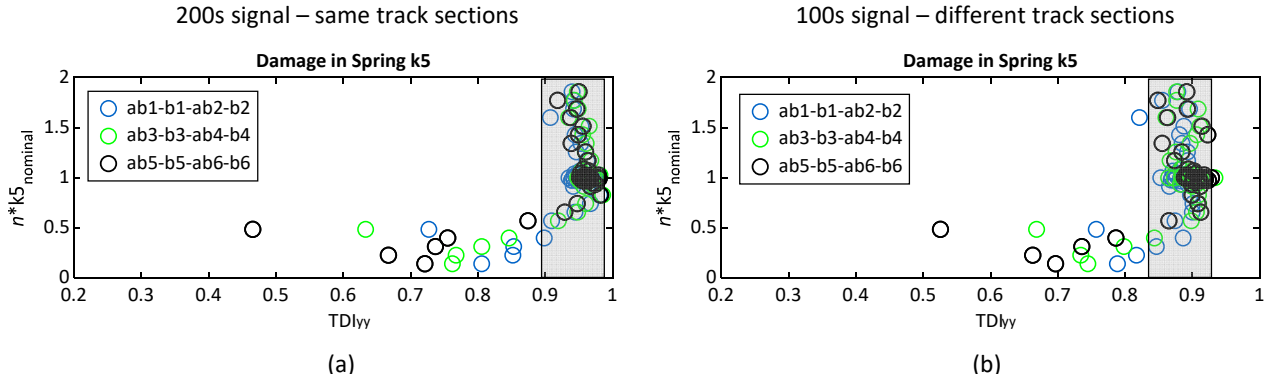

Figure 38 – TDI results using (a) 200s signal and a reference from the same straight track segment; (b) 100s signal with a reference from a different straight track with similar irregularities.

Further work on the TDI methodology can include the use of some type of data analysis process, to aid on the interpretation and crossing of the TDI values obtained across the different groups of sensors. This could allow to identify the damage cases with more precision as well as locating the damaged element. If sufficient data can be obtained via simulations, machine learning might be experimented. Finally, the case of multiple failures is not addressed in the analysis, but the TDI method should be equally sensitive to such occurrences.

8. Contribution to the Second Experimental Campaign

8.1. Motivation

The second experimental campaign aims to demonstrate the condition monitoring strategy developed in LOCATE. The campaign should record quantities involved in the condition indicators identified in WP4, namely, the quantities used for the Transmissibility Damage Indicator (TDI) and Maximum Occurrences (MO) methods and surrogate models. Results from the second campaign will allow understanding the impact of other factors (e.g., speed variation, track condition, and braking) on the sensitivity of the methods used to monitor the condition of bogie components. The results from the experimental campaign will also allow evaluating and correcting the thresholds proposed, which were defined exclusively using computer simulations.

8.2. Sensor System and Operation Conditions

Based on the simulation results presented in Section 7, the sensor system depicted in Figure 39 is proposed to detect damage in the bogie frame and primary suspension. The system consists of six biaxial accelerometers (lateral and vertical directions), one on each axle box, four uniaxial accelerometers (lateral direction) on the bogie frame, and one IMU at the centre of the bogie frame that records longitudinal, lateral, and vertical accelerations and roll, pitch, and yaw speeds. The IMU can be used to calculate the rigid body accelerations at other points in the bogie by differentiating angular velocities. Additionally, the yaw velocity measured by the IMU allows distinguishing straight and curved sections. The goals and frequency domains required for each sensor are described in Table 13. The methods for damage detection require selecting long straight track sections that allow capturing signals with the maximum length possible with the locomotive running at approximately constant speed. For reference, the simulations used to assess damage on the bogie frame involved track sections with a length of approximately 800m. The simulations associated with the evaluation of the condition of the primary suspension involved track sections with a maximum length of 4000m. Nonetheless, multiple straight sections can be used to concatenate the data and obtain the maximum signal length to calculate the power spectral densities. Finally, track irregularities for the track sections considered in the campaign should be recorded, ideally, as close as possible to the time of the campaign.

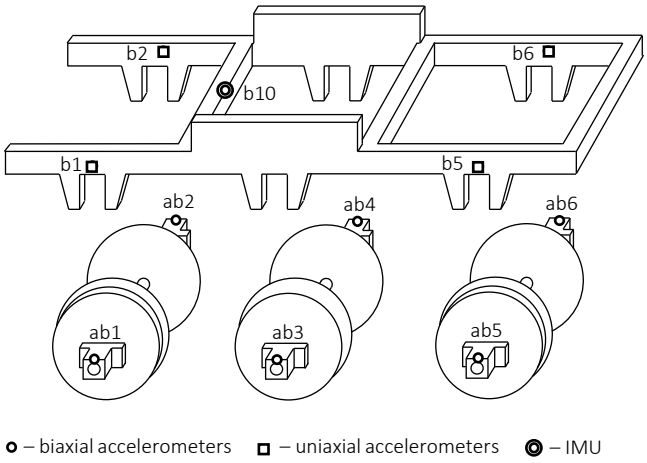

Figure 39 – Sensor system for damage detection in the bogie frame and primary suspension.

Table 12 – Sensors specifications for damage detection in bogie frame and primary suspension.

Type	Sensor	Direction	Frequency domain [Hz]	Monitored System
Uniaxial accelerometer	b1/b2/b5/b6	Lateral (*y*)	1-20	Primary suspension
			10-150	Bogie frame
IMU	b10	Lateral (*y*)	1-150	Bogie frame
		Roll/Pitch/Yaw	1-20	Primary Suspension
Biaxial accelerometer	ab1/ab2/ab3/ ab4/ab5/ab6	Lateral (*y*)	1-20	Primary suspension
		Vertical (*z*)	1-20	Primary suspension

8.3. Data Post-processing

The methods proposed in this deliverable are based on a library of nominal and abnormal vehicle responses. In this database, simulations concerning nominal behaviour provided baselines, while simulations regarding abnormal behaviour allowed defining thresholds. For the TDI and MO methods, the library defines the nominal transmissibility matrix, which is compared to the transmissibility matrix of the measured response to obtain the condition indicators. For the surrogates models, the nominal and abnormal conditions are represented by continuous variables, whose domains are explored to find thresholds. It is sensible to complement or revise the baselines using results from the second measurement campaign. Assuming the locomotive is in nominal condition after leaving the workshop, the recorded measurement can be added to the library as baselines. Vehicle speed is a key variable affecting the vehicle response, and, therefore, baselines must be defined considering different average velocities of the locomotive in the track section selected for measurement.

Figure 40 depicts the proposed data flow concerning the methods for condition monitoring implemented in WP4. Depending on the method, the accelerations are post-processed in the time or frequency domain. The standard deviation of the low-pass filtered lateral acceleration of the

bogie frame is compared with speed-dependent thresholds to assess the condition of the primary suspension. The Power Spectral Densities of the accelerations are used to compute different transmissibility matrices that, separately, allow monitoring the condition of the primary suspension, or the bogie frame, using the TDI method. The MO method complements the TDI method when the value of the TDI is below the threshold defined, either for the bogie frame damage detection or the degradation of suspension elements. It is advisable to store the raw measured data in the time domain to allow other analyses not foreseen in the document.

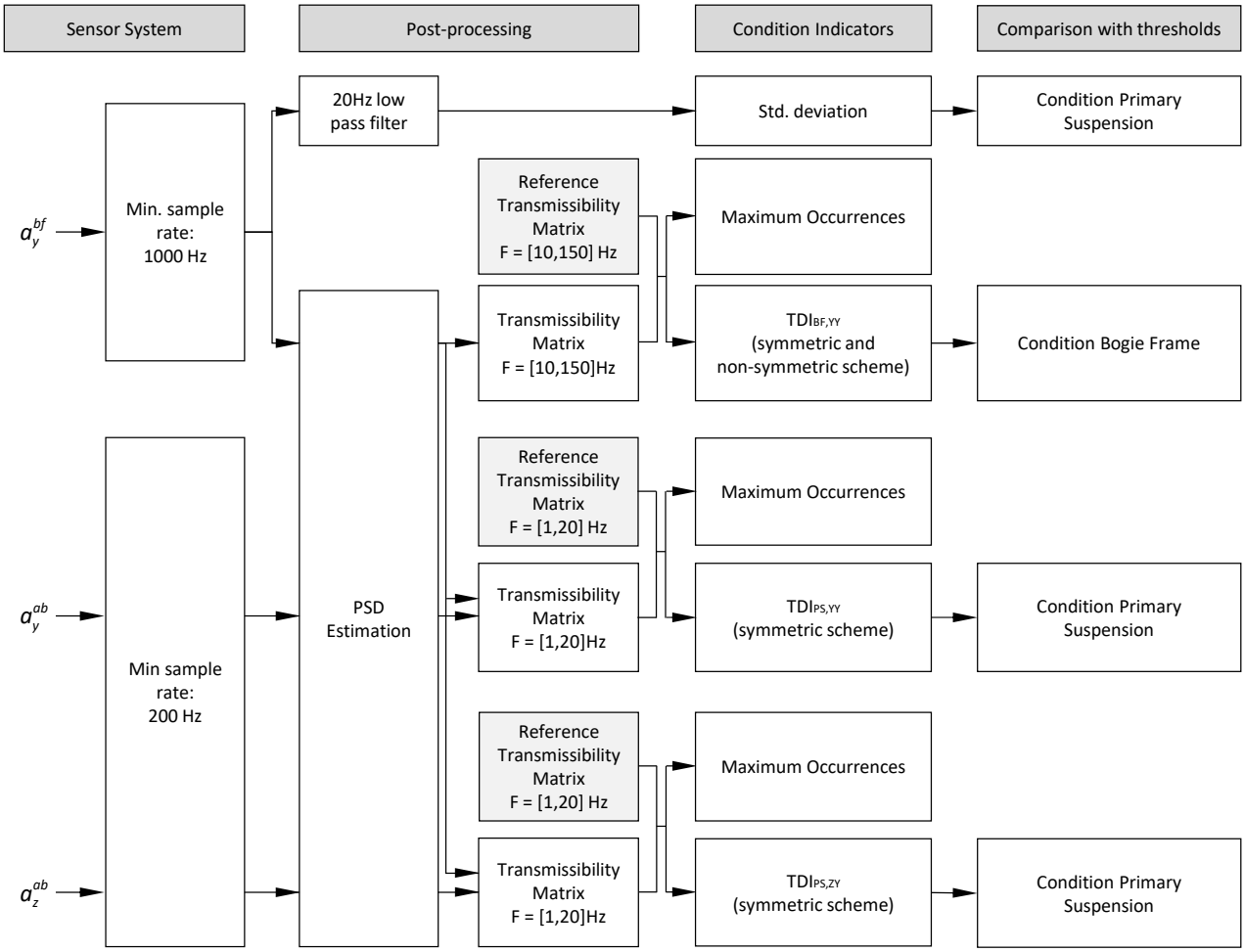

Figure 40 – Data flow for the condition monitoring methods.

8.4. Thresholds for Condition Indicators

Computer simulations of the damaged locomotive and its components allow setting thresholds values for some of the studied quantities. The quantities identified are sensitive to cracks in the bogie frame, buckled or broken springs, and damaged dampers. However, note that these thresholds were defined for specific speed ranges using simulations. They should be reviewed and adapted using data from on-track measurement campaigns. Table 13 lists thresholds for the TDI, defined using the methods described in Sections 7.1.4 and 7.3.3. Table 10 lists the upper and lower thresholds for the standard deviation of the lateral accelerations of the bogie frame measured at position 1, 3, and 5, to detect damage in k_1, k_3, and k_5, as described in Section 7.3.2.

Table 13 – Limit values for quantities used in condition monitoring.

System	Quantity	Description	Speed Range [km/h]	Limit value	Occurrence
Primary Suspension	$TDI_{PS,YY}$	TDI using lateral acceleration at axle boxes and lateral accelerations at bogie frame	25-70	0.85	Buckled/Broken Spring
	$TDI_{PS,ZY}$	TDI using vertical acceleration at axle boxes and lateral accelerations at bogie frame	25-70	0.95	Buckled/Broken Spring or Damaged Damper
Bogie Frame	$TDI_{BF,YY}$	TDI using vertical acceleration at axle boxes and vertical accelerations at bogie frame	57-63	0.7	Crack in Bogie Frame

9. Alternative Approach for Suspension Parameter Estimation Using RLS

In this section, the general configuration of the condition monitoring system of the vehicle suspension system is specified based on the FGC (Ferrocarrils of the Generalitat de Catalunya) diesel locomotive Series 254 (shown in Figure 38) and the suspension layout (shown in Figure 39).

9.1. Definition of Suspension Components

In this type of vehicle, the primary suspension consists of primary rubber and coil springs and dampers (see Figure 39 and Figure 40). The primary rubber chevron spring provides the longitudinal (yaw) and lateral stiffness of the primary suspension, while the coil spring provides the vertical stiffness. The middle axle, the primary damper provides the vertical damping of the primary suspension. The secondary suspension components are mainly the rubber springs (see Figure 39), which provides the vertical, lateral and yaw stiffness of the secondary suspension. In addition, the motors are flexibly connected to the bogie frame with rubber bushings (see Figure 39 and Figure 41). In this project, it is agreed to design a condition monitoring system concerning most of the suspension components related to the vehicle running behaviour. Table 10 summarises the suspension components of the vehicle and their general functions.

Figure 38 – FGC 254 diesel locomotive

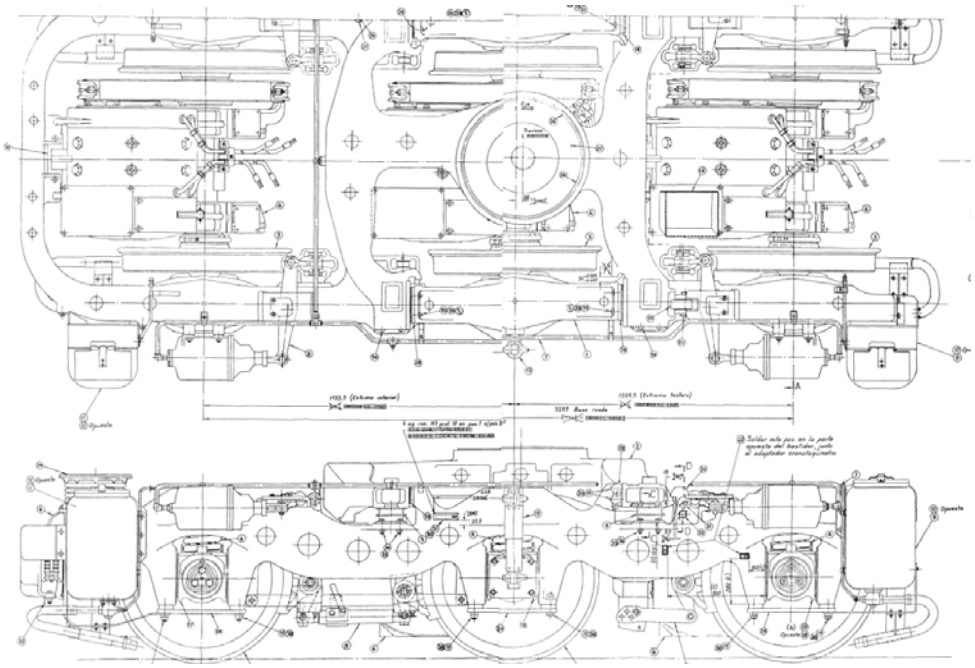

Figure 39 – Bogie plot of FGC 254 locomotive

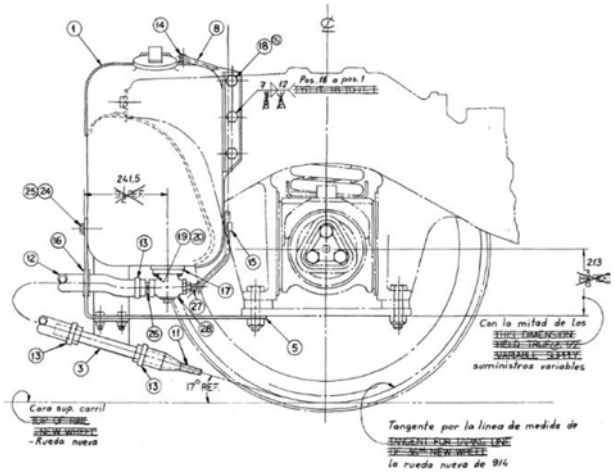

Figure 40 – Wheelset plot for FGC 254 locomotive

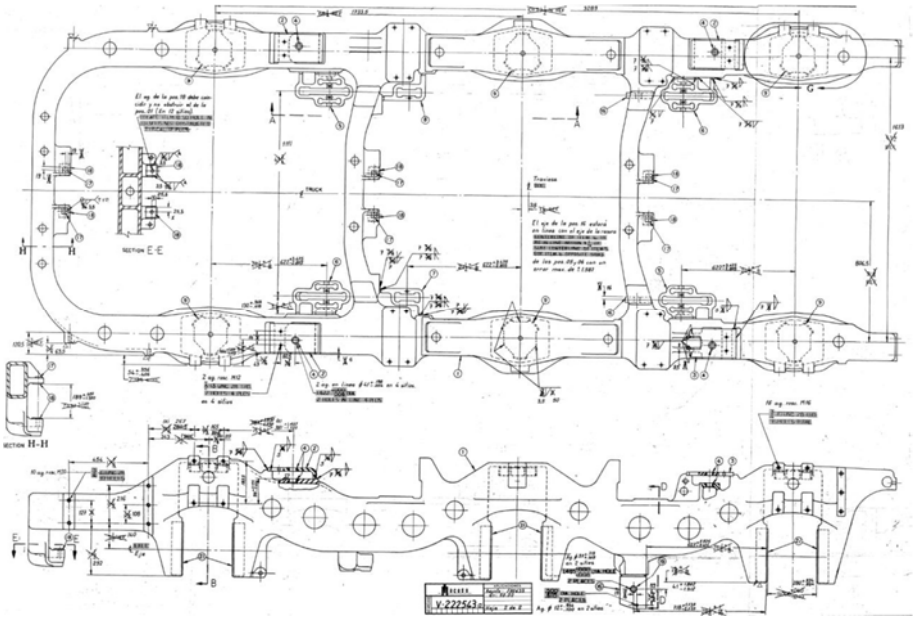

Figure 41 – Bogie frame assembly for FGC 254 locomotive

Table 10 – List of suspension components to be monitored for the FGC 254 locomotive

Suspension Component	Quantity	General Function
Primary coil springs	6 per bogie	Primary stiffness in vertical direction
Primary rubber springs	6 pairs per bogie	Primary stiffness in longitudinal (yaw) and lateral directions
Primary hydraulic dampers	2 per bogie	Primary damping in vertical direction
Secondary rubber springs	4 per bogie (8 per vehicle)	Secondary stiffness in vertical, lateral and yaw directions
Motor connection springs	3 per bogie	Primary stiffness for motor in vertical direction

For the vehicle dynamic system, it is well known that the vehicle suspension is a coupled system. Concerning each body of the vehicle (e.g., carbody, bogie frame and wheelset), there are 6 rigid modes: longitudinal, lateral, vertical, roll, pitch and yaw motions. Actually, each suspension component contributes to at least one mode. In order to realize the fault detection of the suspension system, it is necessary to decouple the contributions of the suspension components. To solve this problem, one straightforward way is to estimate the parameter value of the suspension element from the measured signals. With the identified value of suspension element, any deviation from the normal value can indicate a faulty condition. Table 11 lists the dynamic parameters to be estimated for realizing the fault diagnosis of the suspension components (with reference to Table 10).

Table 11 – Dynamic parameters of suspension components to be identified

Notation	Dynamic parameter	Quantity
K_{px}	Primary longitudinal stiffness	3 averages per bogie
K_{py}	Primary lateral stiffness	3 averages per bogie
K_{pz}	Primary vertical stiffness	6 sets per bogie
C_{pz}	Primary vertical damping coefficient	2 sets per bogie
K_{sx}	Secondary longitudinal stiffness	1 average per bogie
K_{sy}	Secondary lateral stiffness	2 averages per bogie
K_{sz}	Secondary vertical stiffness	4 per bogie
K_{mz}	Motor vertical stiffness	3 per bogie

9.1.1. Subsystem Configuration

In this case study, the condition monitoring of suspension component is achieved by using vibration signals collected at key locations of the running gear. The approach employed is able to realize the fault detection of the anomalies in the suspension system and provide the prompt diagnosis information to the railway operator for an efficient decision-making. In this case, the selection of the condition monitoring components is based on one fault detection method for the suspension system, known as Recursive Least-square Algorithm (RLS). In this section, the hardware selection based on this RLS approach will be illustrated.

The RLS approach relies on the vehicle-mounted equipment to measure the relative displacements and the velocities of the suspension components (springs and dampers), and the absolute accelerations of the bodies (bogie frames, carbodies and/or wheelsets). These physical quantities relate to the vehicle motions and can be measured directly or indirectly. The numerical integration and differentiation can be applied to the measured signals in order to obtain the required physical quantities. Generally speaking, the sensor types applicable could include the accelerometer, displacement transducer, gyroscope and inertial measurement unit (IMU). However, the most commonly used sensor in the railway application is the accelerometer due to its reliability in the harsh operational environment. Theoretically, other sensors could be utilised to realise the same function on the condition, however, their reliability and costs cannot be guaranteed for the operational environment. In this case study, the prototype of the condition monitoring system which uses only accelerometers will be introduced.

Figure 42 illustrates the original sensor layout proposed in the LOCATE project. It is possible to develop a condition monitoring system for the vehicle suspension based on this configuration. The suspension condition monitoring system incorporates three modules: vertical, lateral and yaw modules. Figure 43, Figure 44 and Figure 45 demonstrate the sensor layouts of the vertical, lateral and yaw (longitudinal) modules respectively.

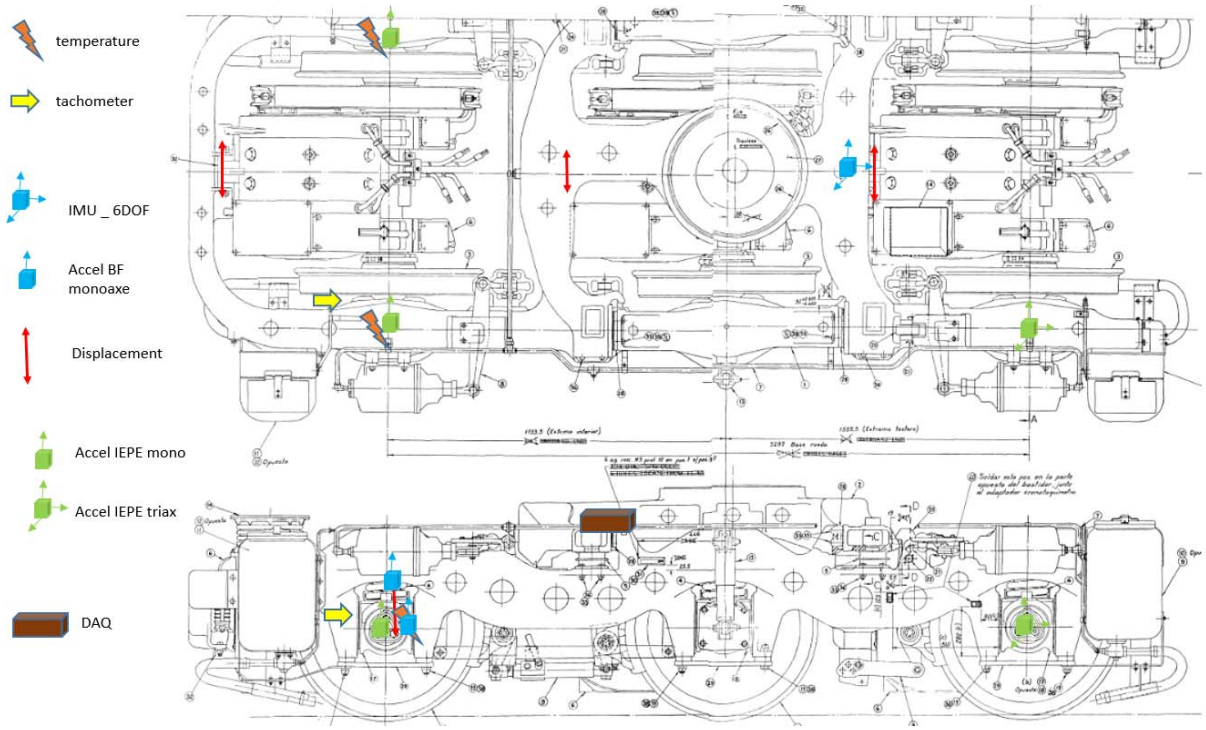

(a)

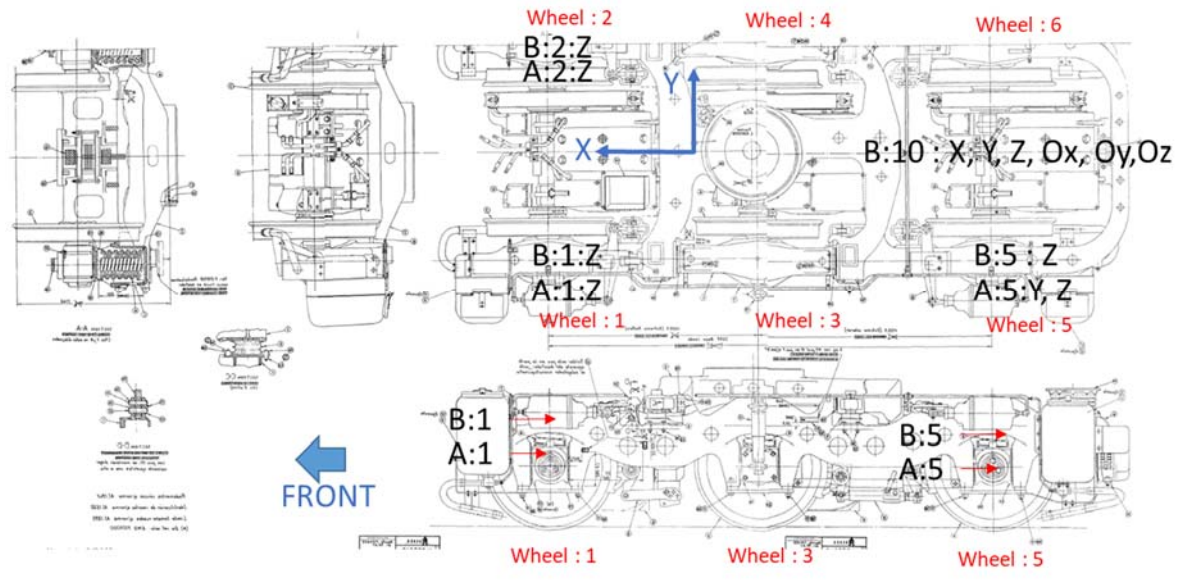

(b)

Figure 42 – Original sensor layout for FGC 254 locomotive bogie

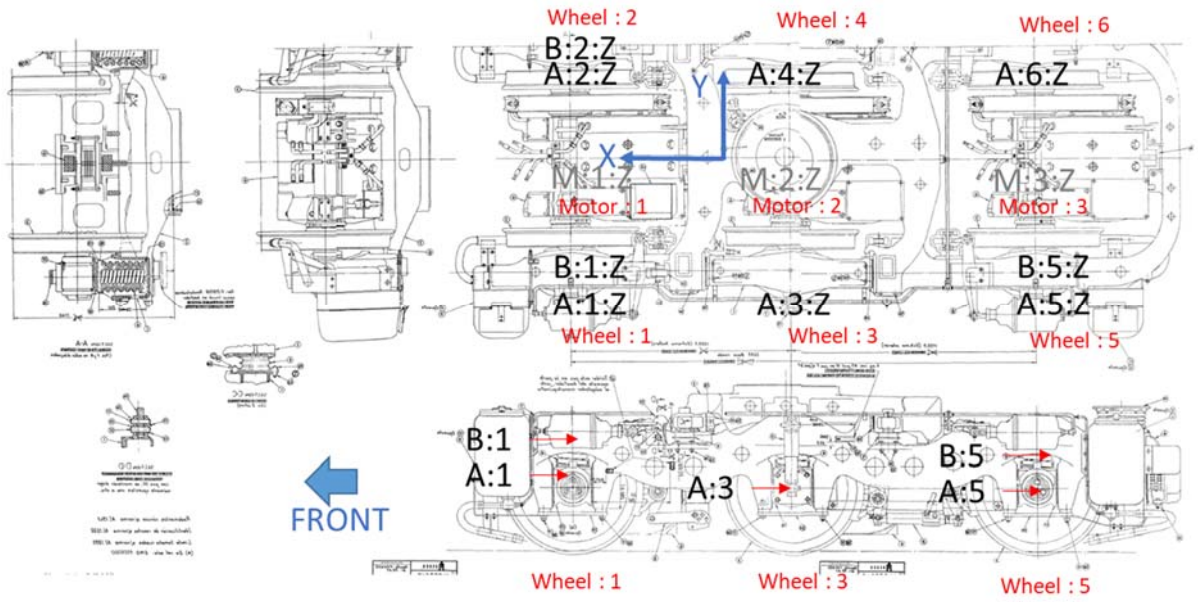

Figure 43 – Sensor layout for condition monitoring of vertical suspension components

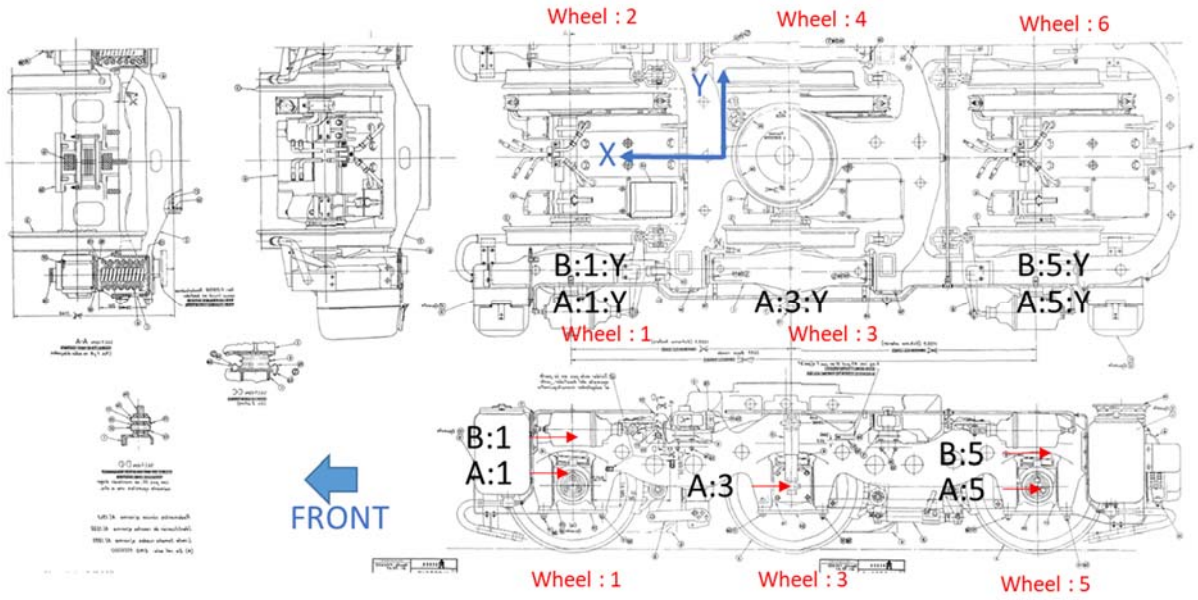

Figure 44 – Sensor layout for condition monitoring of lateral suspension components

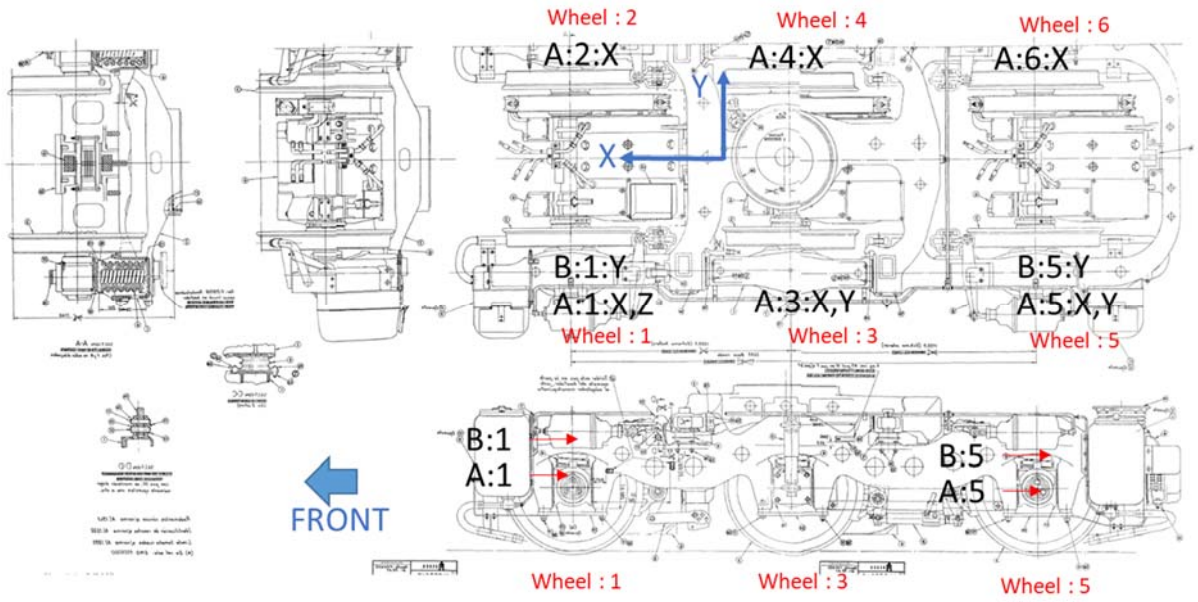

Figure 45 – Sensor layout for condition monitoring of suspension components in yaw direction

Figure 46 is a comprehensive sensor layout of the combination of these condition monitoring modules. In Figure 46, 6 accelerometers are installed on the axle boxes, including three triaxial accelerometers (measuring longitudinal, lateral, and vertical signals) and three biaxial accelerometers (measuring longitudinal and vertical signals). Three accelerometers are mounted on the corners of the bogie frame above the axleboxes, including two biaxial accelerometers (measuring lateral and vertical signals) and one monoaxial accelerometer (measuring the vertical signal). In addition, another three accelerometers are installed on the motors to measure the vertical acceleration of motors. On the carbody, two accelerometers are mounted on the bolster above the secondary springs, including one biaxial accelerometers (measuring lateral and vertical signals) and one monoaxial accelerometer (measuring the vertical signal).

Figure 46 provides the example for the realization of the monitoring system with the sensor installation from the theoretical view, however, the selections of the accelerometers can be more flexible according to the performance requirements. For instance, in order to improve the redundancy and the accuracy of the system, more sensors and/or channels can be added to the monitoring system. On the other side, certain accelerometers or channels could be removed without affecting the diagnosis performance: For example, the accelerometers on the carbody and motor could be removed, since the carbody and motor motions are relatively small compared with wheelsets. Besides, given the wheelbase is known and vehicle speed is recorded during the operation, the acceleration signals from one axle could be approximated as a time delay/advance of the signals measured from a different axle of the same bogie. That is also because for the unsprung mass, the force from the rail is much higher than that from the suspension. Definitely, the sensor reduction should be carried out in a very cautious way. Figure 47 provides a possible sensor layout with a minimum sensor installation.

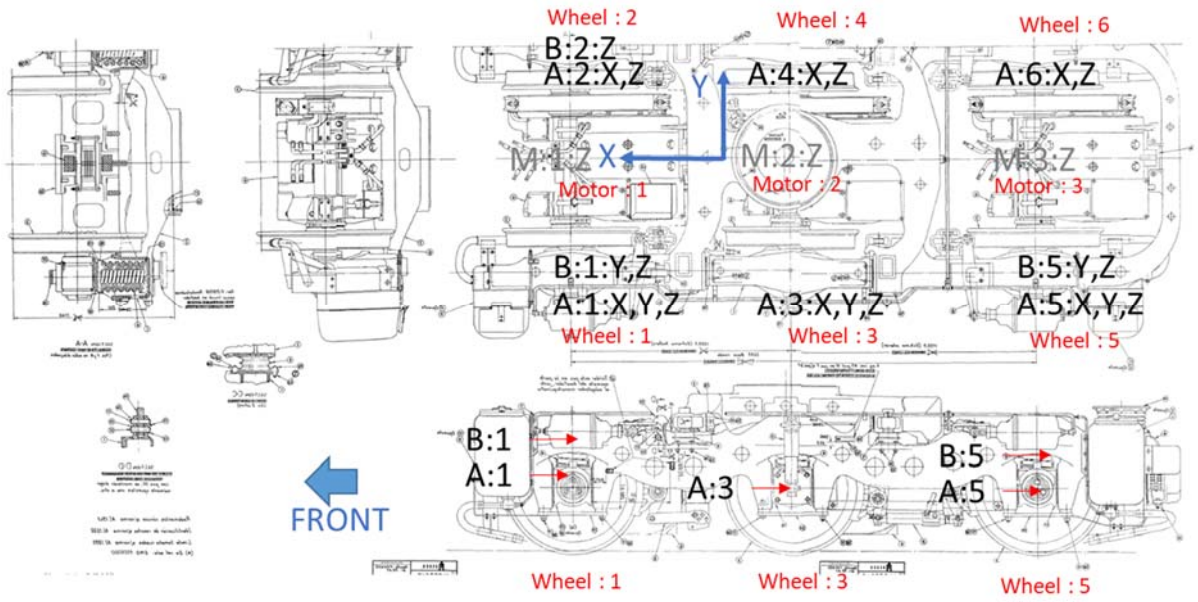

Figure 46 – A comprehensive sensor layout for condition monitoring of all suspension components

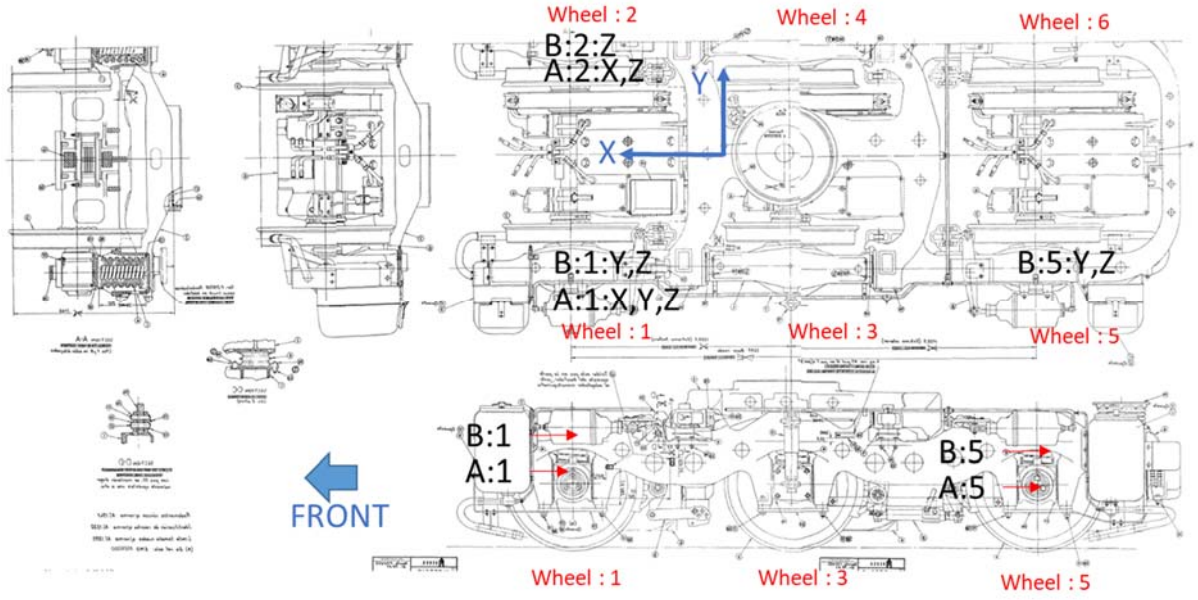

Figure 47 – Sensor layout for condition monitoring of suspensions with minimum sensors

Table 12 lists all the quantities needed for the parameter estimates. All these quantities can be derived readily from the measured acceleration signals together with straightforward geometric calculations. It is possible to acquire the relative displacement of the spring and relative velocity of the damper. The velocity and displacement data can be obtained by the integrations the relative acceleration signals from the accelerometers. The high-pass filtering is required for the convergence of the integration procedure. In reality, the band-pass filtering should be utilised,

because the high-frequency components of the measurements, which may be due to the elastic vibration without obeying the rigid dynamics, should be eliminated from the RLS-based fault detection algorithm.

Table 12 – Deduced quantities from measured signals

Notation	Dynamic parameter	Quantity
D_{px}	Displacements for primary longitudinal stiffness	3 data sets per module
D_{py}	Displacements for primary lateral stiffness	3 data sets per module
D_{pz}	Displacements for primary vertical stiffness	6 data sets per module
V_{pz}	Velocities for primary vertical damping	2 data sets per module
D_{sx}	Displacements for secondary longitudinal stiffness	1 data set per module
D_{sy}	Displacements for secondary lateral stiffness	2 data set per module
D_{sz}	Displacements for secondary vertical stiffness	4 data sets per module
D_{mz}	Displacements for motor linkage vertical stiffness	3 data sets per module
A_{bfz}	Vertical acceleration of bogie frame	1 data set per module
A_{bfy}	Lateral acceleration of bogie frame	1 data set per module
$A_{\mathrm{bf}\psi}$	Yaw angular acceleration of bogie frame	1 data set per module

9.1.1.1. Vertical module

The vertical module monitors the vertical suspension parameters, including primary vertical stiffness, primary vertical damping coefficients, secondary vertical stiffness, and motor vertical stiffness. In the vertical module, the states are the relative displacements for the primary, secondary, and motor vertical stiffness and relative velocities for the primary vertical damping coefficients, 15 quantities in total.

The output observation is the vertical acceleration of the bogie frame. The fundamental dynamic equation is:

$$M_{\mathrm{bf}}A_{\mathrm{bfz}} = \sum_{i=1}^{6} K_{\mathrm{pz}i}D_{\mathrm{pz}i} + \sum_{j=3}^{4} C_{\mathrm{pz}j}V_{\mathrm{pz}j} + \sum_{k=1}^{4} K_{\mathrm{sz}k}D_{\mathrm{sz}k} + \sum_{l=1}^{3} K_{\mathrm{mz}l}D_{\mathrm{mz}l} \tag{32}$$

where M_{bf} is the mass of the bogie frame.

According to the dynamic equation in the form of least square, the estimate parameter matrix is

$$\boldsymbol{\theta}_{\mathbf{z}} = [\, K_{\mathrm{pz1}}\ K_{\mathrm{pz2}}\ K_{\mathrm{pz3}}\ K_{\mathrm{pz4}}\ K_{\mathrm{pz5}}\ K_{\mathrm{pz6}}\ C_{\mathrm{pz3}}\ C_{\mathrm{pz4}}\ K_{\mathrm{sz1}}\ K_{\mathrm{sz2}}\ K_{\mathrm{sz3}}\ K_{\mathrm{sz4}}\ K_{\mathrm{mz1}}\ K_{\mathrm{mz2}}\ K_{\mathrm{mz3}}]^{T} \tag{33}$$

The state matrix is:

$$\mathbf{X}_{\mathbf{z}} = [\, D_{\mathrm{pz1}}\ D_{\mathrm{pz2}}\ D_{\mathrm{pz3}}\ D_{\mathrm{pz4}}\ D_{\mathrm{pz5}}\ D_{\mathrm{pz6}}\ V_{\mathrm{pz3}}\ V_{\mathrm{pz4}}\ D_{\mathrm{sz1}}\ D_{\mathrm{sz2}}\ D_{\mathrm{sz3}}\ D_{\mathrm{sz4}}\ D_{\mathrm{mz1}}\ D_{\mathrm{mz2}}\ D_{\mathrm{mz3}}\ ]^{T} \tag{34}$$

The observation is:

$$Y_{\mathrm{z}} = M_{\mathrm{bf}}A_{\mathrm{bfz}} \tag{35}$$

9.1.1.2. Lateral module

The lateral module monitors the lateral parameters, including primary lateral stiffness and secondary lateral stiffness. In the lateral module, the states are the relative displacements for the primary and secondary lateral stiffness, 5 quantities in total. The observation is the lateral acceleration of the bogie frame.

The fundamental dynamic equation is:

$$M_{\mathrm{bf}}A_{\mathrm{bfy}} = 2K_{\mathrm{py1}}D_{\mathrm{py1}} + 2K_{\mathrm{py2}}D_{\mathrm{py2}} + 2K_{\mathrm{py3}}D_{\mathrm{py3}} + 2K_{\mathrm{sy1}}D_{\mathrm{sy1}} + 2K_{\mathrm{sy2}}D_{\mathrm{sy2}} \tag{36}$$

The estimate parameter matrix is:

$$\boldsymbol{\theta}_{\mathbf{y}} = [\, K_{\mathrm{py1}}\ K_{\mathrm{py2}}\ K_{\mathrm{py3}}\ K_{\mathrm{sy1}}\ K_{\mathrm{sy2}}\ ]^T \tag{37}$$

The state matrix is:

$$\mathbf{X}_{\mathbf{y}} = [\, 2D_{\mathrm{py1}}\ 2D_{\mathrm{py2}}\ 2D_{\mathrm{py3}}\ 2D_{\mathrm{sy1}}\ 2D_{\mathrm{sy2}}\ ]^T \tag{38}$$

The observation is:

$$Y_{\mathrm{y}} = M_{\mathrm{bf}}A_{\mathrm{bfy}} \tag{39}$$

9.1.1.3. Yaw module

The yaw module monitors the longitudinal parameters, including primary longitudinal stiffness and secondary longitudinal stiffness. In the yaw module, the states are the relative displacements for primary and secondary longitudinal stiffness and relative displacements for primary and secondary lateral stiffness, 8 quantities in total. The observation is the yaw acceleration of the bogie frame.

The fundamental dynamic equation is:

$$\begin{aligned} J_{\mathrm{bf\psi}}A_{\mathrm{bf\psi}} = {} & 2K_{\mathrm{px1}}D_{\mathrm{px1}}d_{\mathrm{p}} + 2K_{\mathrm{px2}}D_{\mathrm{px2}}d_{\mathrm{p}} + 2K_{\mathrm{px3}}D_{\mathrm{px3}}d_{\mathrm{p}} + \\ & 2K_{\mathrm{py1}}D_{\mathrm{py1}}l_{\mathrm{p}} - 2K_{\mathrm{py3}}D_{\mathrm{py3}}l_{\mathrm{p}} + 4K_{\mathrm{sx}}D_{\mathrm{sx}}d_{\mathrm{s}} + 2K_{\mathrm{sy1}}D_{\mathrm{sy1}}l_{\mathrm{s}} - 2K_{\mathrm{sy2}}D_{\mathrm{sy2}}l_{\mathrm{s}} \end{aligned} \tag{40}$$

where $J_{\mathrm{bf\psi}}$ is the yaw inertia of the bogie frame. d_{p} is the half of the lateral distance between primary longitudinal springs. l_{p} is the half of the longitudinal distance between lateral springs. d_{s} is the half of the lateral distance between secondary springs. l_{s} is the half of the longitudinal distance between secondary springs.

The estimate parameter matrix is:

$$\boldsymbol{\theta}_{\boldsymbol{\psi}} = [\, K_{\mathrm{px1}}\ K_{\mathrm{px2}}\ K_{\mathrm{px3}}\ K_{\mathrm{py1}}\ K_{\mathrm{py3}}\ K_{\mathrm{sx}}\ K_{\mathrm{sy1}}\ K_{\mathrm{sy2}}\ ]^T \tag{41}$$

The state matrix is:

$$\mathbf{X}_{\boldsymbol{\psi}} = [\, 2D_{\mathrm{px1}}d_{\mathrm{p}}\ \ 2D_{\mathrm{px2}}d_{\mathrm{p}}\ \ 2D_{\mathrm{px3}}d_{\mathrm{p}}\ \ 2D_{\mathrm{py1}}l_{\mathrm{p}}\ \ -2D_{\mathrm{py3}}l_{\mathrm{p}}\ \ 4D_{\mathrm{sx}}d_{\mathrm{s}}\ \ 2D_{\mathrm{sy1}}l_{\mathrm{s}}\ \ -2D_{\mathrm{sy2}}l_{\mathrm{s}}\ ]^T \tag{42}$$

The observation is:

$$Y_{\psi} = J_{\mathrm{bf\psi}}\alpha_{\mathrm{bf\psi}} \tag{43}$$

The accelerations and angular accelerations of the bogie frame are selected as the observation, because the inertias of the bogie frame can be measured readily and do not change with different

loading conditions.

9.1.2. RLS Estimate

The data measured by the condition monitoring system should be utilised in the RLS algorithm [12] for the parameter estimation. The iterative RLS equation is presented as follows:
For each time step t, the parameter estimate update is expressed with a symmetric regression matrix $\mathbf{P}$

$$\widehat{\boldsymbol{\theta}}(t+1) = \widehat{\boldsymbol{\theta}}(t) + \frac{\mathbf{P}(t)\mathbf{X}(t+1)}{1+\mathbf{X}^T(t+1)\mathbf{P}(t)\mathbf{X}(t+1)}\left[Y(t+1) - \mathbf{X}^T(t+1)\widehat{\boldsymbol{\theta}}(t)\right] \quad (44)$$

The regression matrix update is expressed as:

$$\mathbf{P}(t+1) = \mathbf{P}(t) - \frac{\mathbf{P}(t)\mathbf{X}(t+1)\mathbf{X}^T(t+1)\mathbf{P}(t)}{1+\mathbf{X}^T(t+1)\mathbf{P}(t)\mathbf{X}(t+1)} \quad (45)$$

With this iterative scheme, the suspension parameters can be estimated continuously during the operational condition. The parameter deviation of the suspension component due to the fault can be identified promptly. The fault information should be transmitted to the drivers' cabin for the decision-making via the vehicle bus. It can also be transmitted to the railway operator via a wireless communication in order to implement the condition-based maintenance.

This is the most 'robust' version for the identification of the parameter. For the real measurement, this form should be used to obtain a convergent result with a fast identification speed. By restarting the RLS algorithm with a section of data measured during the operation, it is feasible to estimate the suspension parameter during this time period. Theoretically, with the introduction of a forgetting factor λ, it is possible to identify the degradation process of the suspension parameters. The form of the recursive least square is expressed as:
The parameter estimate update is expressed as:

$$\widehat{\boldsymbol{\theta}}(t+1) = \widehat{\boldsymbol{\theta}}(t) + \frac{\mathbf{P}(t)\mathbf{X}(t+1)}{\lambda+\mathbf{X}^T(t+1)\mathbf{P}(t)\mathbf{X}(t+1)}\left[Y(t+1) - \mathbf{X}^T(t+1)\widehat{\boldsymbol{\theta}}(t)\right] \quad (46)$$

The regression matrix update is expressed as:

$$\mathbf{P}(t+1) = \lambda^{-1}\mathbf{P}(t) - \frac{\lambda^{-1}\mathbf{P}(t)\mathbf{X}(t+1)\mathbf{X}^T(t+1)\mathbf{P}(t)}{\lambda+\mathbf{X}^T(t+1)\mathbf{P}(t)\mathbf{X}(t+1)} \quad (47)$$

9.1.2.1. Implementation of RLS with MATLAB/Simulink

This RLS based condition monitoring algorithm can be implemented with MATLAB/Simulink software in a relatively simple way. Figure 48 shows a general Simulink plot for this RLS based approach for the suspension condition monitoring. The measured acceleration signals related to the suspension components are integrated into displacement or velocity signals. The measured accelerations related to the observations are multiplied with the mass to obtain the inertia forces. The identical bandpass filtering is applied to these two sets of signals. The filtered displacement and velocity signals are fed into the 'Regressors' port and the filtered force signals are fed into the 'Output' port. The output of RLS estimator is the estimated suspension parameters.

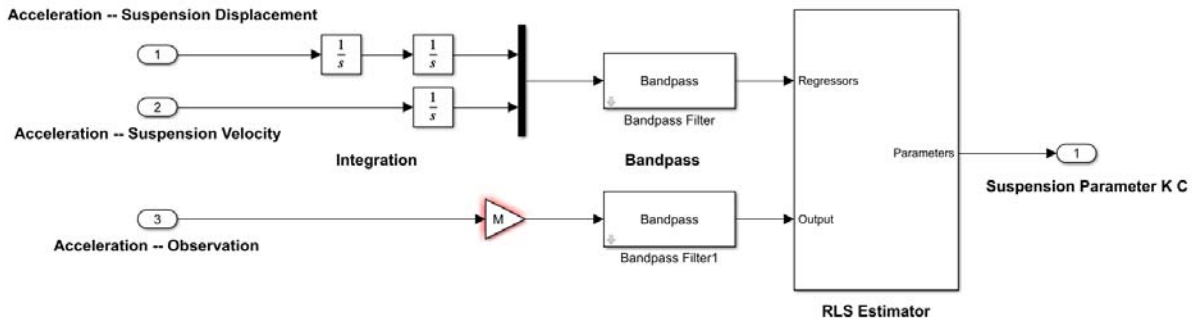

Figure 48 – Implementation of RLS based approach with MATLAB/Simulink

Due the simplicity of this approach, the RLS based model can be complied to relatively simple C/C++ codes. These codes can be run within a low-cost electronic device, such as Raspberry-Pie. In this sense, the suspension condition monitoring system can function online with a low computational requirement during the operation.

In fact, theoretically it could be more efficient to use a derivative form to estimate the suspension parameters, since the RLS parameter estimate can get a convergent result with a faster rate in this way. It means a derivative operation is applied to all the input acceleration signals, including for both suspensions and observations. The derivative form for this RLS approach is shown in Figure 49. However, it is necessary to mention that a derivative operation can amplify the signal noise. Therefore, a derivative form should be used in more cautious way.

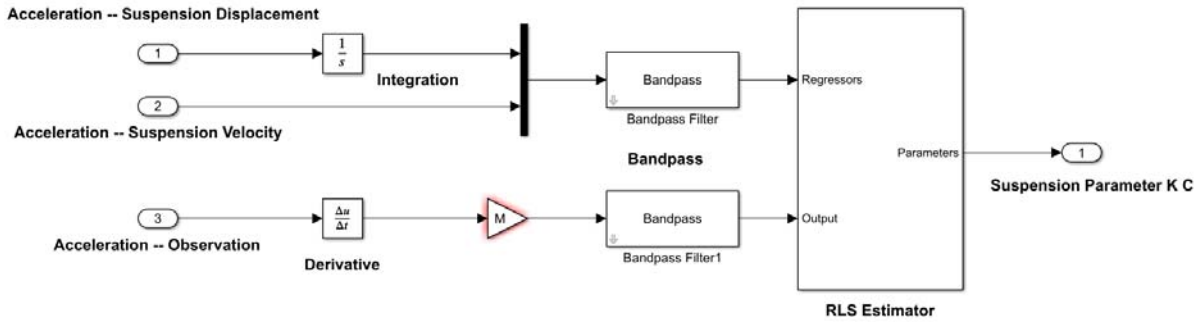

Figure 49 – Implementation of RLS based approach with MATLAB/Simulink – Derivative form

Figure 50, Figure 51 and Figure 52 show the Simulink models of RLS based condition monitoring methods for the vertical module, lateral module and yaw module, respectively.

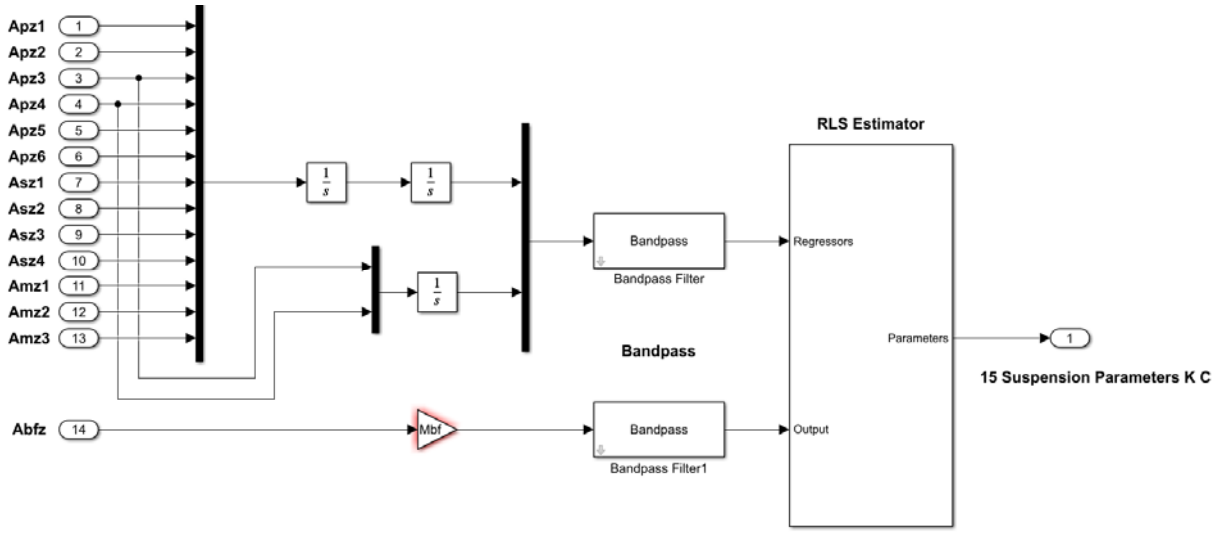

Figure 50 – Simulink model of RLS based condition monitoring approach – Vertical module

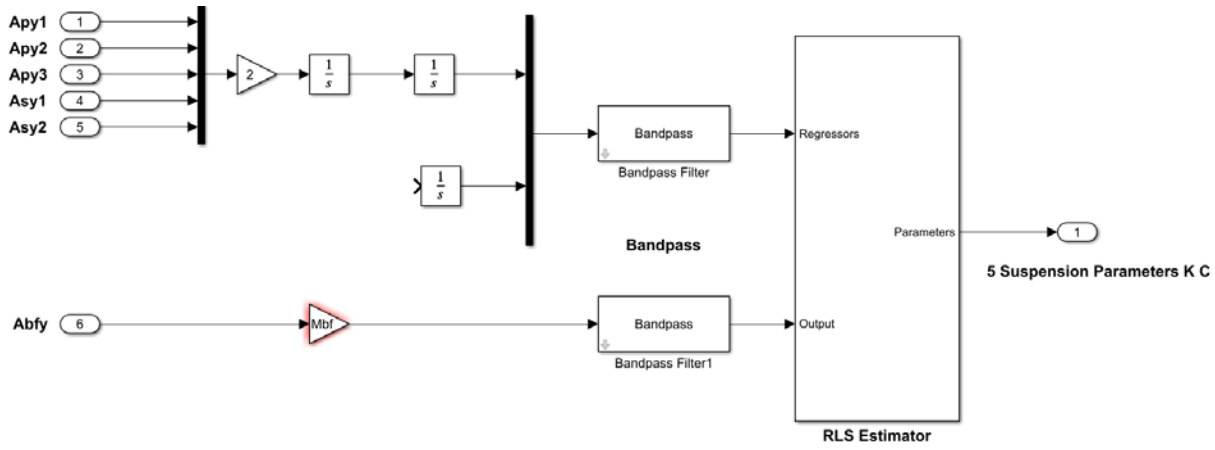

Figure 51 – Simulink model of RLS based condition monitoring approach – Lateral module

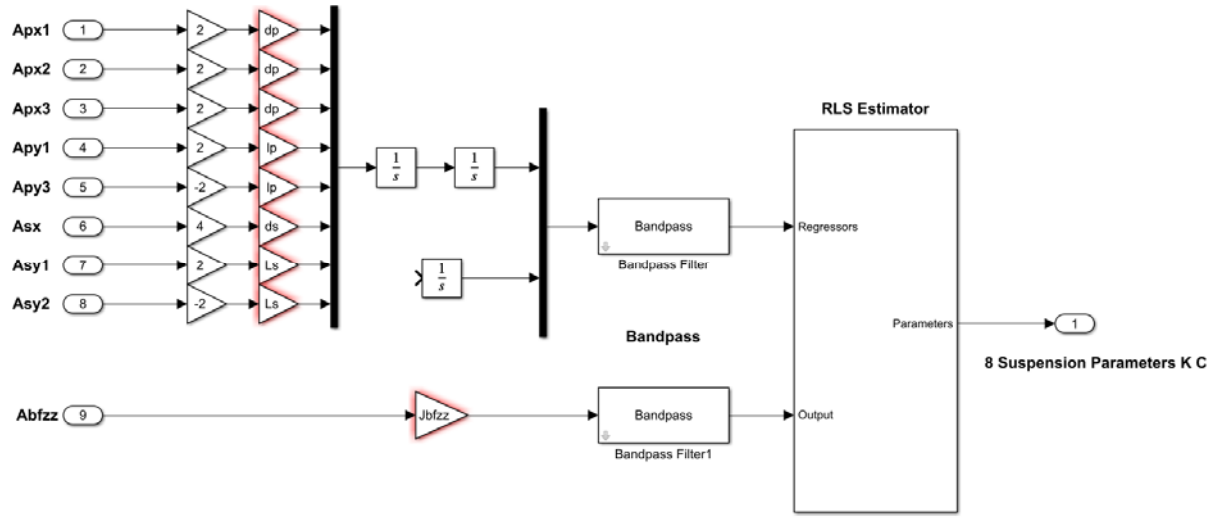

Figure 52 – Simulink model of RLS based condition monitoring approach – Yaw module

According to an extensive on-field investigation carried out by IST, in the primary lateral and longitudinal suspensions of FGC 254 locomotive there was no rubber spring between the bogie frame and the axle-box. Instead, there are some clearances and friction surfaces between the bogie frame and axle-box in the longitudinal and lateral directions. In this sense, the RLS method based on the linear system is no longer suitable for the fault detection in these directions because of the highly nonlinear effects of the clearance and friction. To be exact, since the dry friction force is not related to the amplitude of the relative velocity, it is impossible to estimate its 'damping coefficient' from a linear RLS model. In fact, these dry friction forces are not neglectable in the acceleration of the bogie frame. Therefore, it is very difficult for the RLS based algorithm to identify the linear suspension parameters from the system. Generally speaking, FGC 254 is a relatively old type of locomotive. These types of locomotives are not widely utilised in the present railway industry.

9.2. Condition Monitoring of Suspension System of Co-Co Locomotive with RLS Approach

Under the framework of this project, HUD decide to utilise another standard-gauge heavy-duty Co-Co locomotive to implement this RLS-based condition monitoring strategy. This locomotive prototype represents a currently widely used locomotive type with many linear suspension components, such as coil springs and viscous dampers. The total mass of this heavy-duty six axle locomotive is 126 t. The yaw stiffness of the primary suspension is 60 MN/m per axle. The bogie wheelbase of this locomotive is 4.2 m.

9.2.1. Vampire Modelling of Co-Co Locomotive

A Vampire model of this vehicle is employed to generate 'virtual measurements' to demonstrate the newly developed condition monitoring system. Figure 53 is a multi-body plot of this locomotive in the Vampire simulation environment, where all the suspension components are shown.

In this Vampire model, the primary coil spring and secondary rubber spring are modelled as shear spring elements. The share spring element considers the translational vertical and horizontal stiffnesses and the rotational shear and torsional stiffnesses. The primary rubber bushing is modelled as a bush element. The bush element considers both the stiffness and the damping of the element in all translational and rotational directions. The primary vertical damper, secondary lateral damper and yaw damper are modelled as damper elements. The damper element takes into account the behaviour of a damper-spring in series scenario. The 6 motors are modelled as individual masses with 6 DOFs. The connection between the motor and the wheelset is modelled as a bush element with no stiffness in rotational direction but very large stiffness in other directions. The linkage between the motor and bogie frame is modelled as a pin-link element. The pin-link element considers the stiffness and damping only along the linkage axle. The traction rod and roll bar are also modelled as bush elements in longitudinal and roll direction, respectively.

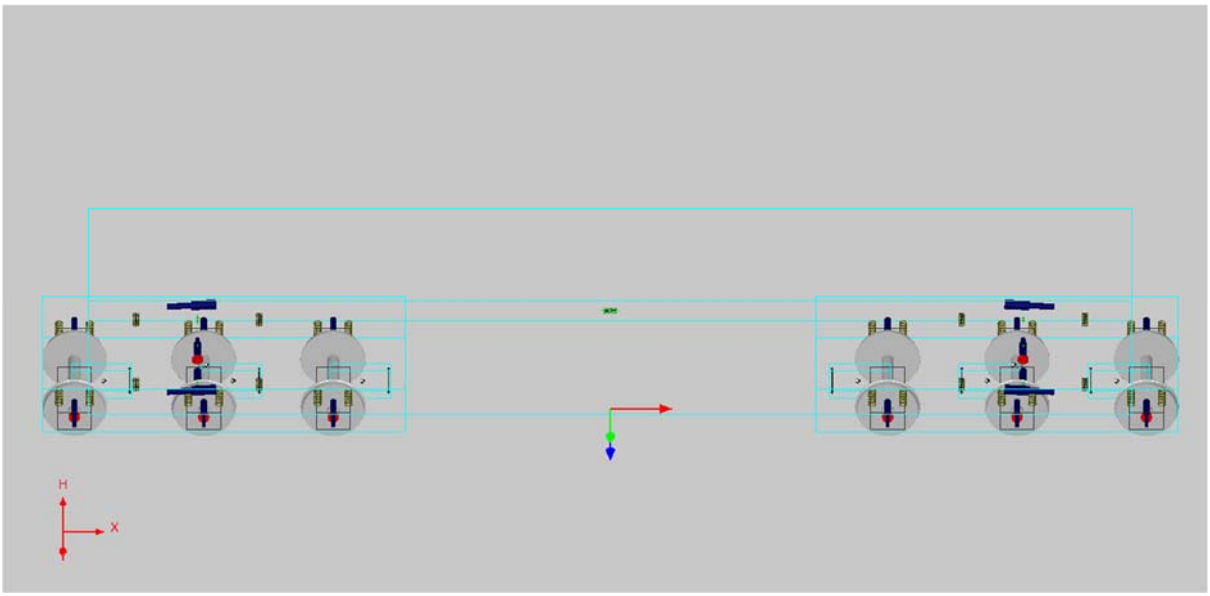

Figure 53 – Multi-body model of six axle locomotive in Vampire environment

With the reference of Table 12, the output quantities of this locomotive model from Vampire simulation results are listed in Table 13. The location layout of the sensor installation can be very similar to the sensor layout of FGC 254 locomotive. Figure 54 exhibits a complete sensor (accelerometer) layout for the condition monitoring of suspension components of this Co-Co locomotive.

Table 13 – Output quantities from Vampire simulation results

Notation	Dynamic parameter	Quantity
D_{px}	Displacements for primary longitudinal stiffness	3 data sets per module
D_{py}	Displacements for primary lateral stiffness	3 data sets per module
D_{pz}	Displacements for primary vertical stiffness	6 data sets per module
V_{pz}	Velocities for primary vertical damping	6 data sets per module
D_{sx}	Displacements for secondary longitudinal stiffness	1 data set per module
D_{sy}	Displacements for secondary lateral stiffness	1 data set per module
D_{sz}	Displacements for secondary vertical stiffness	4 data sets per module
V_{sy}	Velocity for secondary lateral damping	1 data set per module
V_{sx}	Velocity for secondary yaw damping	1 data set per module
D_{mz}	Displacements for motor linkage vertical stiffness	3 data sets per module
V_{mz}	Velocities for motor linkage vertical damping	3 data sets per module
A_{bfz}	Vertical acceleration of bogie frame	1 data set per module
A_{bfy}	Lateral acceleration of bogie frame	1 data set per module
$A_{bf\psi}$	Yaw angular acceleration of bogie frame	1 data set per module

In Figure 54, the red block represents the accelerometer installed on the vehicle. The arrow shows the direction of the acceleration measurement. 6 accelerometers (3 triaxial and 3 biaxial), labelled as 'W', are mounted on the axle-boxes to measure the vertical, lateral and longitudinal

accelerations of the axle-boxes. Three monoaxial accelerometers, labelled as 'M', are installed on the motors to measure their vertical motions. Three accelerometers (2 biaxial and 1 monoaxial), labelled as 'F', are mounted on the corners of the bogie frame to obtain the vertical, lateral and yaw accelerations of the bogie frame. One monoaxial accelerometer, labelled as 'C', is installed on the carbody to measure its vertical acceleration above the bogie pivot. Most motions of the carbody are much smaller than that of the bogie frame and wheelsets except the carbody pitch. All the motions of the suspension components and the observed bogie frame accelerations can be measured and/or calculated from this plot.

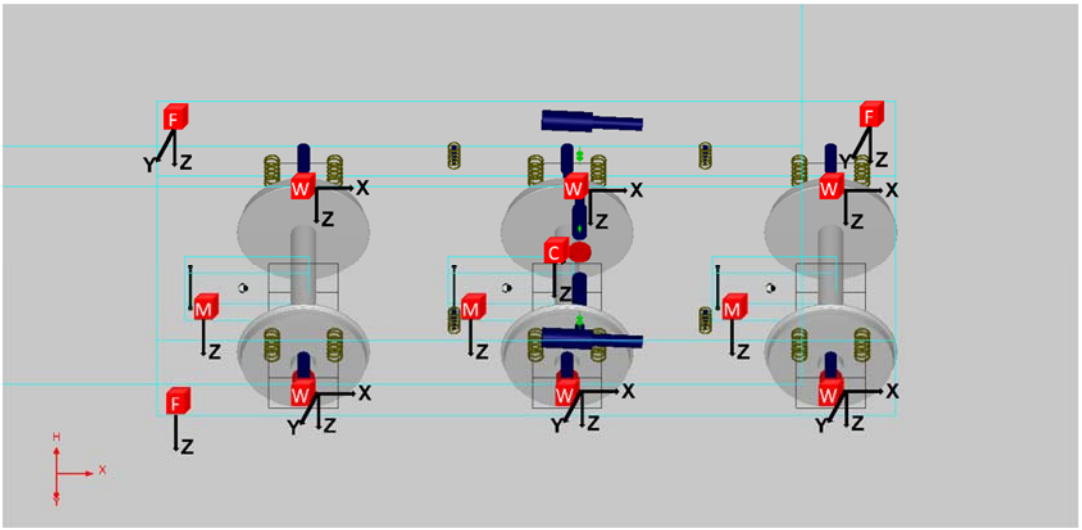

Figure 54 – Sensor layout for condition monitoring of Co-Co locomotive

9.2.2. RLS Estimation Model for Co-Co Locomotive

Correspondingly, the mathematical model for the vertical, lateral and yaw modules can be deduced according to the locomotive suspension configurations.

9.2.2.1. Vertical module

The vertical module monitors the vertical suspension parameters, including primary vertical stiffness, primary vertical damping coefficients, secondary vertical stiffness, and motor vertical stiffness and damping coefficients. In the vertical module, the states are the relative displacements for the primary, secondary, and motor vertical stiffness and relative velocities for the primary vertical damping coefficients and motor damping coefficients, 22 quantities in total. The output observation is the vertical acceleration of the bogie frame. The fundamental dynamic equation is:

$$M_{\mathrm{bf}}A_{\mathrm{bfz}} = \sum_{i=1}^{6} K_{\mathrm{pz}i}D_{\mathrm{pz}i} + \sum_{j=1}^{6} C_{\mathrm{pz}j}V_{\mathrm{pz}j} + \sum_{k=1}^{4} K_{\mathrm{sz}k}D_{\mathrm{sz}k} + \sum_{l=1}^{3} K_{\mathrm{mz}l}D_{\mathrm{mz}l} + \sum_{l=1}^{3} C_{\mathrm{mz}l}V_{\mathrm{mz}l} \qquad (48)$$

where M_{bf} is the mass of the bogie frame.

According to the dynamic equation in the form of least-square, the estimate parameter matrix is

$$\boldsymbol{\theta}_{\mathbf{z}} = \begin{matrix}[\, K_{\mathrm{pz1}}\ K_{\mathrm{pz2}}\ K_{\mathrm{pz3}}\ K_{\mathrm{pz4}}\ K_{\mathrm{pz5}}\ K_{\mathrm{pz6}}\ C_{\mathrm{pz1}}\ C_{\mathrm{pz2}}\ C_{\mathrm{pz3}}\ C_{\mathrm{pz4}}\ C_{\mathrm{pz5}}\ C_{\mathrm{pz6}}\ K_{\mathrm{sz1}}\ K_{\mathrm{sz2}}\ \dots \\ \dots K_{\mathrm{sz3}}\ K_{\mathrm{sz4}}\ K_{\mathrm{mz1}}\ K_{\mathrm{mz2}}\ K_{\mathrm{mz3}}\ C_{\mathrm{mz1}}\ C_{\mathrm{mz2}}\ C_{\mathrm{mz3}}]^T \end{matrix} \tag{49}$$

The state matrix is:

$$\mathbf{X}_{\mathbf{z}} = \begin{matrix}[\, D_{\mathrm{pz1}}\ D_{\mathrm{pz2}}\ D_{\mathrm{pz3}}\ D_{\mathrm{pz4}}\ D_{\mathrm{pz5}}\ D_{\mathrm{pz6}}\ V_{\mathrm{pz1}}\ V_{\mathrm{pz2}}\ V_{\mathrm{pz3}}\ V_{\mathrm{pz4}}\ V_{\mathrm{pz5}}\ V_{\mathrm{pz6}}\ D_{\mathrm{sz1}}\ D_{\mathrm{sz2}}\ \dots \\ \dots D_{\mathrm{sz3}}\ D_{\mathrm{sz4}}\ D_{\mathrm{mz1}}\ D_{\mathrm{mz2}}\ D_{\mathrm{mz3}}\ V_{\mathrm{mz1}}\ V_{\mathrm{mz2}}\ V_{\mathrm{mz3}}]^T \end{matrix} \tag{50}$$

The observation is:

$$Y_{\mathrm{z}} = M_{\mathrm{bf}} A_{\mathrm{bfz}} \tag{51}$$

9.2.2.2. Lateral module

The lateral module monitors the lateral parameters, including primary lateral stiffness, secondary lateral stiffness and secondary lateral damping coefficients. In the lateral module, the states are the relative displacements for the primary and secondary lateral stiffness, and relative velocity for the secondary lateral damper, 5 quantities in total. The observation is the lateral acceleration of the bogie frame. The fundamental dynamic equation is:

$$M_{\mathrm{bf}} A_{\mathrm{bfy}} = 2K_{\mathrm{py1}} D_{\mathrm{py1}} + 2K_{\mathrm{py2}} D_{\mathrm{py2}} + 2K_{\mathrm{py3}} D_{\mathrm{py3}} + 4K_{\mathrm{sy}} D_{\mathrm{sy}} + 2C_{\mathrm{sy}} V_{\mathrm{sy}} \tag{52}$$

The estimate parameter matrix is:

$$\boldsymbol{\theta}_{\mathbf{y}} = [\, K_{\mathrm{py1}}\ K_{\mathrm{py2}}\ K_{\mathrm{py3}}\ K_{\mathrm{sy}}\ C_{\mathrm{sy}}\ ]^T \tag{53}$$

The state matrix is:

$$\mathbf{X}_{\mathbf{y}} = [\, 2D_{\mathrm{py1}}\ 2D_{\mathrm{py2}}\ 2D_{\mathrm{py3}}\ 4D_{\mathrm{sy}}\ 2V_{\mathrm{sy}}\ ]^T \tag{54}$$

The observation is:

$$Y_{\mathrm{y}} = M_{\mathrm{bf}} A_{\mathrm{bfy}} \tag{55}$$

9.2.2.3. Yaw module

The yaw module monitors the parameters in yaw direction, including primary longitudinal stiffness, secondary longitudinal stiffness, and secondary yaw damping. In the yaw module, the states are the relative displacements for primary and secondary longitudinal stiffness, relative displacements for primary and secondary lateral stiffness, and relative velocities for secondary yaw damping, 8 quantities in total. The observation is the yaw acceleration of the bogie frame. The fundamental dynamic equation is:

$$\begin{aligned} J_{\mathrm{bf}\psi} A_{\mathrm{bf}\psi} = {} & 2K_{\mathrm{px1}} D_{\mathrm{px1}} d_{\mathrm{p}} + 2K_{\mathrm{px2}} D_{\mathrm{px2}} d_{\mathrm{p}} + 2K_{\mathrm{px3}} D_{\mathrm{px3}} d_{\mathrm{p}} + \\ & 2K_{\mathrm{py1}} D_{\mathrm{py1}} l_{\mathrm{p}} - 2K_{\mathrm{py3}} D_{\mathrm{py3}} l_{\mathrm{p}} + 4K_{\mathrm{sx}} D_{\mathrm{sx}} d_{\mathrm{s}} + 4K_{\mathrm{sy}} D_{\mathrm{sy}} l_{\mathrm{s}} + 2C_{\mathrm{sx}} V_{\mathrm{sx}} d_{\mathrm{d}} \end{aligned} \tag{56}$$

*w*here $J_{\mathrm{bf}\psi}$ is the yaw inertia of the bogie frame. d_{p} is the half of the lateral distance between primary longitudinal springs. l_{p} is the half of the longitudinal distance between lateral springs. d_{s}

is the half of the lateral distance between secondary springs. l_s is the half of the longitudinal distance between secondary springs. d_d is the half of the lateral distance between the yaw dampers.

The estimate parameter matrix is:

$$\boldsymbol{\theta}_{\boldsymbol{\psi}} = [\, K_{px1}\ K_{px2}\ K_{px3}\ K_{py1}\ K_{py3}\ K_{sx}\ K_{sy}\ C_{sx}\,]^T \tag{57}$$

The state matrix is:

$$\mathbf{X}_{\boldsymbol{\psi}} = [\, 2D_{px1}d_p\ \ 2D_{px2}d_p\ \ 2D_{px3}d_p\ \ 2D_{py1}l_p\ \ -2D_{py3}l_p\ \ 4D_{sx}d_s\ \ 4D_{sy}l_s\ \ 2C_{sx}d_d\,]^T \tag{58}$$

The observation is:

$$Y_{\psi} = J_{bf\psi}\alpha_{bf\psi} \tag{59}$$

9.2.2.4. Implementation of RLS for Co-Co locomotive in MATLAB/Simulink

Based on the same principal with FGC 254 locomotive, Figure 55, Figure 56 and Figure 57 show the Simulink plots of condition monitoring approaches for the lateral, yaw and vertical modules of this Co-Co locomotive, respectively. In these models, the differentiations are utilised for the states variables (regressors) and observations (outputs) to obtain fast convergent estimations.

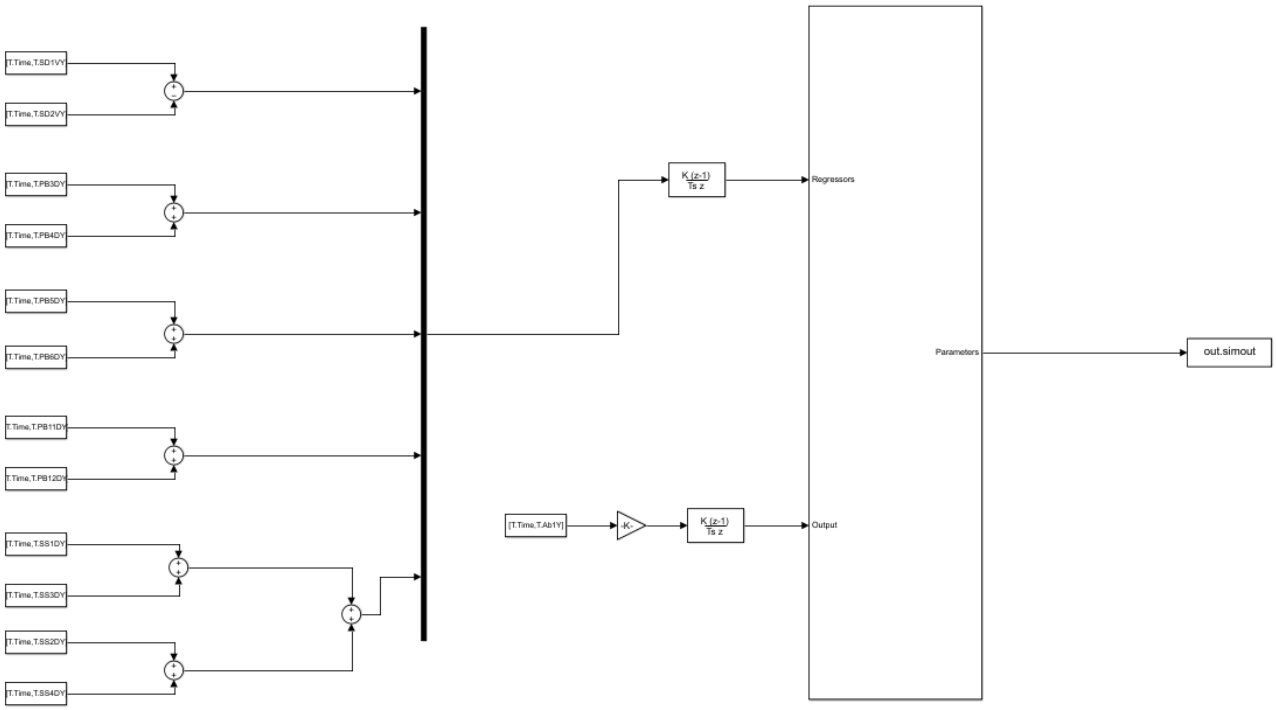

Figure 55 – Simulink plot of RLS-based condition monitoring approach – Lateral module of Co-Co locomotive

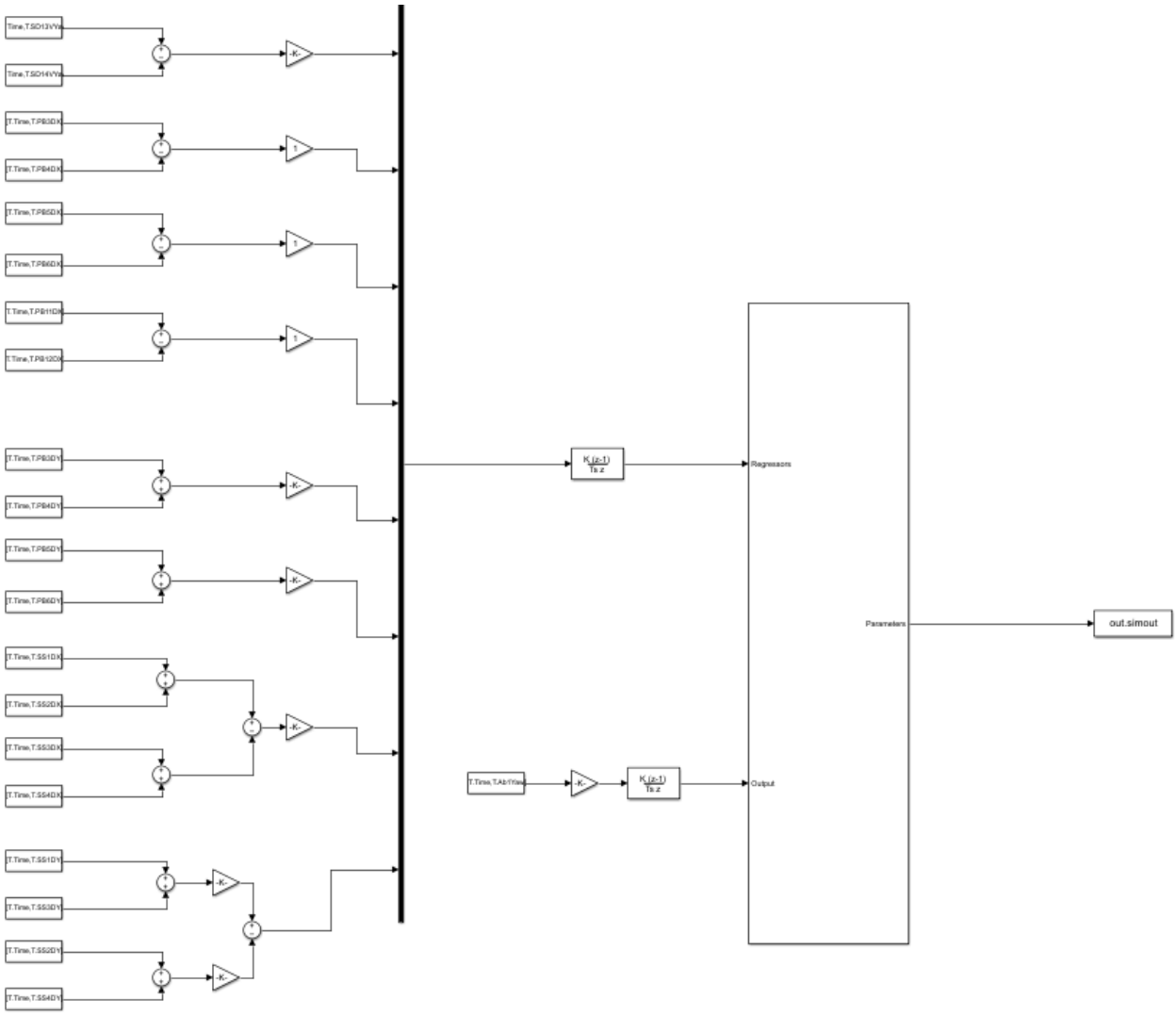

Figure 56 – Simulink plot of RLS-based condition monitoring approach – Yaw module of Co-Co locomotive

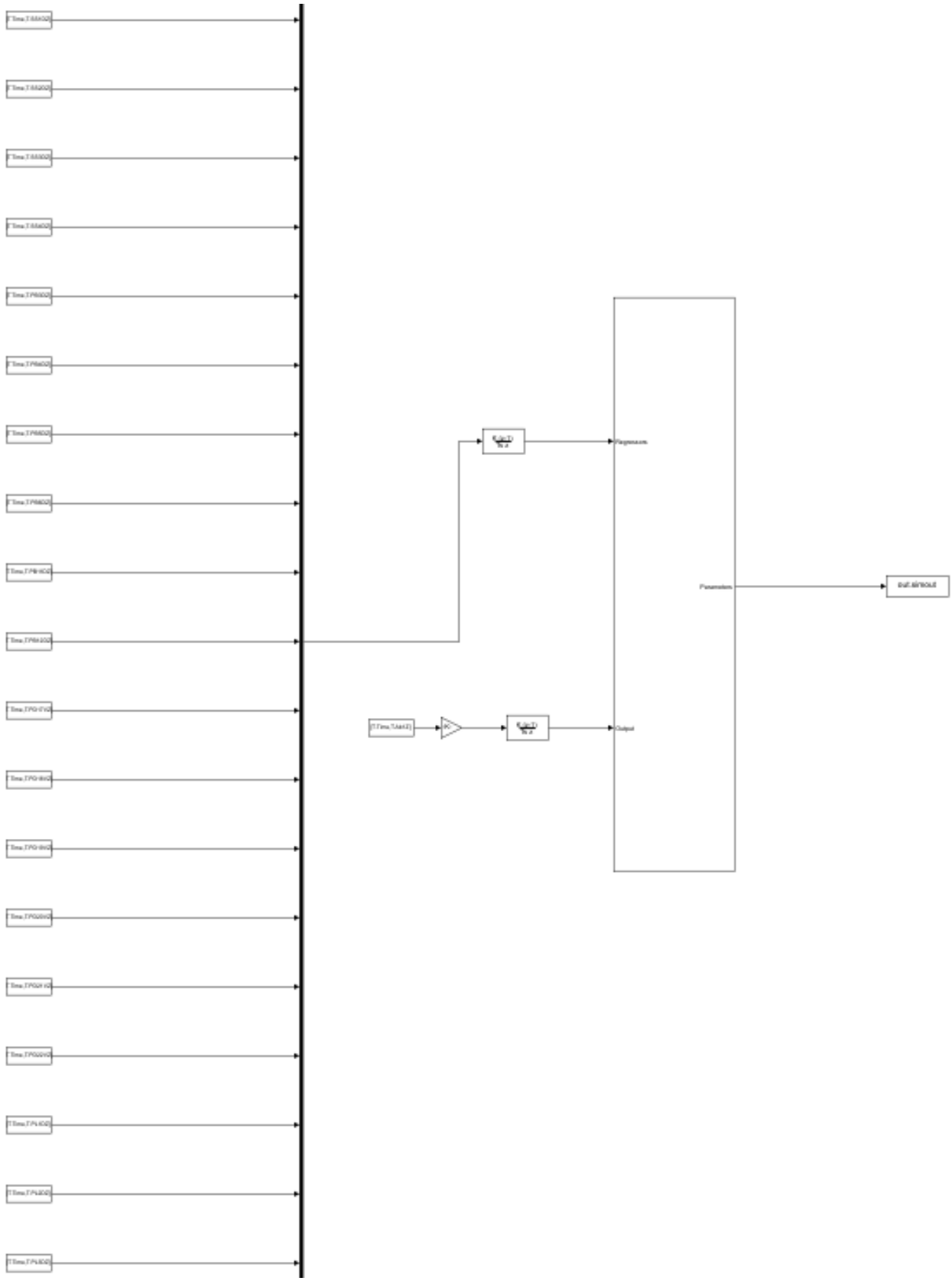

Figure 57 – Simulink plot of RLS-based condition monitoring approach – Vertical module of Co-Co locomotive

9.2.3. Multi-body Simulation with Vampire Software

To validate the feasibility of the proposed condition monitoring strategy, several Vampire simulations are used to generate the virtual measurements for the fault-free and faulty vehicle scenarios. Both the fault-free and faulty cases utilise the same track case.

The locomotive was simulated operating at a speed of 100 km/h on straight track with representative track irregularities, 'Track-160'. The conventional 56E1 rail profile (inclined at 1:20) and P8 wheel profile has been utilised in the simulations. The output data generated from the simulated vehicle were exported at a sampling frequency of 1 kHz (sampling time of 1 ms), which is a common sampling frequency for acceleration measurements. A track length of 3,000 m has been used in the simulations. Overall, 108,000 data samples were collected for each output channel from each Vampire simulation.

The Vampire output data was converted into the required variables in the MATLAB workspace. Simulink reads these variables into the RLS block (in System Identification Toolbox) as regressors and an observation. The data exported from the RLS block are the time series of the estimated suspension parameters. Because the sampling frequency of the Vampire output channel is 1 kHz, the calculation frequency in RLS block is also set as 1 kHz. To obtain the most robust estimate of the parameter from the RLS estimator, the forgetting factor in RLS is set as 1.

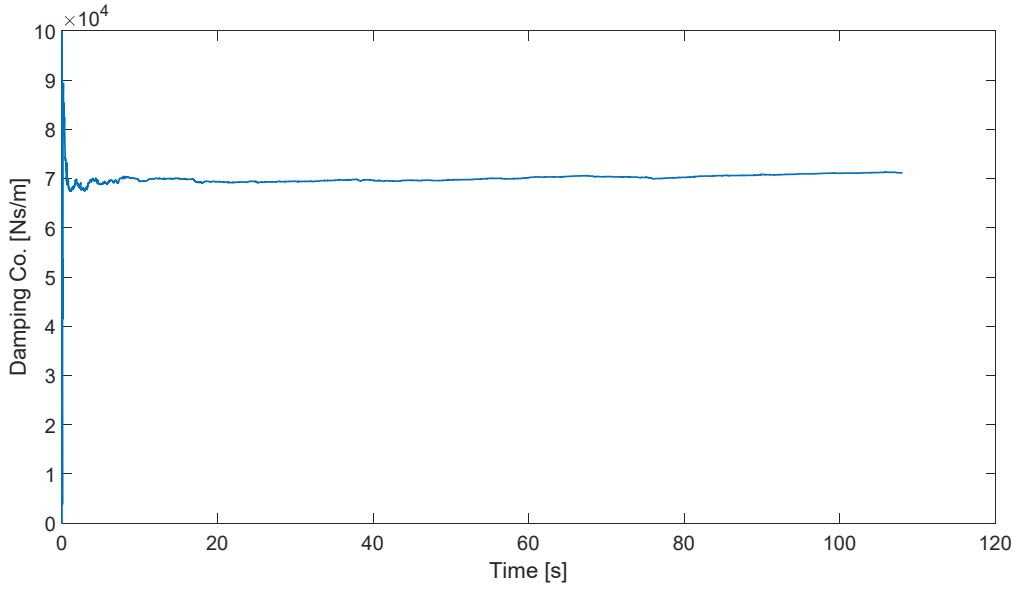

Figure 58 – Estimate of secondary lateral damping coefficient – Fault-free

9.2.4. Estimation Result for Fault-Free Vehicle

Corresponding to the track case above, a transient simulation is carried out in Vampire regarding a fault-free vehicle model. All the output channels are related to the front bogie. With the usage of the previously mentioned Simulink model, several key parameters estimated for a faulty-free vehicle are shown below.

From the lateral module, the secondary lateral damping coefficient and primary lateral

stiffness can be estimated. The secondary lateral damping coefficient is shown in Figure 58; it has a nominal value of 75 kNs/m (per damper) in the simulated locomotive model. The primary lateral stiffness of three axles is shown in Figure 59. In the simulated locomotive model, the front and rear axle have a large lateral stiffness of 10.5 MN/m (per bushing), while the middle axle has a very small stiffness of 0.5 MN/m (per bushing).

It can be seen that the estimates of the secondary lateral damping coefficient and primary lateral stiffness are very closely matched to the values defined in the Vampire locomotive model. Because the lateral force generated by the secondary spring is very small, it is difficult to observe this force component in the lateral acceleration of the bogie frame. However, the estimated of lateral stiffness of the secondary spring is still of a similar magnitude to the value in the simulation model.

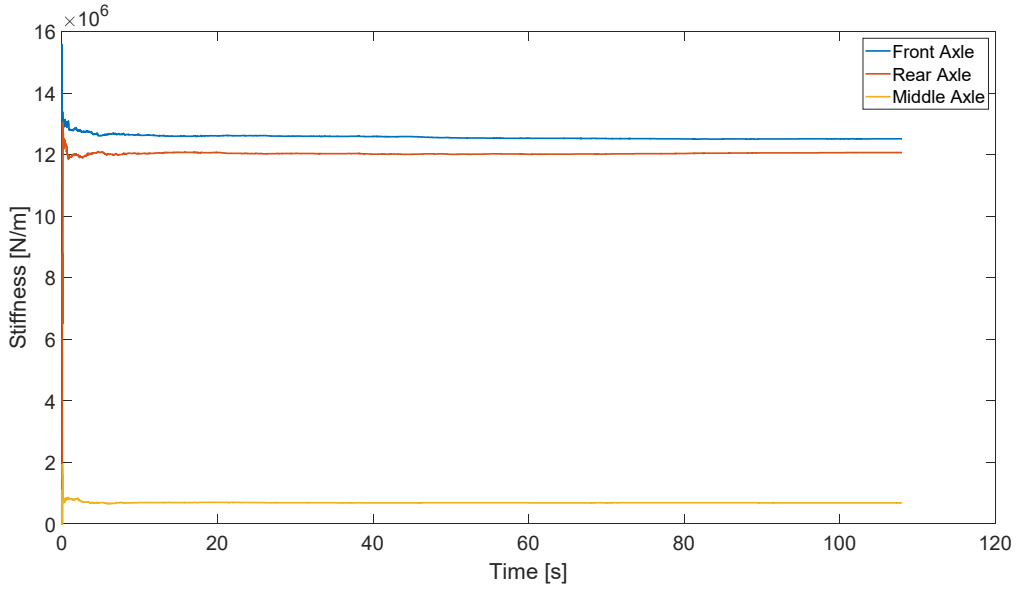

Figure 59 – Estimate of primary lateral stiffness – Fault-free

From the yaw module, the damping coefficient of the secondary yaw damper, primary longitudinal stiffness and primary lateral stiffness (front and rear axles) can be estimated. The damping coefficient of the secondary yaw damper is shown in Figure 60; its nominal value in the simulation model is 150 kNs/m (per damper). The primary longitudinal stiffness of three axles is shown in Figure 61; its nominal value for each axle is 30 MN/m (per bushing). The primary lateral stiffness can be estimated in yaw module as well, as shown in Figure 62.

It can be seen that the estimates of the damping coefficient of the yaw damper and primary longitudinal and lateral stiffness correlate well with the values defined in the Vampire simulation model. Because the yaw torques generated by the secondary spring are very small, it is difficult to observe these torques in the yaw acceleration of the bogie frame. The estimate of lateral and longitudinal stiffness of the secondary spring is still of the same magnitude as the value contained in the simulation model.

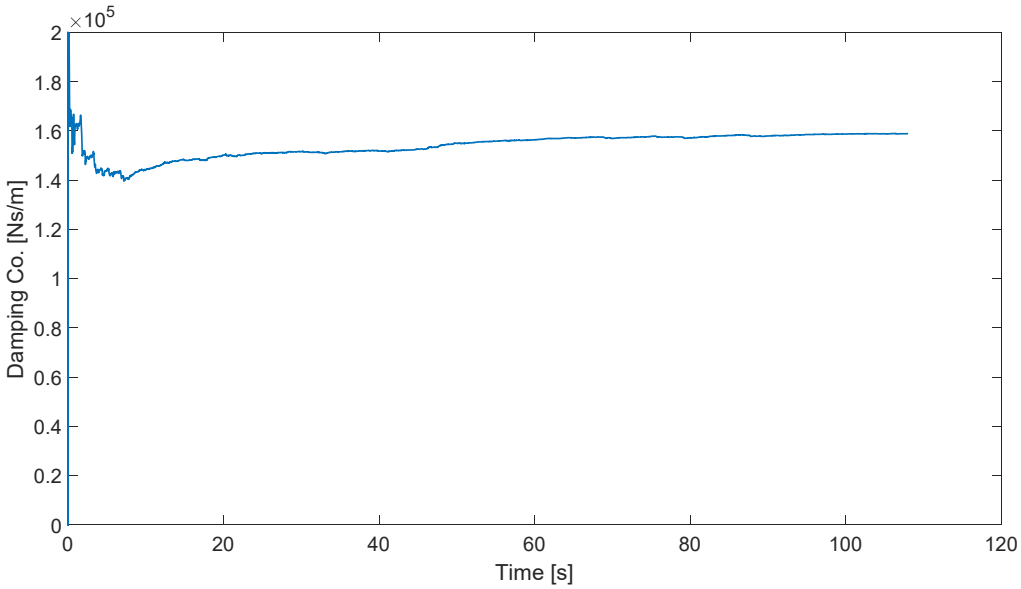

Figure 60 – Estimate of damping coefficient of secondary yaw damper – Fault-free

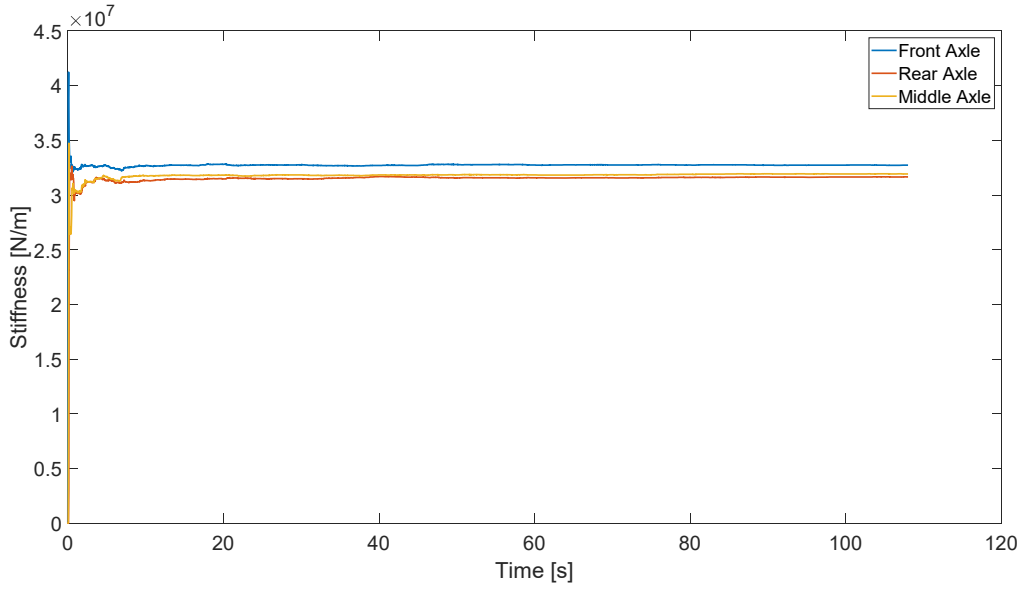

Figure 61 – Estimate of primary longitudinal stiffness – Fault-free

For the vertical module, the estimate of the secondary vertical stiffness is shown in Figure 63, which has a nominal value in the simulation model is 10 MN/m (per spring). It can be seen that all the estimated stiffnesses are very accurate. Figure 64 shows the estimate of the stiffness of the motor linkage, which has a nominal value in the simulation model is 10 MN/m (per link). These estimates are still approximate to the simulation value. Figure 65 exhibits the estimate of primary vertical stiffness, which has a nominal value in the simulation is 0.8 MN/m (per axle-box). The four estimates are very similar to the simulation values.

Due to the suspension design of this vehicle, the damping coefficient of the primary vertical

damper is small. In this sense, the vertical acceleration of the bogie frame mainly reflects the suspension forces by the secondary vertical spring and motor link of large stiffness. The weak forces generated by the primary vertical dampers are difficult to be identified from bogie frame acceleration, but the estimates are still in the same scale with the value in the simulation model.

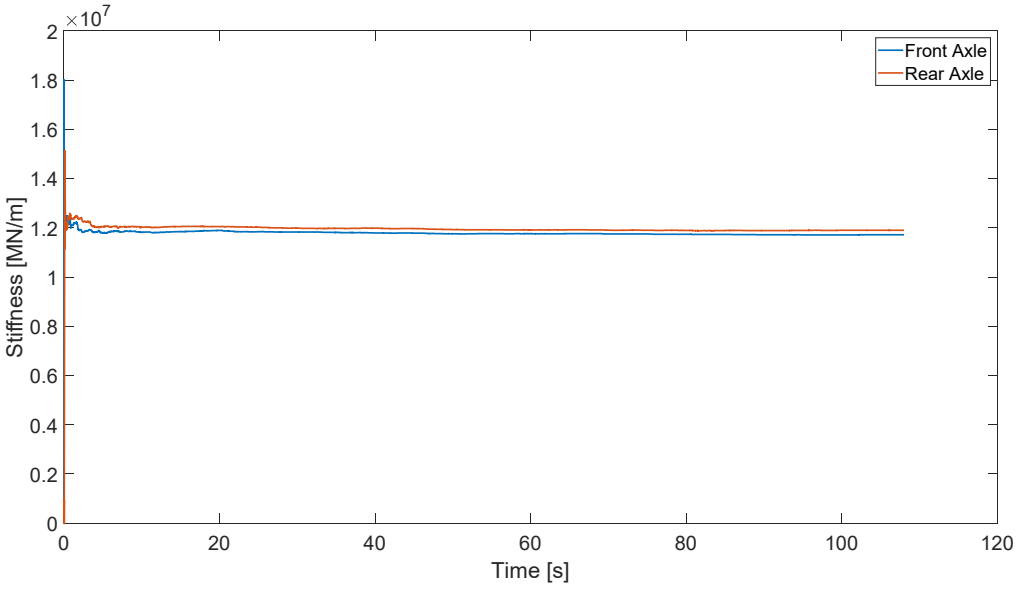

Figure 62 – Estimate of primary lateral stiffness (front and rear) – Fault-free

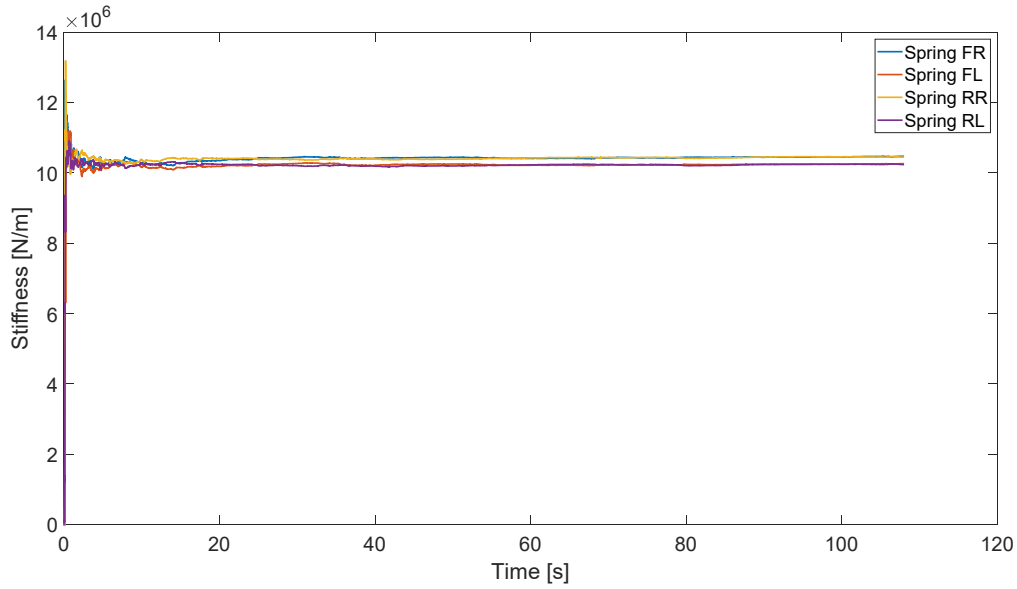

Figure 63 – Estimate of secondary vertical stiffness – Fault-free

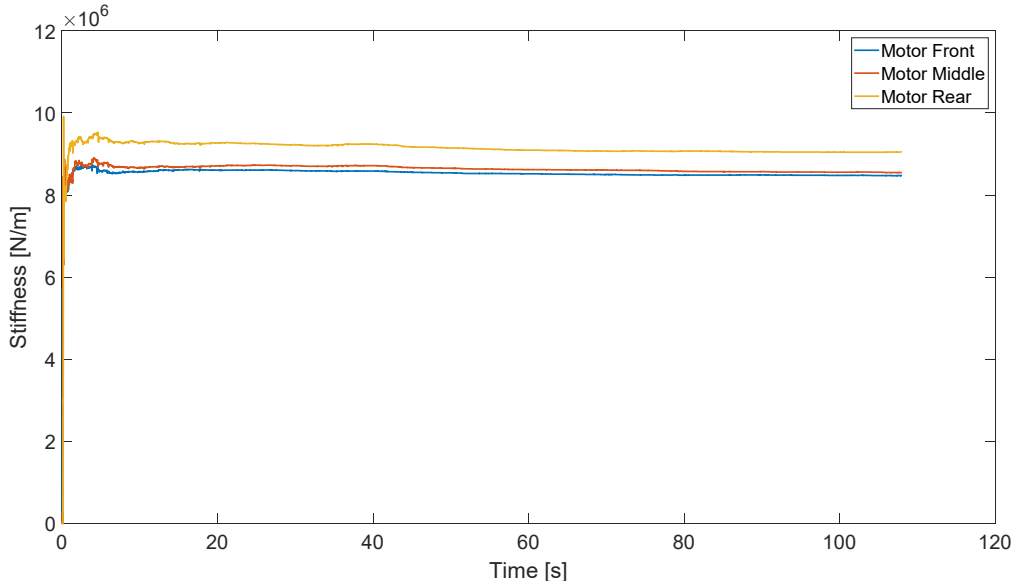

Figure 64 – Estimate of motor link stiffness – Fault-free

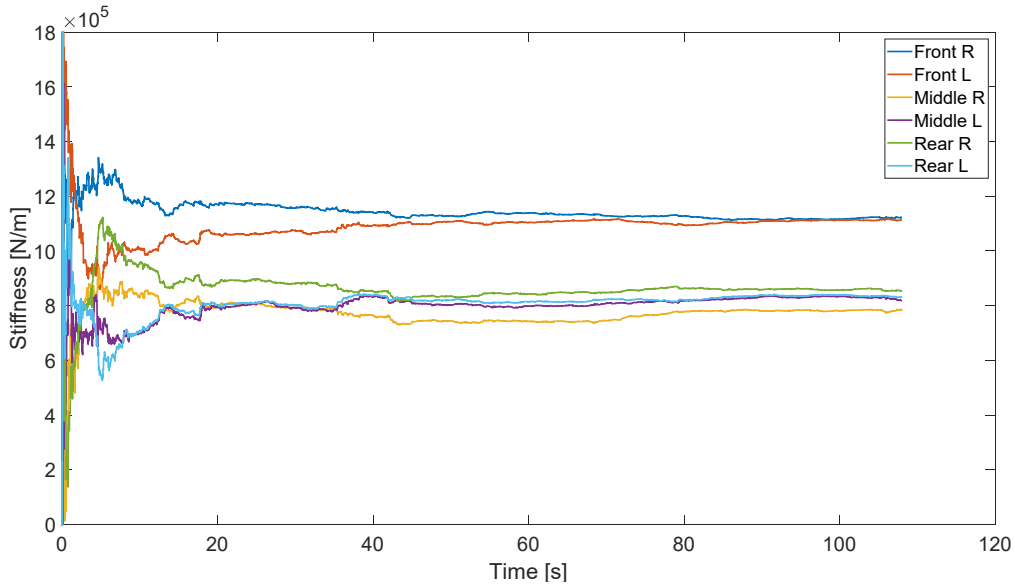

Figure 65 – Estimate of primary vertical stiffness – Fault-free

9.2.5.Suspension Fault Detection & Isolation by RLS Estimation

9.2.5.1. Fault case

To investigate the feasibility of this parameter-based fault detection approach, several 'artificial' suspension faults were added to the leading bogie of the Vampire vehicle model. These suspension faults included:

- Damping of secondary yaw dampers set to zero.
- Damping of secondary lateral dampers set to zero.
- Stiffness of one secondary vertical rubber spring set to 2 times of its normal stiffness value.

- Primary lateral stiffness and longitudinal stiffness of one primary rubber bushing set to be 2 times of their normal values.

A higher stiffness is likely to be indicative of a degraded rubber spring component due to the loss of in flexibility. These suspension faults are only general examples of possible fault scenarios mainly for the investigation in this report. In Figure 66, the suspension components with faults are marked with circles.

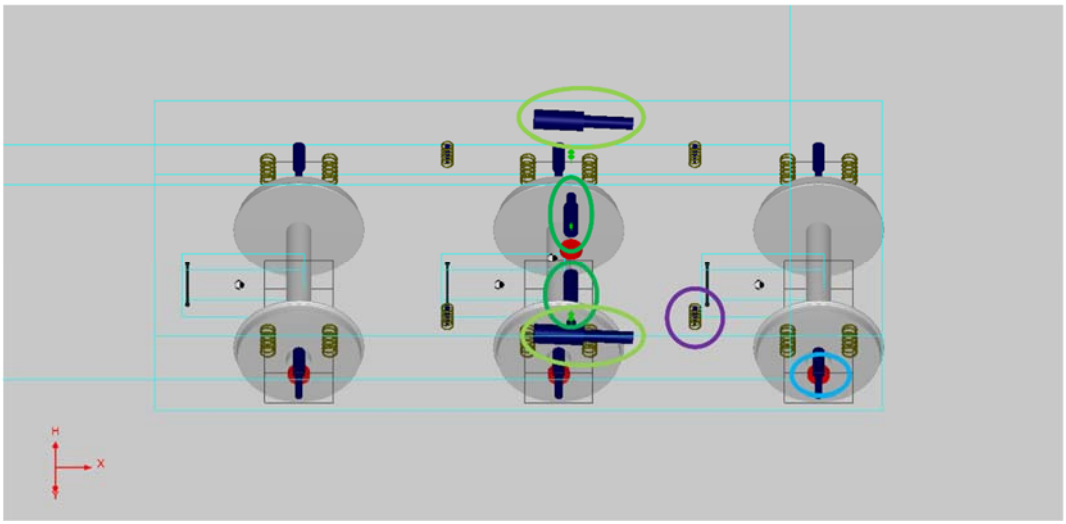

Figure 66 – Bogie plot with marked faulty suspension elements

With such a vehicle model and parameter alterations, the identical track case is simulated at the same vehicle speed. From the simulation result, on its own it is very difficult to distinguish the abnormal behaviour of the faulty vehicle from the resulting vibration signal compared with a fault-free vehicle. This phenomenon is very common for the railway vehicle since many suspension components are designed to control the vibration response of the vehicle even in a faulty condition.

9.2.5.2. Parameter estimation result of fault case

Identically, the vibration signals exported from the Vampire simulations were introduced into the three modules of the Simulink models for parameter estimation.
For the lateral module, the secondary lateral damping coefficient is shown in Figure 67. Its value set in the simulation model is zero, while the normal value should be 75 kNs/m (per damper). It can be seen from the figure, that the RLS estimates a very small value for the damping coefficient, indicating a degraded condition.

Also from the lateral model, the estimate of primary lateral stiffness of three axles is shown in Figure 68. In the normal condition, the front and rear axle have a lateral stiffness of 10.5 MN/m (per bushing), while the middle axle has a very small stiffness of 0.5 MN/m (per bushing). Here in this faulty vehicle model, the lateral stiffness of the front axle should be 15.5 MN/m (the average of two bushings). It can be seen that the estimate of the primary lateral stiffness of the front axle is very similar to this value. Meanwhile, the other stiffness estimates are still approximate to their normal values.

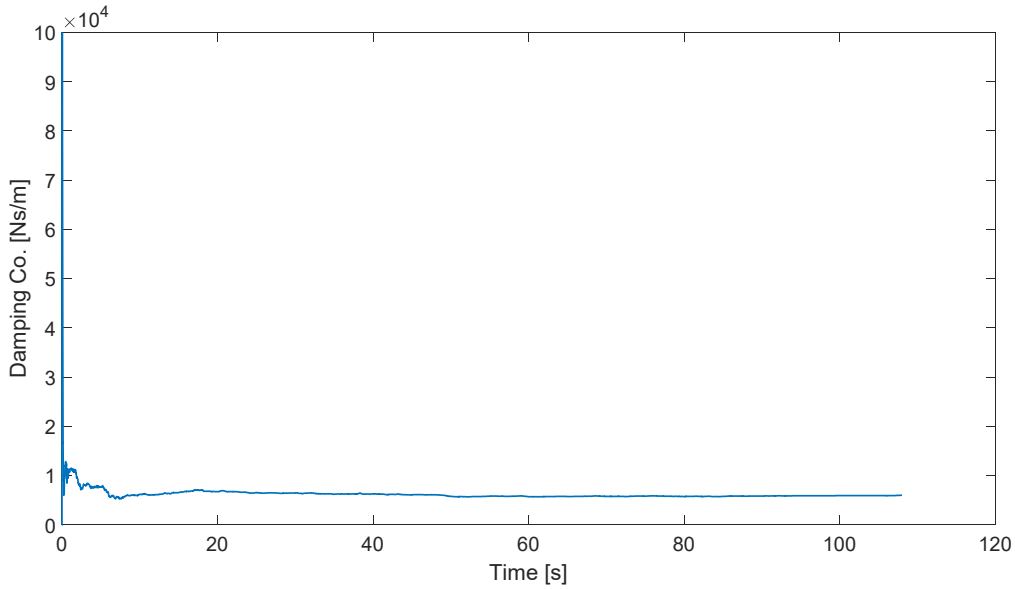

Figure 67 – Estimate of secondary lateral damping coefficient – faulty vehicle

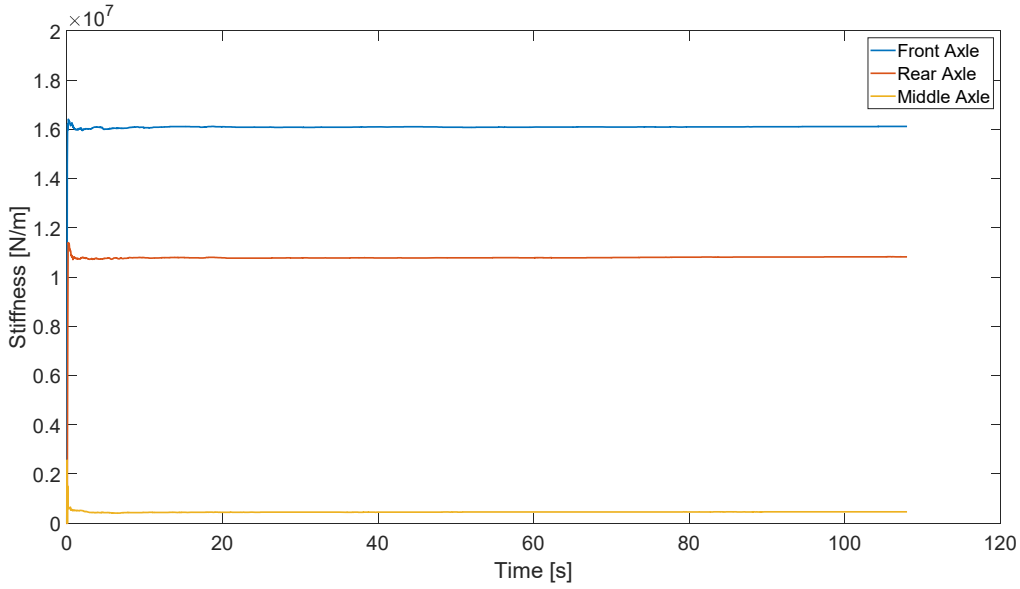

Figure 68 – Estimate of primary lateral stiffness – faulty vehicle

For the yaw module, the damping coefficient of the secondary yaw damper is shown in Figure 69. Its normal value is 150 kNs/m (per damper), while its value in this Vampire simulation is zero. It can be seen from Figure 69 that the model estimates a very small value for the damping coefficient indicating a degraded condition.

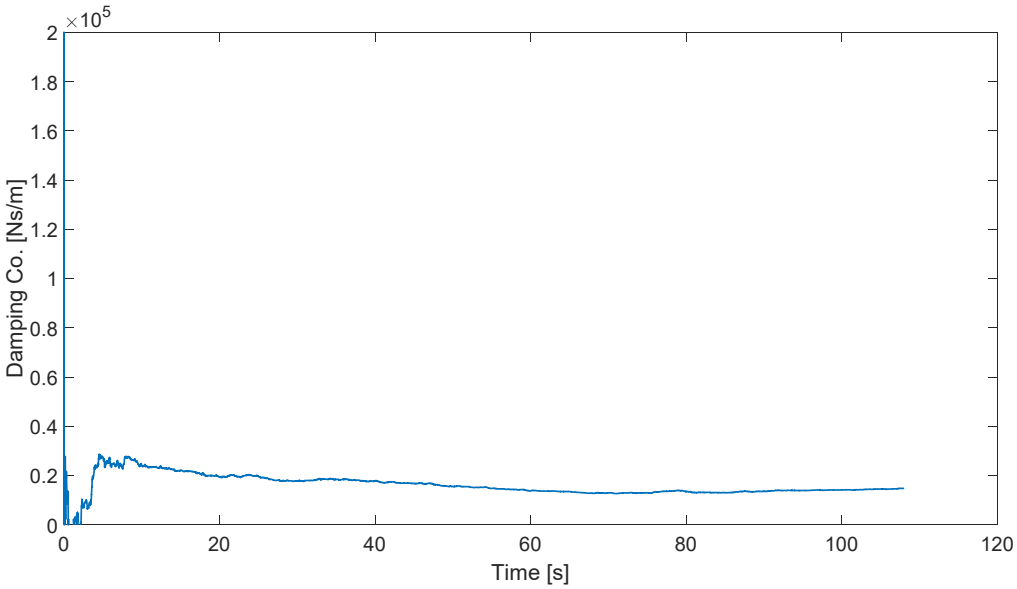

Figure 69 – Estimate of damping coefficient of secondary yaw damper – faulty vehicle

For the yaw module, the estimate of primary longitudinal stiffness is shown in Figure 70. Its nominal value for each axle is 30 MN/m (per bushing). However, the longitudinal stiffness value of the front axle should be 45 MN/m (per bushing, average of a pair of bushings) in this fault model. From Figure 70, the estimates for the rear and middle axles are almost identical to the nominal values. The estimate for the front axle is higher than the others and similar to the value used in the faulty vehicle simulations. Besides, the primary lateral stiffness (front and rear axles) estimated in yaw module is shown in Figure 71. It can be seen that its result is very similar with the one identified by the lateral module.

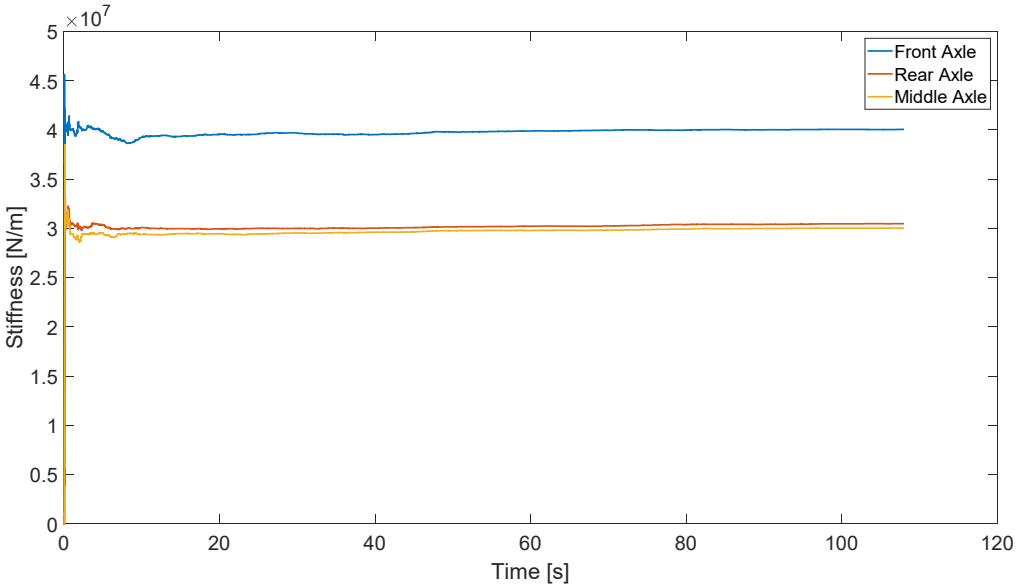

Figure 70 – Estimate of primary longitudinal stiffness – faulty vehicle

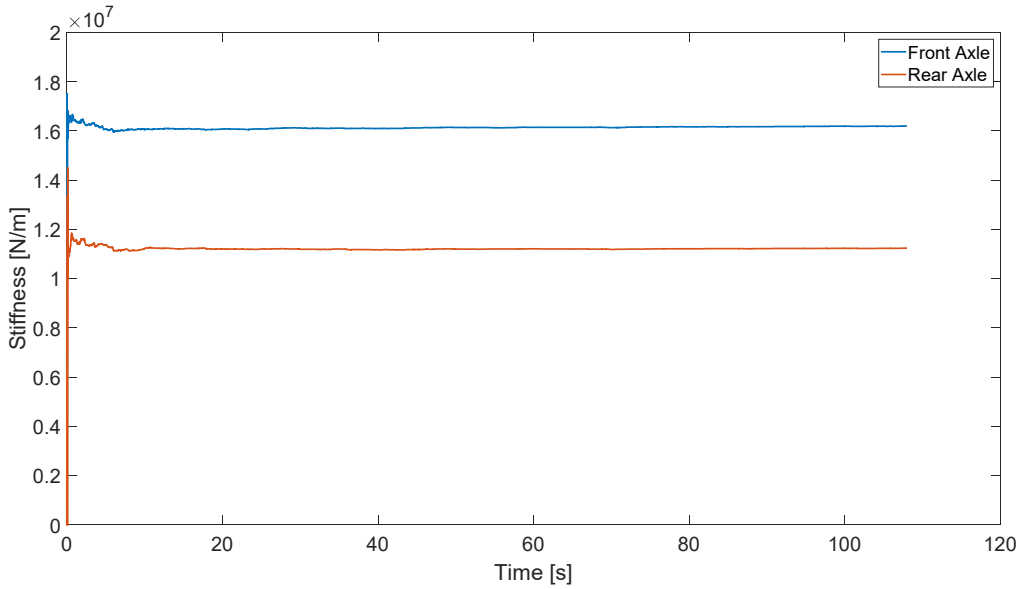

Figure 71 – Estimate of primary lateral stiffness – faulty vehicle

For the vertical module, the estimate of the secondary vertical stiffness is shown in Figure 72. Its normal is 10 MN/m (per spring); In this simulation, the stiffness value of the front right rubber spring is set to be 20 MN/m. From Figure 72, the stiffness estimate of the front right spring is definitely higher than the other estimates. Although this vertical model does not deliver very accurate estimation due to the similarities of input signals, it is obvious that some variation from the nominal value can be detected for the secondary springs.

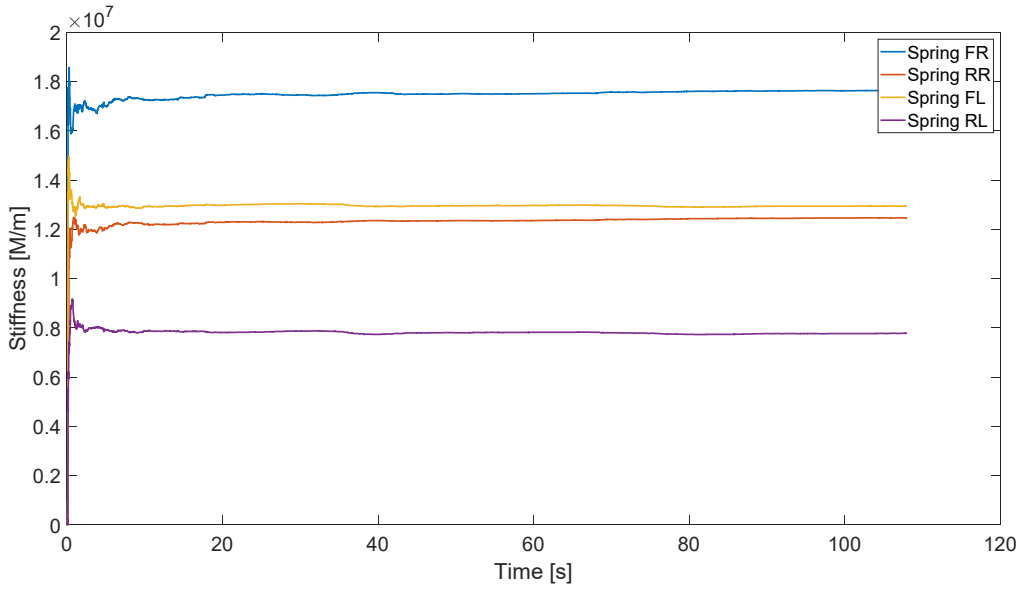

Figure 72 – Estimate of secondary vertical stiffness – faulty vehicle

9.3. Summaries

In the framework of LOCATE WP4, this work is parallel to the development of 'Digital Twin' and aiming at exploring an alternative solution for the vehicle condition monitoring with a 'smart diagnostic' approach. Instead of a comparison of the faulty and fault-free signals, this fault detection method takes the advantage of the relationship between the measured signals to directly identify the parameter in a quantitively manner.

Due to the complexity of the vehicle system, the fault detection and identification of the suspension parameters can be very challenging. Because so many suspension components exist in the railway vehicle, especially the locomotive, the dynamic behaviours of the vehicle are influenced by different suspension forces and their coupling effects. In many cases, it is very difficult to identify the suspension fault by the comparisons of the vibration signals between the faulty condition and fault-free condition. Besides, the vehicle vibration also depends on the external excitations, such as the track irregularities.

In spite of the complexity of the vehicle suspension system, the dynamic model of the vehicle is determined and can be analysed with known mathematical model. Based on Newton's second law, the acceleration of the sprung mass is determined by the sums of the suspension forces. The motion of the suspension component, velocity for damper and displacement for spring, can be obtained directly or indirectly from sensor measurements. Specifically, the accelerometer which is the most commonly used sensor in vehicle dynamics. As the vibration signals are measured in a large quantity (with high sampling frequencies), the stiffness or the damping coefficient can be estimated based on a Least-square approach if the suspension system can be regarded as a linear system. However, the ordinary Least-square is not suitable for the estimate of the suspension parameter from vibration signals due to the ill-conditioned inverse matrix. In contrast, the Recursive Least-square (RLS) is capable of solving this problem with its memory and correlation characteristics, i.e., an optimal Kalman gain.

A condition monitoring system for the suspension of FGC Series 254 locomotive is illustrated in this report. The FGC Series 254 is an old type of locomotive with many clearances and dry friction pairs. These mechanical features constitute high non-linearities in its suspension components. By the investigation of the multi-body simulation data from FGC Series 254 locomotive, the forces by the non-linear elements are not neglectable in the acceleration observations based on RLS method because of their large amplitudes. HUD decide to utilize another relatively new type of Co-Co locomotive for the demonstration of this condition monitoring strategy within this project.

For this six-axle locomotive, a validated Vampire multi-body model is used to generate the motion output in the simulation. These output data represent the 'virtual measurements' in the operational conditions for the purpose of validating the RLS approach. In this RLS-based suspension condition monitoring system, three modules are developed in accordance with the layout of this locomotive's suspension, including: vertical module, lateral module and yaw module. These modules are implemented in a MATLAB/Simulink environment. A Simulink model for this RLS method can be readily converted into C/C++ code. The converted code can be executed in a low-cost electronic computing device, such as Raspberry-Pie.

In the parameter estimation of the Co-Co locomotive, the main suspension parameters can be reliability estimated, especially the large stiffness parameters. Several suspension faults with parameter deviations were added into the vehicle model within the multi-body simulations. By

using this RLS fault detection method, the suspension fault can be identified quantitively with the parameter estimate. Since this RLS method is based on the parameter estimation with Input-Output model, the estimation result is not sensitive to the operational condition. However, it is necessary to mention that the RLS method need to be developed dedicatedly according to the target vehicle. Different vehicles have different suspension layouts with a varieties of parameter configurations, which can affect the motion equations of the RLS models. Certain suspension components contribute very little to the observed sprung mass acceleration, making their parameters difficult to estimate. These factors should be considered carefully in order to obtain a reasonable model for the condition monitoring system, meanwhile, the cost for the condition monitoring system is also an important issue.

10. Conclusions

10.1. Main Findings

This deliverable describes the models developed and the methods implemented to evaluate the condition of bogie components using dynamic simulations. The results of multibody simulations represent the nominal and abnormal response of the vehicle, providing a database of the locomotive reference behaviour. This database supports the identification of the health of the bogie components. The failure modes addressed in WP4 are cracks in the bogie frame and wheelsets, and the degradation of elements in the primary suspension. Condition assessment is accomplished using damage detection methods based on the transmissibility concept, such as the Transmissibility Damage Indicator (TDI) and Maximum Occurrences (MO) methods. The degradation of primary suspension elements is also assessed using surrogate modelling. The main conclusions of the research activities reported in this deliverable are:

- A static analysis based on standard EN 13749 was used to define an appropriate location for a crack in the welded connections between the front transversal beam and the side frames. The lateral accelerations measured at selected points in the bogie frame were obtained from a set of simulations of the vehicle-track interaction considering different crack sizes and a constant speed of 60km/h. The transmissibility matrix of the measured response is computed in the frequency range of 10-150Hz, and the results show the TDI method is sensitive to damage if the crack area is at least 63% of the cross-section of the welded connection. Further increasing the crack area reduces the TDI value. The symmetric and non-symmetric schemes used to compute TDI suggest a threshold of 0.7.
- The results from the flexible multibody simulations rely on the sensitivity of the natural frequencies and vibration modes of the structure to the existence of damage. The modal analysis of the wheelset shows the natural frequencies are only sensitive to cracks perpendicular to the axle if their depth is higher than 25% of the axle diameter. Therefore, this method is unlikely to detect damage in the wheelset before the crack grows exponentially.
- The TDI method can measure changes in transmissibilities caused by damage in the primary suspension. It is sensitive to a 50% reduction of the nominal value of spring stiffness and a 40% increase or decrease of the nominal value of the damping coefficient of the viscous damper. TDI is sensitive to damage in the primary suspension given the sources of variability in the simulations, i.e., track irregularities, speed and uncertainty about the nominal values of the mechanical properties.
- After detecting damage in the bogie frame using the TDI method, the MO method identifies the entry corresponding to the highest difference between the nominal and measured transmissibility matrices. The indices of this entry correspond to the pair of sensors detecting damage. The sensitivity of the MO method depends both on the frequency range considered for the response and the position of the sensors. However, when damage is

detected on springs it can only indicate if the damaged spring is in the leading wheelset or on the other two. The method cannot isolate damage in the middle and rear wheelset.

- Surrogate models of the standard deviation of the lateral acceleration of the bogie frames show good fit, low absolute percentage error, and sensitivity to spring damage. The stiffness values used in the simulations range from 10 to 190% of the nominal stiffness. However, it is not clear what values are acceptable before the spring can be considered damaged. Upper and lower stiffness limits were defined for discrete speed intervals based on the variance of the surrogate. Finally, the maximum and minimum of the surrogate within the stiffness limits constitute the threshold for the response.
- A Recursive Least Square method for the estimation of the primary suspension parameters is presented. The RLS method is suitable to monitor the condition of suspension systems that can be represented by linearised models. Since this RLS method is based on the parameter estimation with Input-Output model, the estimation result is not sensitive to the operational condition.

10.2. Future Developments

The work developed in WP4 contributes to the development and implementation of strategies for online condition monitoring. However, there are a few points requiring further investigation:

- The flexible multibody simulations run to assess the impact of bogie frame damage on its dynamics are computationally expensive (4.2 hours to simulate 1 second). Improving the efficiency of the methods will allow investigating cracks in other locations and provide a more explicit evolution of the system response as a function of damage. Moreover, it is relevant to investigate the sensitivity of the TDI and MO methods to crack areas between 20% and 63% of the welded connection.
- The methods involving transmissibilities would benefit from a data post-processing to associate different combinations of sensors to the different damage scenarios. Machine learning might be helpful if the number of simulations is large enough.
- This work did not address simultaneous failures of the vehicle elements. However, the methods presented should also apply to such cases. Nevertheless, the effectiveness of these methods for simultaneous failures should be addressed.
- There is a need to develop a systematic methodology to build a library of reference behaviour using experimental data. This methodology must deal with the variability of speed during measurements, which is an inevitable consequence of the regular operation of railway vehicles.
- The simulations considered only a straight track geometry, and, consequently, indicators relevant to curvature might have been eliminated (e.g., surrogates involving statistical quantities of the angular speeds). Future work building on this report and considering curvature should explore indicators comprehensively.

11. References

[1] Bruni S, Vinolas J, Berg M, et al. Modelling of suspension components in a rail vehicle dynamics context. Veh Syst Dyn. 2011;49:1021–1072.
[2] Berg M. A non-linear rubber spring model for rail vehicle dynamics analysis. Veh Syst Dyn. 1998;30:197–212.
[3] Sun YQ, Cole C. Vertical dynamic behavior of three-piece bogie suspensions with two types of friction wedge. Multibody Syst Dyn. 2008;19:365–382.
[4] Berghuvud A, Stensson A. Consequences of nonlinear characteristics of a secondary suspension in a three-piece freight car bogie. Veh Syst Dyn. 2001;36:37–55.
[5] Harder RF. Dynamic modeling and simulation of three-piece freight vehicle suspensions with non-linear frictional behaviour using ADAMS/Rail. Proc IEEE/ASME Jt Railr Conf. 2001;185–191.
[6] Wu Q, Luo S, Xu Z, et al. Coupler jackknifing and derailments of locomotives on tangent track. Veh Syst Dyn. 2013;51:1784–1800.
[7] S. Iwnicki. Handbook of Rail Vehicle Dynamics. 2006.
[8] Iverson WC. Analysis of the Reconstruction of Rail Geometry from Curvature Data. IEEE Trans Ind Appl. 1974;IA-10:368–379.
[9] Pombo J, Ambrósio J. An alternative method to include track irregularities in railway vehicle dynamic analyses. Nonlinear Dyn. 2012;68:161–176.
[10] Cole C, Spiryagin M, Wu Q, et al. Modelling, simulation and applications of longitudinal train dynamics. Veh Syst Dyn. 2017;55:1498–1571.
[11] EN14363:2016 E. EN 14363:2016+A1:2018 Railway applications - Testing and Simulation for the acceptance of running characteristics ofrailway vehicles - Running Behaviour and stationary tests. European Committee for Standardization (CEN), Brussels; 2018. 2016;
[12] Polach O, Böttcher A. A new approach to define criteria for rail vehicle model validation. Veh Syst Dyn. 2014;52:125–141.
[13] Polach O, Böttcher A, Vannucci D, et al. Validation of simulation models in the context of railway vehicle acceptance. Proc Inst Mech Eng Part F J Rail Rapid Transit. 2015;229:729–754.
[14] Flores P, Machado M, Seabra E, et al. A parametric study on the baumgarte stabilization method for forward dynamics of constrained multibody systems. J Comput Nonlinear Dyn. 2011;6.
[15] Gear CW, Petzold L. ODE Methods for the Solutions of Differential/Algebraic Equations. SIAM J Numer Anal. 1984;21:716–728.
[16] Nikravesh PE. Computer-Aided Analysis of Mechanical Systems. Prentice-Hall, Englewood Cliffs, New Jersey. 1988.
[17] Ambrósio JAC, Neto MA, Leal RP. Optimization of a complex flexible multibody systems with composite materials. Multibody Syst Dyn. 2007;18:117–144.
[18] Agrawal OP, Shabana AA. Application of deformable-body mean axis to flexible multibody system dynamics. Comput Methods Appl Mech Eng. 1986;56:217–245.
[19] Bae DS, Han JM, Choi JH. A Virtual Body and Joint for Constrained Flexible Multibody Dynamics. Vol 7A 17th Bienn Conf Mech Vib Noise. American Society of Mechanical Engineers; 1999. p. 91–97.
[20] Gonçalves J, Ambrósio J. Advanced modelling of flexible multibody systems using virtual bodies. Comput Assist Mech Eng Sci. 2002;9:373–390.

[21] Pombo JC, Ambrósio JAC. MUltiBOdy DYnamics Analysis Program - MUBODyn: User's Manual. Lisbon. 2006.
[22] Magalhães H, Marques F, Liu B, et al. Implementation of a non-Hertzian contact model for railway dynamic application. Multibody Syst Dyn. 2020;48:41–78.
[23] Fontul M, Ribeiro AMR, Silva JMM, et al. Transmissibility matrix in harmonic and random processes. Shock Vib. 2004;11:563–571.
[24] Maia NMM, Almeida RAB, Urgueira APV, et al. Damage detection and quantification using transmissibility. Mech Syst Signal Process. 2011;25:2475–2483.
[25] Heylen W, Lammens S, Sas P. Modal Analysis Theory and Testing. K.U. Leuven - PMA, Belgium; 1998. p. 340.
[26] Sampaio RPC, Maia NMM, Silva JM., et al. On the Use of Transmissibility for Damage Detection and Location. Eur COST F3 Conf Syst Identif Struct Heal Monit. Madrid, Spain; 2000. p. 363–376.
[27] Sampaio RPC, Maia NMM, Ribeiro AMR, et al. Transmissibility Techniques for Damage Detection. 19th Int Modal Anal Conf. Kissimmee, Florida, USA; 2001.
[28] Santner TJ, Williams BJ, Notz WI. The Design and Analysis of Computer Experiments [Internet]. New York, NY: Springer New York; 2003. Available from: http://link.springer.com/10.1007/978-1-4757-3799-8.
[29] Sacks, J., Welch, W.J., Mitchell, T.J., Wynn, H.P.: Design and Analysis of Computer Experiments. Stat. Sci. 4, 409–423 (1989).
[30] Forrester AIJ, Sóbester A, Keane AJ. Engineering Design via Surrogate Modelling [Internet]. Wiley; 2008. Available from: https://onlinelibrary.wiley.com/doi/book/10.1002/9780470770801.
[31] Gramacy, R. B. (2020), Surrogates: Gaussian Process Modeling, Design, and Optimization for the Applied Sciences (1st ed.), Boca Raton, FL: Chapman & Hall/CRC.
[32] Hastie T, Tibshirani R, Friedman J. The Elements of Statistical Learning [Internet]. New York, NY: Springer New York; 2009. Available from: http://link.springer.com/10.1007/978-0-387-84858-7.
[33] Saltelli A, Andres TH, Homma T. Sensitivity analysis of model output. Comput Stat Data Anal [Internet]. 1993;15:211–238. Available from: https://linkinghub.elsevier.com/retrieve/pii/016794739390193W.
[34] Homma T, Saltelli A. Importance measures in global sensitivity analysis of nonlinear models. Reliab Eng Syst Saf [Internet]. 1996;52:1–17. Available from: https://linkinghub.elsevier.com/retrieve/pii/0951832096000026.
[35] EN 13749:2011 Railway applications - Wheelsets and bogies - Method of specifying the structural requirements of bogie frames. European Committee for Standardization (CEN), Brussels; 2011. 2011;
[36] Fu D, Wang W, Dong L. Analysis on the fatigue cracks in the bogie frame. Eng Fail Anal. 2015;58:307–319.
[37] Yan J, Jin H, Sun H, et al. Active monitoring of fatigue crack in the weld zone of bogie frames using ultrasonic guided waves. Sensors (Switzerland). 2019;19.
[38] Wang W, Bai J, Wu S, et al. Experimental investigations on the effects of fatigue crack in urban metro welded bogie frame. Appl Sci. 2020;10.
[39] Bachschmid N, Tanzi E, Pennacchi P. Cracked rotors: A survey on static and dynamic behaviour including modelling and diagnosis. Crack. Rotors A Surv. Static Dyn. Behav. Incl. Model. Diagnosis. 2010.

Annex A – MUBODyn FGC 254 Model

Table A.1 – FGC 254 Vehicle Body: Mass and inertia properties and initial positions of the CM of the rigid bodies.

ID	Body	Mass [kg]	Inertia properties [kg.m^2]			Initial position [m]		
			I_{roll}	I_{pitch}	I_{yaw}	X_0	Y_0	Z_0
101	Vehicle body	50860	56798	505047	513774	0	0	2.325

Table A.2 – FGC 254 Bogie: Mass and inertia properties and initial positions of the CM of the rigid bodies.

ID	Body	Mass [kg]	Inertia properties [kg.m^2]			Initial position [m]		
			I_{roll}	I_{pitch}	I_{yaw}	X_0	Y_0	Z_0
201	Bogie Frame	3090	1854	5864	7508	0	0	0.613
202	Wheelset Front	1243	418	103	418	1.8345	0	0.457
203	Wheelset Middle	1243	418	103	418	0.279	0	0.457
204	Wheelset Rear	1243	418	103	418	-1.4545	0	0.457
205	Axle box Front Left	60	1	1	1	1.8345	0.7665	0.457
206	Axle box Front Right	60	1	1	1	1.8345	-0.7665	0.457
207	Axle box Front Left	60	1	1	1	0.279	0.7665	0.457
208	Axle box Front Right	60	1	1	1	0.279	-0.7665	0.457
209	Axle box Front Left	60	1	1	1	-1.4545	0.7665	0.457
210	Axle box Front Right	60	1	1	1	-1.4545	-0.7665	0.457
211	Front Motor	2002	211	268	307	1.419	0	0.487
212	Middle Motor	2002	211	268	307	-0.1365	0	0.487
213	Rear Motor	2002	211	268	307	-1.87	0	0.487
214	Bolster	817	168	332	478	0.189	0	0.939

Table A.3 – Subsystem 2 – FGC 254 Bogie: Perfect kinematic joints of the primary suspension.

ID	Joint	Bodies		Body *i*						Body *j*					
		i	*j*	P_i (ξ_j / η_j / ζ_j)			Q_i (ξ_j / η_j / ζ_j)			P_j (ξ_j / η_j / ζ_j)			Q_j (ξ_j / η_j / ζ_j)		
1	Revolute	202	205	0	0.7665	0	0	0.8665	0	0	0	0	0	-0.1	0
2	Revolute	202	206	0	-0.7665	0	0	-0.8665	0	0	0	0	0	0.1	0
3	Revolute	203	207	0	0.7665	0	0	0.8665	0	0	0	0	0	-0.1	0
4	Revolute	203	208	0	-0.7665	0	0	-0.8665	0	0	0	0	0	0.1	0
5	Revolute	204	209	0	0.7665	0	0	0.8665	0	0	0	0	0	-0.1	0
6	Revolute	204	210	0	-0.7665	0	0	-0.8665	0	0	0	0	0	0.1	0
7	Rigid	201	211	0	0	0	0	0	0	0	0	0	0	0	0
8	Rigid	201	212	0	0	0	0	0	0	0	0	0	0	0	0
9	Rigid	201	213	0	0	0	0	0	0	0	0	0	0	0	0

Table A.4 – Subsystem 2 – FGC254 Bogie: Kinematic joints with clearance of the primary suspension.

ID	Joint	Bodies		Body *i*						Body *j*					
		i	*j*	P_i (ξ_j / η_j / ζ_j)			Q_i (ξ_j / η_j / ζ_j)			P_j (ξ_j / η_j / ζ_j)			Q_j (ξ_j / η_j / ζ_j)		
1	Prismatic	205	201	0	0.04	-0.122	0	0.04	0.122	-0.0255	0.8065	-1	-0.0255	0.8065	1
2	Prismatic	205	201	0	0.04	-0.122	0	0.04	0.122	3.6945	0.8065	-1	3.6945	0.8065	1
3	Prismatic	205	201	0	-0.1475	-0.062	0	-0.1574	0.086	1.8345	-1.311	-1	1.8345	-1.311	1
4	Prismatic	206	201	0	-0.04	-0.122	0	-0.04	0.122	-0.0255	-0.8065	-1	-0.0255	-0.8065	1
5	Prismatic	206	201	0	-0.04	-0.122	0	-0.04	0.122	3.6945	-0.8065	-1	3.6945	-0.8065	1
6	Prismatic	206	201	0	0.1475	-0.062	0	0.1574	0.086	1.8345	1.311	-1	1.8345	1.311	1
7	Prismatic	207	201	0	0.04	-0.122	0	0.04	0.122	-1.581	0.8065	-1	-1.581	0.8065	1
8	Prismatic	207	201	0	0.04	-0.122	0	0.04	0.122	2.139	0.8065	-1	2.139	0.8065	1
9	Prismatic	207	201	0	-0.1475	-0.062	0	-0.1574	0.086	0.279	-1.311	-1	0.279	-1.311	1
10	Prismatic	208	201	0	-0.04	-0.122	0	-0.04	0.122	-1.581	-0.8065	-1	-1.581	0.8065	1
11	Prismatic	208	201	0	-0.04	-0.122	0	-0.04	0.122	2.139	-0.8065	-1	2.139	-0.8065	1
12	Prismatic	208	201	0	0.1475	-0.062	0	0.1574	0.086	0.279	1.311	-1	0.279	1.311	1
13	Prismatic	209	201	0	0.04	-0.122	0	0.04	0.122	-3.3145	0.8065	-1	-3.3145	0.8065	1
14	Prismatic	209	201	0	0.04	-0.122	0	0.04	0.122	0.4055	0.8065	-1	0.4055	0.8065	1
15	Prismatic	209	201	0	-0.1475	-0.062	0	-0.1574	0.086	-1.4545	-1.311	-1	-1.4545	-1.311	1
16	Prismatic	210	201	0	-0.04	-0.122	0	-0.04	0.122	-3.3145	-0.8065	-1	-3.3145	-0.8065	1
17	Prismatic	210	201	0	-0.04	-0.122	0	-0.04	0.122	0.4055	-0.8065	-1	0.4055	-0.8065	1
18	Prismatic	210	201	0	0.1475	-0.062	0	0.1574	0.086	-1.4545	1.311	-1	-1.4545	1.311	1

Table A.5 – Subsystem 2 – FGC 254 Bogie: Geometric characteristics of the kinematic joints with clearance of the primary suspension.

ID	Joint	Radius journal body *i* [m]	Radius bearing body *j* [m]
1,2,4,5,7,8,10,11,13,14,16,17	Cylindrical	0.139	2
3,6,9,12,15,18	Cylindrical	0.06	2

Table A.6 – Subsystem 2 – FGC 254 Bogie: Kinematic joints with clearance of the Bogie-Bolster connection.

ID	Joint	Bodies		Body *i*						Body *j*					
		i	*j*	P_i (ξ_j / η_j / ζ_j)			Q_i (ξ_j / η_j / ζ_j)			P_j (ξ_j / η_j / ζ_j)			Q_j (ξ_j / η_j / ζ_j)		
1	Revolute	201	214	0.877	0.6955	-0.284	0.877	0.8065	0.284	-1.3	0.664	-0.042	-1.3	1	-0.042
2	Revolute	201	214	0.877	-0.6955	-0.284	0.877	-0.8065	0.284	-1.3	-0.664	-0.042	-1.3	-1	-0.042
3	Revolute	201	214	-0.293	0.6955	-0.284	-0.293	0.8065	0.284	1.507	0.664	-0.042	1.507	1	-0.042
4	Revolute	201	214	-0.293	-0.6955	-0.284	0.877	-0.8065	0.284	1.507	-0.664	-0.042	1.507	-1	-0.042

Table A.7 – FGC 254 Bogie: Geometric characteristics of the clearance kinematic joints of the SS.

ID	Joint	Radius journal body *i* [m]	Radius bearing body *j* [m]
1-4	Prismatic	0.01	2

Table A.8 – Subsystem 2 – FGC 254 Bogie: Linear force elements of the primary suspension.

ID	Bodies		Stiffness *k* [kN/m]	Damping Coef. *C* [kN/ms]	Undeformed length l_0 [m]	P_i (ξ_i / η_i / ζ_i)			P_j (ξ_j / η_j / ζ_j)		
	i	*j*									
1	201	205	680	0	0.402	1.8345	0.8065	0.316	0	0.04	0.155
2	201	205	209.5	0	0.2	1.8345	0.9065	0.1575	0	-0.06	0.3135
3	201	205	209.5	0	0.2	1.9345	0.8065	0.1575	-0.1	0.04	0.3135
4	201	206	680	0	0.402	1.8345	-0.8065	0.316	0	-0.04	0.155
5	201	206	209.5	0	0.2	1.8345	-0.9065	0.1575	0	0.06	0.3135
6	201	206	209.5	0	0.2	1.9345	-0.8065	0.1575	-0.1	-0.04	0.3135
7	201	207	680	0	0.402	0.279	0.8065	0.316	0	0.04	0.155
8	201	207	209.5	0	0.2	0.279	0.9065	0.1575	0	-0.06	0.3135
9	201	207	209.5	0	0.2	0.379	0.8065	0.1575	-0.1	0.04	0.3135
10	201	207	0	20	0.2	0.279	1.0795	0.278	0	0.31	0
11	201	208	680	0	0.402	0.279	-0.8065	0.316	0	-0.04	0.155
12	201	208	209.5	0	0.2	0.279	-0.9065	0.1575	0	0.06	0.3135
13	201	208	209.5	0	0.2	0.379	-0.8065	0.1575	-0.1	-0.04	0.3135
14	201	208	0	20	0.2	0.279	-1.0795	0.278	0	-0.31	0
15	201	209	680	0	0.402	-1.4545	0.8065	0.316	0	0.04	0.155
16	201	209	209.5	0	0.2	-1.4545	0.9065	0.1575	0	-0.06	0.3135
17	201	209	209.5	0	0.2	-1.3545	0.8065	0.1575	-0.1	0.04	0.3135
18	201	210	680	0	0.402	-1.4545	-0.8065	0.316	0	-0.04	0.155
19	201	210	209.5	0	0.2	-1.4545	-0.9065	0.1575	0	0.06	0.3135
20	201	210	209.5	0	0.2	-1.3545	-0.8065	0.1575	-0.1	-0.04	0.3135

Table A.9 – Subsystem 2 – FGC 254 Bogie: Linear force elements Bogie-Bolster connection.

ID	Bodies		Stiffness *k* [kN/m]	Damping Coef. *C* [kN/ms]	Undeformed length l_0 [m]	P_i (ξ_i / η_i / ζ_i)			P_j (ξ_j / η_j / ζ_j)		
	i	*j*									
1	201	214	1750	7	0.308	1.041	0.8065	0.038	0.852	0.8065	-0.017
2	201	214	650	7	0.2	1.041	0.7065	0.1735	0.852	0.9065	-0.1525
3	201	214	650	7	0.2	0.941	0.8065	0.1735	0.952	0.8065	-0.1525
4	201	214	1750	7	0.308	1.041	-0.8065	0.038	0.852	-0.8065	-0.017
5	201	214	650	7	0.2	1.041	-0.7065	0.1735	0.852	-0.9065	-0.1525
6	201	214	650	7	0.2	0.941	-0.8065	0.1735	0.952	-0.8065	-0.1525
7	201	214	1750	7	0.308	-0.407	0.8065	0.038	-0.596	0.8065	-0.017
8	201	214	650	7	0.2	-0.407	0.7065	0.1735	-0.596	0.9065	-0.1525
9	201	214	650	7	0.2	-0.307	0.8065	0.1735	-0.696	0.8065	-0.1525
10	201	214	1750	7	0.308	-0.407	-0.8065	0.038	-0.596	-0.8065	-0.017
11	201	214	650	7	0.2	-0.407	-0.7065	0.1735	-0.596	-0.9065	-0.1525
12	201	214	650	7	0.2	-0.307	-0.8065	0.1735	-0.696	-0.8065	-0.1525

Table A.10 – Connection Subsystems 1 and 2 – Kinematic joints with clearance of the pivot.

ID	Joint	Bodies		Body *i*						Body *j*					
		i	*j*	P_i (ξ_j / η_j / ζ_j)			Q_i (ξ_j / η_j / ζ_j)			P_j (ξ_j / η_j / ζ_j)			Q_j (ξ_j / η_j / ζ_j)		
1	Revolute	101	214	5.075	0	-1.223	5.075	0	-1.158	0.128	0	0.163	0.128	0	1.163
2	Revolute	101	214	4.425	0	-1.223	4.425	0	-1.158	0.128	0	0.163	0.128	0	1.163
3	Revolute	101	214	4.75	0.325	-1.223	4.75	0.325	-1.158	0.128	0	0.163	0.128	0	1.163
4	Revolute	101	214	4.75	-0.325	-1.223	4.75	-0.325	-1.158	0.128	0	0.163	0.128	0	1.163

Table A.11 – Connection Subsystems 1 and 2: Geometric characteristics of the kinematic joints with clearance of the pivot.

ID	Joint	Radius ball body *i* [m]	Radius socket body *j* [m]
1-4	Revolute	0.01	0.3365

Table A.12 – Connection Subsystems 1 and 2 – Kinematic joints with clearance of the side bearers.

ID	Joint	Bodies		Body *i*						Body *j*					
		i	*j*	P_i (ξ_j / η_j / ζ_j)			Q_i (ξ_j / η_j / ζ_j)			P_j (ξ_j / η_j / ζ_j)			Q_j (ξ_j / η_j / ζ_j)		
1	Revolute	101	214	5.474	0.765	-1.318	5.474	0.765	-1	0.852	0.765	0.058	0.852	0.765	1.058
2	Revolute	101	214	5.474	-0.765	-1.318	5.474	-0.765	-1	0.852	-0.765	0.058	0.852	-0.765	1.058
3	Revolute	101	214	4.026	0.765	-1.318	4.026	0.765	-1	-0.596	0.765	0.058	-0.596	0.765	1.058
4	Revolute	101	214	4.026	-0.765	-1.318	4.026	-0.765	-1	-0.596	-0.765	0.058	-0.596	-0.765	1.058

Table A.13 – Connection Subsystems 1 and 2: Geometric characteristics of the kinematic joints with clearance of the side bearers.

ID	Joint	Radius journal body *i* [m]	Radius bearing body *j* [m]
1-2	Prismatic	0.057	2

Annex B – MUBODyn FGC 62.000 Model

Table B.1 – Subsystem 1 – FGC62.000 Vehicle Body: Mass and inertia properties and initial positions of the CM of the rigid bodies.

ID	Body	Mass [kg]	Inertia properties [kg.m^2]			Initial position [m]		
			I_{roll}	I_{pitch}	I_{yaw}	X_0	Y_0	Z_0
101	Vehicle body	53096	59407	366523	365988	0	0	2.235

Table B.2 – Subsystem 1 – FGC62.000 Vehicle Body: Mass and inertia properties and initial positions of the CM of the rigid bodies.

ID	Body	Mass [kg]	Inertia properties [kg.m^2]			Initial position [m]		
			I_{roll}	I_{pitch}	I_{yaw}	X_0	Y_0	Z_0
201	Bolster	366	106	9	108	0	0	0.482
202	Side Frame Left	446	15	138	127	0	0.76	0.449
203	Side Frame Right	446	15	138	127	0	-0.76	0.449
204	Wheelset Front	990	338	54	338	0.8	0	0.381
205	Wheelset Rear	990	338	54	338	-0.8	0	0.381

Table B.3 – Subsystem 2 – FGC 62.000 Bogie: Primary suspension non-linear force elements.

ID	Bodies		Force characteristic	P_i (ξ_i / η_i / ζ_i)			P_j (ξ_j / η_j / ζ_j)		
	i	j							
1	204	202	F1	0	0.83	0	0.8	0.07	0.432
2	204	202	F1	0	0.69	0	0.8	-0.07	0.432
3	204	202	F2	0	0.76	0	0.8	-0.5	-0.068
4	204	202	F3	0	0.76	0	1.3	0	-0.068
5	204	202	F3	0	0.76	0	0.3	0	-0.068
6	204	203	F1	0	-0.83	0	0.8	-0.07	0.432
7	204	203	F1	0	-0.69	0	0.8	0.07	0.432
8	204	203	F2	0	-0.76	0	0.8	0.5	-0.068
9	204	203	F3	0	-0.76	0	1.3	0	-0.068
10	204	203	F3	0	-0.76	0	0.3	0	-0.068
11	205	202	F1	0	0.83	0	-0.8	0.07	0.432
12	205	202	F1	0	0.69	0	-0.8	-0.07	0.432
13	205	202	F2	0	0.76	0	-0.8	-0.5	-0.068
14	205	202	F3	0	0.76	0	-1.3	0	-0.068
15	205	202	F3	0	0.76	0	-0.3	0	-0.068
16	205	203	F1	0	-0.83	0	-0.8	-0.07	0.432
17	205	203	F1	0	-0.69	0	-0.8	0.07	0.432
18	205	203	F2	0	-0.76	0	-0.8	0.5	-0.068
19	205	203	F3	0	-0.76	0	-1.3	0	-0.068
20	205	203	F3	0	-0.76	0	-0.3	0	-0.068

Table B.4 – Subsystem 2 – FGC 62.000 Bogie: Linear force elements of the primary suspension.

ID	Bodies		Stiffness k [kN/m]	Damping Coef. C [kN/ms]	Undeformed length l_0 [m]	P_i (ξ_i / η_i / ζ_i)			P_j (ξ_j / η_j / ζ_j)		
	i	j									
1	204	202	0	20	0.5	0	0.83	0	0.8	0.07	0.432
2	204	202	0	20	0.5	0	0.69	0	0.8	-0.07	0.432
3	204	202	0	20	0.5	0	0.76	0	0.8	-0.5	-0.068
4	204	202	0	20	0.5	0	0.76	0	1.3	0	-0.068
5	204	202	0	20	0.5	0	0.76	0	0.3	0	-0.068
6	204	203	0	20	0.5	0	-0.83	0	0.8	-0.07	0.432
7	204	203	0	20	0.5	0	-0.69	0	0.8	0.07	0.432
8	204	203	0	20	0.5	0	-0.76	0	0.8	0.5	-0.068
9	204	203	0	20	0.5	0	-0.76	0	1.3	0	-0.068
10	204	203	0	20	0.5	0	-0.76	0	0.3	0	-0.068
11	205	202	0	20	0.5	0	0.83	0	-0.8	0.07	0.432
12	205	202	0	20	0.5	0	0.69	0	-0.8	-0.07	0.432
13	205	202	0	20	0.5	0	0.76	0	-0.8	-0.5	-0.068
14	205	202	0	20	0.5	0	0.76	0	-1.3	0	-0.068
15	205	202	0	20	0.5	0	0.76	0	-0.3	0	-0.068
16	205	203	0	20	0.5	0	-0.83	0	-0.8	-0.07	0.432
17	205	203	0	20	0.5	0	-0.69	0	-0.8	0.07	0.432
18	205	203	0	20	0.5	0	-0.76	0	-0.8	0.5	-0.068
19	205	203	0	20	0.5	0	-0.76	0	-1.3	0	-0.068
20	205	203	0	20	0.5	0	-0.76	0	-0.3	0	-0.068

Table B.5 – Subsystem 2 – FGC 62.000 Bogie: Linear force elements of the spring nest.

ID	Bodies		Stiffness k [kN/m]	Damping Coef. C [kN/ms]	Undeformed length l_0 [m]	P_i (ξ_i / η_i / ζ_i)			P_j (ξ_j / η_j / ζ_j)		
	i	j									
1	204	202	550	0	0.273	0.075	0.12	-0.24	0.75	0.88	-0.06
2	204	202	550	0	0.273	-0.075	0.12	-0.24	-0.075	0.88	-0.06
3	204	202	550	0	0.273	0.075	-0.12	-0.25	0.075	0.64	-0.06
4	204	202	550	0	0.273	-0.075	-0.12	-0.24	0.075	0.64	-0.06
5	204	202	160	0	0.5	0	-0.25	-0.1335	0	1.01	-0.1665
6	204	203	160	0	0.5	0.25	0	-0.1335	-0.25	0.76	-0.1665
7	204	203	550	0	0.273	0.075	-0.12	-0.24	0.75	-0.88	-0.06
8	204	203	550	0	0.273	-0.075	-0.12	-0.24	-0.075	-0.88	-0.06
9	204	203	550	0	0.273	0.075	0.12	-0.25	0.075	-0.64	-0.06
10	204	203	550	0	0.273	-0.075	0.12	-0.24	0.075	-0.64	-0.06
11	205	202	160	0	0.5	0	0.25	-0.1335	0	-1.01	-0.1665
12	205	202	160	0	0.5	0.25	0	-0.1335	-0.25	-0.76	-0.1665

Table B.6 – Subsys 2 – FGC 62.000 Bogie: Bolster-side frames bumpstops nonlinear force elements.

ID	Bodies		Force characteristic	P_i (ξ_i / η_i / ζ_i)			P_j (ξ_j / η_j / ζ_j)		
	i	*j*							
1	202	201	F4	0	0	0.033	0	0.26	0
2	202	201	F5	0.5	0	0.033	0	0.76	0
3	202	201	F5	-0.5	0	0.033	0	0.76	0
4	203	201	F4	0	0	0.033	0	-0.26	0
5	203	201	F5	0.5	0	0.033	0	-0.76	0
6	203	201	F5	-0.5	0	0.033	0	-0.76	0

Table B.7 – Subsys 2 – FGC 62.000 Bogie: Bolster-side frames bumpstops Linear force elements.

ID	Bodies		Stiffness *k* [kN/m]	Damping Coef. *C* [kN/ms]	Undeformed length l_0 [m]	P_i (ξ_i / η_i / ζ_i)			P_j (ξ_j / η_j / ζ_j)		
	i	*j*									
1	202	201	0	20	0.5	0	0	0.033	0	0.26	0
2	202	201	0	20	0.5	0.5	0	0.033	0	0.76	0
3	202	201	0	20	0.5	-0.5	0	0.033	0	0.76	0
4	203	201	0	20	0.5	0	0	0.033	0	-0.26	0
5	203	201	0	20	0.5	0.5	0	0.033	0	-0.76	0
6	203	201	0	20	0.5	-0.5	0	0.033	0	-0.76	0

Table B.8 – Subsys 2 – FGC 62.000 Bogie: Non-linear force elements friction wedges.

ID	Bodies		Force characteristic	P_i (ξ_i / η_i / ζ_i)			P_j (ξ_j / η_j / ζ_j)		
	i	*j*							
1	202	201	D1	0	0	-0.25	0	0.76	0.25
2	202	201	D2	0	-0.5	0.033	0	0.76	0
3	203	201	D1	0	0	0.25	0	-0.76	0.25
4	203	201	D2	0	0.5	0.033	0	-0.76	0

Table B.9 – Connection Subsystems 1 and 2 – Nonlinear force elements of the pivot.

ID	Bodies		Force characteristic	P_i (ξ_i / η_i / ζ_i)			P_j (ξ_j / η_j / ζ_j)		
	i	*j*							
1	101	201	F6	4.95	0	-1.303	0.15	0	0.15
2	101	201	F6	4.65	0	-1.303	-0.15	0	0.15
3	101	201	F6	4.8	0.15	-1.303	0	0.15	0.15
4	101	201	F6	4.8	-0.15	-1.303	0	-0.15	0.15

Table B.10 – Connection Subsys 1 and 2 – Linear force elements of the pivot.

ID	Bodies		Stiffness k [kN/m]	Damping Coef. C [kN/ms]	Undeformed length l_0 [m]	P_i (ξ_i / η_i / ζ_i)			P_j (ξ_j / η_j / ζ_j)		
	i	j									
1	101	201	0	20	0.3007	4.95	0	-1.303	0.15	0	0.15
2	101	201	0	20	0.3007	4.65	0	-1.303	-0.15	0	0.15
3	101	201	0	20	0.3007	4.8	0.15	-1.303	0	0.15	0.15
4	101	201	0	20	0.3007	4.8	-0.15	-1.303	0	-0.15	0.15
5	101	201	60000	20	0.15	4.8	0	-1.603	0.15	0	0.15
6	101	201	60000	20	0.15	4.8	0	-1.603	-0.15	0	0.15
7	101	201	60000	20	0.15	4.8	0	-1.603	0	0.15	0.15
8	101	201	60000	20	0.15	4.8	0	-1.603	0	-0.15	0.15

Table B.11 – Connection Subsystems 1 and 2 – pivot friction damping non-linear force elements.

ID	Bodies		Force characteristic	P_i (ξ_i / η_i / ζ_i)			P_j (ξ_j / η_j / ζ_j)		
	i	j							
1	101	201	D3	4.95	0	-1.603	0.15	0.15	0.15
2	101	201	D3	4.65	0	-1.603	-0.15	-0.15	0.15
3	101	201	D3	4.8	0.15	-1.603	-0.15	0.15	0.15
4	101	201	D3	4.8	-0.15	-1.603	0.15	0.15	0.15

Table B.12 – Connection Subsys 1 and 2 – Non-linear force elements of the sidebearers.

ID	Bodies		Force characteristic	P_i (ξ_i / η_i / ζ_i)			P_j (ξ_j / η_j / ζ_j)		
	i	j							
1	101	201	F7	4.8	0.62	-1.303	0	0.62	0.15
2	101	201	F7	4.8	-0.62	-1.303	0	-0.62	0.15

Table B.13 – Connection Subsys 1 and 2 –Linear force elements of the sidebearers.

ID	Bodies		Stiffness k [kN/m]	Damping Coef. C [kN/ms]	Undeformed length l_0 [m]	P_i (ξ_i / η_i / ζ_i)			P_j (ξ_j / η_j / ζ_j)		
	i	j									
1	101	201	0	20	0.3007	4.8	0.62	-1.303	0	0.62	0.15
2	101	201	0	20	0.3007	4.8	-0.62	-1.303	0	-0.62	0.15

Table B.14 – Connection Subsys 1 and 2 – Sidebearers friction damping nonlinear force elements.

ID	Bodies		Force characteristic	P_i (ξ_i / η_i / ζ_i)			P_j (ξ_j / η_j / ζ_j)		
	i	j							
1	101	201	D2	4.8	0.62	-1.303	0	0.62	0.15
2	101	201	D2	4.8	-0.62	-1.303	0	-0.62	0.15

Table B.15 – Force characteristic of non-linear force elements of the primary suspension.

Force characteristics		Force characteristics		Force characteristics	
F1		F2		F3	
Length *X* [m]	Force [kN]	Length *X* [m]	Force [kN]	Length *X* [m]	Force [kN]
0.495	-300	0.4928	-300	0.49	-300
0.498	-120	0.4958	-120	0.493	-120
0.499	-60	0.4968	-60	0.494	-60
0.4995	-30	0.4973	-30	0.4945	-30
0.4999	-6	0.4977	-6	0.495	-6
0.5	0	0.4978	0	0.5	0
0.5001	0	0.5	0	0.505	0
0.5005	0	0.5022	0	0.5051	0
0.501	0	0.5023	6	0.5055	0
0.502	0	0.5027	30	0.506	0
0.505	0	0.5032	60	0.507	0
-	-	0.5042	120	0.51	0
-	-	0.5072	300	-	-

Table B.16 – Force characteristic of bolster-side frames bumpstops non-linear force elements.

Force characteristics		Force characteristics	
F4		F5	
Length *X* [m]	Force [kN]	Length *X* [m]	Force [kN]
0.491	-300	0.494	-300
0.494	-120	0.497	-120
0.495	-60	0.498	-60
0.4955	-30	0.4985	-30
0.4959	-6	0.4989	-6
0.496	0	0.499	0
0.5	0	0.5	0
0.504	0	0.501	0
0.5041	6	0.5011	0
0.5045	30	0.5015	0
0.505	60	0.502	0
0.506	120	0.503	0
0.509	300	0.506	0

Table B.17 – Force characteristic of non-linear force elements of the pivot and sidebearers.

Force characteristic		Force characteristic	
F6		F7	
Length *X* [m]	Force [kN]	Length *X* [m]	Force [kN]
0.295	-300	0.275	-300
0.298	-120	0.278	-120
0.299	-60	0.279	-60
0.2995	-30	0.2795	-30
0.2999	-6	0.2799	-6
0.3	0	0.28	0
0.3001	0	0.3	0
0.3005	0	0.3001	0
0.301	0	0.3005	0
0.302	0	0.31	0
0.305	0	0.32	0
0.31	0	0.33	0
0.35	0	0.35	0
0.4	0	0.4	0

Table B.18 – Force characteristic of non-linear force elements of the friction wedge and pivot/sidebearers friction damping.

Force characteristic		Force characteristic		Force characteristic	
D1		D2		D3	
Speed *v* [m/s]	Force [kN]	Speed *v* [m/s]	Force [kN]	Speed *v* [m/s]	Force [kN]
-10	-9.966	-10	-9.966	-10	-17.362
-1	-9.966	-1	-9.966	-1	-17.362
-0.1	-9.966	-0.1	-9.966	-0.1	-17.362
-0.02	-9.966	-0.02	-9.966	-0.02	-17.362
-0.015	-9.966	-0.015	-9.966	-0.015	-17.362
-0.01	-9.966	-0.01	-9.966	-0.01	-17.362
-0.0075	-7.4745	-0.0075	-7.4745	-0.0075	-13.0215
-0.005	-4.983	-0.005	-4.983	-0.005	-8.681
-0.0025	-2.4915	-0.0025	-2.4915	-0.0025	-4.34
0	0	0	0	0	0
0.0025	4.6985	0.0025	2.4915	0.0025	4.34
0.005	9.397	0.005	4.983	0.005	8.681
0.0075	14.0955	0.0075	7.4745	0.0075	13.0215
0.01	18.794	0.01	9.966	0.01	17.362
0.015	18.794	0.015	9.966	0.015	17.362
0.02	18.794	0.02	9.966	0.02	17.362
0.1	18.794	0.1	9.966	0.1	17.362
1	18.794	1	9.966	1	17.362
10	18.794	10	9.966	10	17.362

Annex C – MUBODyn Coupler Model Connecting FGC 254 to FGC 62.000

Table C.1 – Subsystem 1 – Knuckle Coupler: Mass and inertia properties and initial positions of the CM of the rigid bodies.

ID	Body	Mass [kg]	Inertia properties [kg.m^2]			Initial position [m]		
			I_{roll}	I_{pitch}	I_{yaw}	X_0	Y_0	Z_0
101	Knuckle Front	100	10	100	100	0.43	0	0.87
102	Link Front	100	10	100	100	0.96	0	0.87
103	Knuckle Rear	100	10	100	100	-0.43	0	0.87
104	Link Rear	100	10	100	100	-0.96	0	0.87

Table C.2 – Subsystem 1 – FGC254 Bogie: Kinematic joints with clearance of the knuckle-knuckle connection.

ID	Joint	Bodies		Body *i*						Body *j*					
		i	*j*	P_i (ξ_j / η_j / ζ_j)			Q_i (ξ_j / η_j / ζ_j)			P_j (ξ_j / η_j / ζ_j)			Q_j (ξ_j / η_j / ζ_j)		
1	Revolute	101	103	-0.43	0	0.065	-0.43	0	-0.065	0.43	0	0.074	0.43	0	-0.074

Table C.3 – Subsystems 1 – Knuckle Coupler: Geometric characteristics of the kinematic joints with clearance of the knuckle-knuckle connection.

ID	Joint	Radius journal body *i* [m]	Radius bearing body *j* [m]
1-2	Prismatic	0.1	0.11

Table C.4 – Subsystem 1 – Knuckle Coupler: Perfect kinematic joints of the knuckle-link connection.

ID	Joint	Bodies		Body *i*						Body *j*					
		i	*j*	P_i (ξ_j / η_j / ζ_j)			Q_i (ξ_j / η_j / ζ_j)			P_j (ξ_j / η_j / ζ_j)			Q_j (ξ_j / η_j / ζ_j)		
1	Revolute	101	102	0.43	0	0	0.43	0	0.25	-0.1	0	0	-0.1	0	-0.25
2	Revolute	103	104	-0.43	0	0	-0.43	0	0.25	0.1	0	0	0.1	0	-0.25

Table C.5 – Subsystem 1 – Knuckle Coupler: Non-linear force elements of the knuckle-knuckle connection.

ID	Bodies		Force characteristic	P_i (ξ_i / η_i / ζ_i)			P_j (ξ_j / η_j / ζ_j)		
	i	*j*							
1	101	102	F8	0	0.25	0	0	0.25	0
2	103	104	F8	0	-0.25	0	0	-0.25	0

Table C.6 – Connection Subsystem 1 to FGC 254 and FGC62.000– Perfect kinematic joints of the coupler-vehicles connection.

ID	Joint	Bodies		Body *i*						Body *j*					
		i	*j*	P_i (ξ_i / η_j / ζ_j)			Q_i (ξ_j / η_j / ζ_j)			P_j (ξ_j / η_j / ζ_j)			Q_j (ξ_j / η_j / ζ_j)		
1	Prismatic	FGC254 101	102	-7.013	0	-1.455	-6.913	0	-1.455	-0.1	0	0	-0.5	0	0
2	Prismatic	104	FGC62.000 101	0.1	0	0	-0.5	0	0	5.6563	0	-1.365	5.5563	0	-1.365

Table C.7 – Connection Subsystem 1 and Vehicles 1 and 2 –- Linear force elements of the coupler-vehicles draft gear.

ID	Bodies		Stiffness *k* [kN/m]	Damping Coef. *C* [kN/ms]	Undeformed length l_0 [m]	P_i (ξ_i / η_i / ζ_i)			P_j (ξ_j / η_j / ζ_j)		
	i	*j*									
1	FGC254 101	102	80000	20	0.2	-7.013	0	-1.455	-0.1	0	0
2	104	FGC62.000 101	80000	20	0.2	0.1	0	0	5.7563	0	-1.365

Table C.8 – Force characteristic of non-linear force elements knuckle-knuckle connection.

Force characteristic	
F8	
Length *X* [m]	Force [kN]
0.833	-300
0.836	-120
0.837	-60
0.8375	-30
0.8379	-6
0.838	0
0.845	0
0.855	0
0.859	0
0.860	0
0.861	0
0.865	0
0.875	0
0.882	0
0.8821	6
0.8825	30
0.883	60
0.884	120
0.887	300